CRANFIELD UNIVERSITY

FABIEN MARTINEZ

Drag study of the nacelles of a tidal stream device using CFD

SCHOOL OF ENGINEERING
MSc by Research

MSc by Research
Academic Year: 2008 - 2010

Supervisor: Dr Florent Trarieux
November 2010

CRANFIELD UNIVERSITY

SCHOOL OF ENGINEERING
Offshore Engineering and Naval Architecture

MSc by Research

Academic Year 2008 – 2010

FABIEN MARTINEZ

Drag study of the nacelles of a tidal stream device using CFD

Supervisor: Dr Florent Trarieux

November 2010

This thesis is submitted in partial fulfilment of the requirements for the degree of MSc by Research
(NB. This section can be removed if the award of the degree is based solely on examination of the thesis)

ABSTRACT

Nowadays, renewable energy is in full growth. In particular, offshore wind farms will be at the centre of UK energetic strategy in the coming years. However, other types of marine renewable are still at an early development stage. That is the case for tidal energy. Many projects have been undertaken but there is no candidate for competitive commercial applications yet.

Deltastream is one of these numerous pioneering projects. It consists of a set of three marine current turbines mounted on a triangular base put down onto the seabed. The device is not moored and no harm is done to the environment. However, that makes the structure more sensitive to water flows. And it is important to ensure that it will remain at its location and not being carried along with the tidal streams.

Using CFD, the present study aims to evaluate the drag on the nacelles of the structure and come up with solutions to reduce it as much as possible.

Keywords:

Renewable energy – fluid dynamics – Deltastream – marine current turbine – tidal energy

ACKNOWLEDGEMENTS

I would like to thank my girlfriend Paula and my parents for always being on my side and supporting me during a difficult period of my life.

Amongst the many friends I met in Cranfield I would like to extend my warmest thanks to Mustafa, Xavier, Olivia and Etienne.

Thanks to my supervisor Dr Trarieux for giving me the opportunity to discover the field of research and to learn new subjects.

TABLE OF CONTENTS

LIST OF FIGURES

1 BACKGROUND

1.1 Energy crisis

Sources of conventional energy such as coal, oil or gas tend to decrease considerably and pessimistic predictions announce their progressive disappearance in the decades to come. However, the energy demand becomes more and more important with populations growing on Earth and the emergence of countries like China or India.

Hence, on one hand there is a rarefaction of energy resources and on the other hand high energy requirements. This complex situation leads the world towards an important energy crisis which consequences could be disastrous for the politic and economic stability of our planet.[1]

1.2 Climate change and environmental concerns

Furthermore, since the early 1990's the scientific community pointed out the issue of environmental changes on Earth. Temperatures have been subject to increase, ices are melting at the poles and extreme meteorological events are becoming more frequent and violent. It is recognized that these observations are the main consequences of global warming (or climate change). The exact causes of climate change are not yet clearly identified, contrarily to its above mentioned consequences. However, it has been recognized that the global phenomenon is instigated by increased levels of "greenhouse gases" emissions. Amongst the panel of "greenhouse gases" contributing to global warming, carbon dioxide has the most negative effect on the environment. The production and use of energy worldwide produces 60% of the total CO2 emissions.[2]

1.3 The need for renewable energy

National governments started to show awareness of the energy and climate change issues and the necessity to undertake joint actions to bring solutions to reduce carbon emissions and achieve energy supply. New energy policies have been defined and more interest have been shown to the low carbon emissions sources of energy better known as renewable energy.

Climate change concerns and high oil prices are then the main drivers for the development of renewable energies. The term renewable energy designates the energy generated from natural and sustainable sources such as sunlight, wind, rain, tides or geothermal heat. These sources of energy are available at all time in nature and will never vanish as they are continuously replenished.

Renewable energy can take several forms. The more spread forms being wind power, solar energy, hydropower, bio-fuels and geothermal energy.[3]

1.3.1 Wind power

Wind is used to run wind turbines generators. Nowadays, the rated power of a WTG can be comprised between 600 kW and 5 MW. The power output is directly dependent on the cube of wind speed. The faster the wind flows, the more power is generated. As a result, wind turbine generators (WTGs) are preferably installed in region of strong and constant winds. For instance, high altitudes and offshore locations offer an attractive potential for developing wind farms. Even if the wind energy is one of the most advanced in the category of renewable energy, a lot more progress remains possible to achieve better productivity and efficiency. Most of the wind farms worldwide are onshore based, but the developers tend to go offshore where wind resources are estimated to be much more important with mean wind speed approximately 90% greater than onshore. Wind power does not release any greenhouse gases in operation.[4]

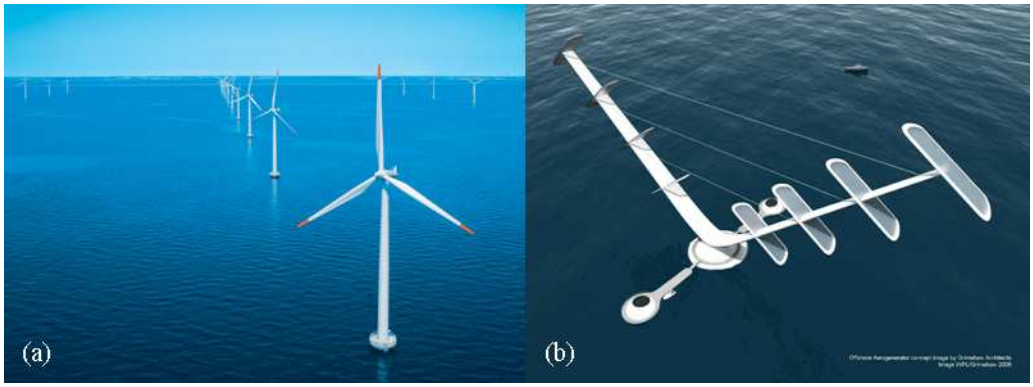

Figure 1-1: (a) A view of the Nysted offshore wind park (courtesy Siemens); (b) NOVA offshore vertical axis turbine project (courtesy Grimshaw)

1.3.2 Hydropower

Energy is present in water. Luckily, this energy can be harnessed and used. Different types of hydroelectricity are available.

- Large-scale hydroelectricity dams
- Micro hydroelectricity systems
- Damless hydroelectric systems that generate power from the kinetic energy from rivers and oceans with no need for a dam
- Ocean energy

The last category is of particular interest to us. Ocean energy covers all those technologies that harness energy from the marine environment. Marine current power, tidal power and ocean thermal energy conversion (TEC) are part of ocean energy.[5]

Figure 1-2: Large-scale hydroelectricity dam (courtesy of IER)

1.3.3 Solar energy

Solar energy harnesses energy from the sun through solar radiations. Electricity is produced using photovoltaic cells or heat engines. A solar device captures converts and distributes solar energy.[3]

Figure 1-3: (a) Solar panel (courtesy BP); (b) Giant photovoltaic array, Ontario, Canada (courtesy greenenergyreporter.com)

1.3.4 Bio-fuels

Bio-fuels are liquid fuels produced from plant materials and waste. Two categories of bio-fuels are commonly distinguished.

Bio-alcohol such as bio-ethanol is obtained by the fermentation of sugar generally from plant materials (e.g. sugar beet). Bio-ethanol is used as a fuel for

vehicles in its pure form or as an additive to gasoline and is widely spread in Brazil and the United States.

Bio-diesel is the other form of bio-fuels. Bio-diesel can be produced from vegetable oils and used as a vehicle fuel. Again this can be done with bio-diesel in its pure form, but most of the time it is employed as an additive. It is commonly used in Europe.

Bio-fuels aim to reduce pollutants emissions arising from the use of vehicles. On the contrary of all of the other renewable energy presented in this section, the main purpose of their use is transportation.[3]

1.3.5 Geothermal energy

Geothermal energy takes advantages of the heat of the Earth itself. The heat is tapped from some meters to kilometers deep into the Earth's crust. Three kind of power station are generally used in geothermal energy. These are categorized as:

- Dry steam plants (steam is taken out of fractures in the ground and use to turn a turbine spinning a generator)
- Flash plants (hot water [over 20° C] is taken out of the ground; steam and water phases are separated and steam is used to drive a turbine.[3]

1.4 UK energy policy

Based on 2007 figures, UK's annual electricity consumption is estimated to be around 350 TWh with a generating capacity of approximately 76 GW.[1]

The current energy market for UK is organized as follows. Coal power stations provide 37% of the energy distributed in UK, gas power plant provides 36% of the needs in electricity, 18% arise from nuclear and only 4% comes from renewable. However, this generation mix is quite likely to change in the new few years. Indeed, the programmed decommissioning of coal, oil and nuclear power stations will allow renewables to gain more importance.[1]

Important investment in new generation capacity is essential to face the lack meant by the conventional power stations closures.

"Renewable energy has a key role to play in reducing carbon emissions and achieving security of supply" [1]

UK presents amongst the best renewable resources in Europe, particularly very good wind and marine (wave and tidal) resources [6]. Then, government decided to orient its energetic strategy towards a more important development of renewables. Indeed, renewables present several advantages. First of all they are less polluting, then they use sustainable resources and finally electricity production can be achieved within UK solving the problem of security of supply and energetic independence. For these reasons, renewables will be importantly integrated to the future generation mix, with already a lot of offshore wind farm projects under construction.[5; 7; 8]

However, the current status of renewable technologies does not make them competitive enough on the energy market place when compared to more conventional energy sources. In order to help their development, UK government decided to adopt an adequate policy.

The main objective of this new policy is to reach the targets set by the Kyoto protocol (1997). Following this protocol, and in accordance with EU directives, UK agreed to reduce its carbon dioxide emissions by 12.5% from their 1990's level by 2012. Even, UK launched a Climate Change Program in 2000 with the idea to go beyond this target and reduce its emissions by 20% by 2010.[1]

In the frame of the climate change program, different measures have been undertaken to favor the development of renewables. The climate change bill is one of them, with an objective of decreasing UK's emissions by 60% from 1990's levels by 2050.[1]

Furthermore, renewable obligations require that energy suppliers in UK produce a percentage of the total energy they sell using renewable sources. This percentage is annually reviewed and was set to around 9% in 2008. It is

expected to reach a value close to 15% in 2015/2016 (BERR website). Licensed energy suppliers are financially penalized if they do not rely on green power in their energy production through renewable obligation certificates (ROCs). On the other hand, those who integrate green power in their energy generation mix are rewarded through the same certificates.

Finally, the climate change Levy (a tax) applies to energy supplied to non-domestic consumers and generated from conventional sources and nuclear. When the energy supplied is produced from renewables an exemption of climate change Levy applies. The money collected through the application of the CCL is then redistributed to organizations that promote energy efficiency like the Carbon Trust for instance.

All together these measures encourage energy suppliers to “go green” and consider renewables as a serious alternative to energy production. By financial support, they intend to reduce the gap that makes competition with conventional sources to tough for renewables as green technologies are less advanced and established than their predecessor, and hence are more costly.[3]

2 TIDAL ENERGY REVIEW

Europe presents the best tidal resource worldwide. United Kingdom possesses half the total of this potential extractable power. When security of energy supply is threatened due to the diminution of fuel resources and high energetic dependence on other countries, tidal energy could be the warrant of future energy security for Great Britain. Furthermore, with no carbon dioxide emissions in operation, tidal energy devices have a role to play in the effort to reach the targets set by European and British energy policies.

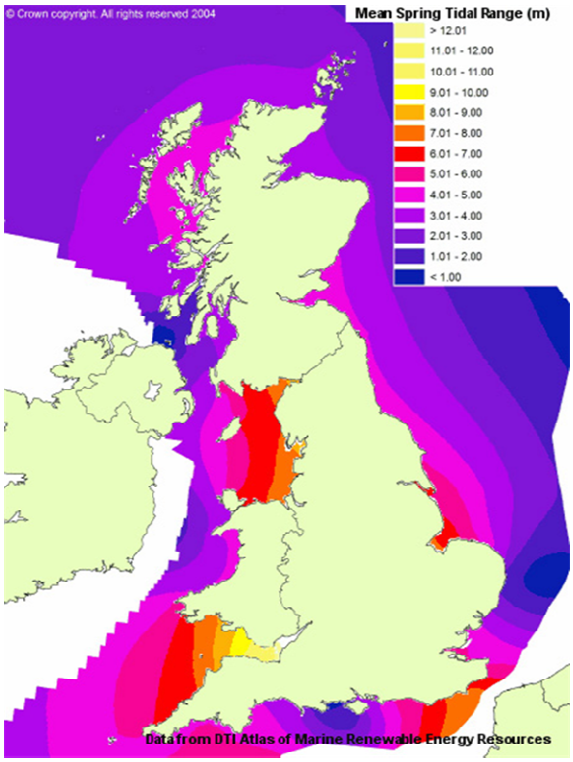

Figure 2-1: UK mean spring tidal range (courtesy DTI)

The importance of the resource combined with the predictable nature of tides could make tidal energy even more attractive than wind energy or other form of renewables.[6; 9]

2.1 The nature of the tides

Tides are the periodic changes of water levels observed at the surface of the Earth and caused by the gravitational action of the Moon and the Sun on Earth.

2.1.1 History of tidal knowledge

Three centuries before Christ, Aristotle was the first to recognize the link existing between the tides and the Moon but in these times Earth-centered astronomy did not allow him to fully understand this phenomenon.

In the middle Ages, Copernicus came with his heliocentric view of the solar system and opened the way to progress for tidal science.

Later, in the middle of the seventeenth century, three different theories were being seriously examined to explain the tides.

1. Johannes Kepler proposed the idea that Moon exerted a gravitational attraction on the water of the ocean, balanced by the Earth's attraction on the waters. Without such a balancing force emanating from Earth, waters would have simply been elevated in the sky and would stick to the Moon's body.
2. A second theory was advanced by Galileo who believed the rotation of Earth led to a motion of the seas. The modification of this motion by the shape of the sea floor generated tides.
3. The last theory is due to Descartes. The French scientist presented the space as full of invisible matter. The rotation of the Moon around Earth would compress the matter in a way that it would transmit pressure to the sea, hence giving place to the tides.

Although all of these approaches were respectable, Isaac Newton was the one to finally give the best explanation to the tidal process. He used the example of tides to illustrate his equilibrium theory and introduce the concept of force in a heliocentric solar system.

Later on, Laplace and Kelvin provided a more mathematical approach to model and predict the tides.[9]

2.1.2 Newton's law of gravitation

The rise and fall of waters at the surface of our planet occurs in response to gravitational effect of the Moon and the Sun.

According to Newton, the gravitational force between two bodies depends on the product of their masses and the inverse square of the distance between them. In other words, if an object A (of mass m_a) interacts with an object B (of mass m_b) and located at a distance D from A, then the gravitational force F between A and B can be expressed as follows:

$$F = \frac{Gm_a m_b}{D^2} \quad \textbf{(2-1)}$$

Where G is the so-called universal gravitational constant which is generally given the value of $6.67300 \times 10^{-11}\, m^3.kg^{-1}.s^{-2}$.

2.1.3 Tidal force

The amount of gravitational force acting on the Earth may be different at various positions on the Earth body as it is affected by the distance of the attracting object. Hence it is common practice to consider the gradient of the gravitational force (its variation over distance) also referred as a *tidal force*.

The tidal force across a distance dD is:

$$dF = \left(\frac{dF}{dD}\right) dD = \frac{2Gm_a m_b}{D^3} dD \quad \textbf{(2-2)}$$

The tidal force is proportional to the mass m_a and m_b. Plus, the tidal force is inversely proportional to the distance D cubed.

To determine what has strongest tidal effects on the Earth between the Sun and the Moon, we can determine the ratio:

$$\frac{F_{tidal,moon}}{F_{tidal,sun}} = \frac{m_{moon}}{m_{sun}}\left(\frac{D_{sun}}{D_{moon}}\right)^3 \approx 2.2 \qquad \textbf{(2-3)}$$

$m_{moon} = 7.3477 \times 10^{22}\ kg;\ m_{sun} = 1.9891 \times 10^{30} kg\ ; D_{moon} = 384{,}402\ km$

$D_{sun} = 149{,}597{,}870\ km$

From (2-3), even though the Sun is heavier than the moon (2.7×10^7 times) but 389 times as far away from Earth, the Sun's tide raising force is less important than that of the Moon. The Sun plays a less important role than the Moon in the tidal process.[10]

2.1.4 The tidal mechanism

We consider two points at the surface of the Earth x and x' (Figure 2-1). The point x is the closest to the Moon, meanwhile x' is located further. The center of the Earth is the point O.

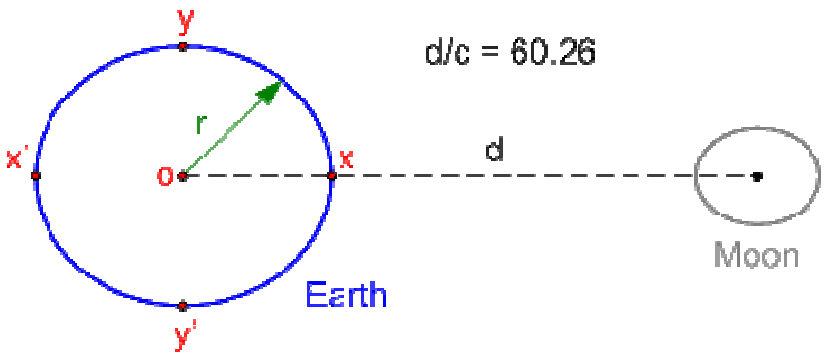

Figure 2-1: schematic representation of the Earth-Moon system

The radius of Earth is about one sixtieth of the distance the Moon and the Earth centers (Figure 2-1). Hence, the radius of our planet is a significant proportion of the distance separating the two celestial bodies. As a result, the force exerted by the Moon at x is higher than the force exerted at O which is in turn higher than the force at x'. The relative magnitudes of these forces are illustrated in Figure 2-2.

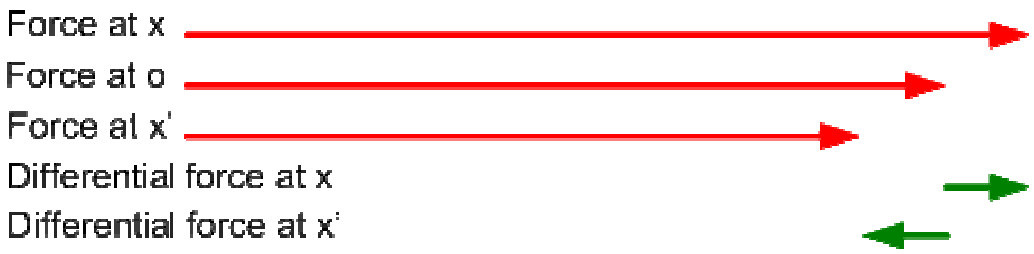

Figure 2-2: Relative magnitude of Earth-Moon system interactions

At point x' the Earth is attracted away from the water due to the gravitational action of the Moon. At point x the water is pulled away from the Earth due to the Moon attraction. As a result, the water envelope around Earth transforms into an ellipsoid as shown on Figure 2-3. The perpendicular points to the Moon-Earth axis (y and y') are equidistant from the Moon, like the centre of the Earth o, and, as a result, the gravitational attraction of the Moon is the same for all of these three points (y, y', o).

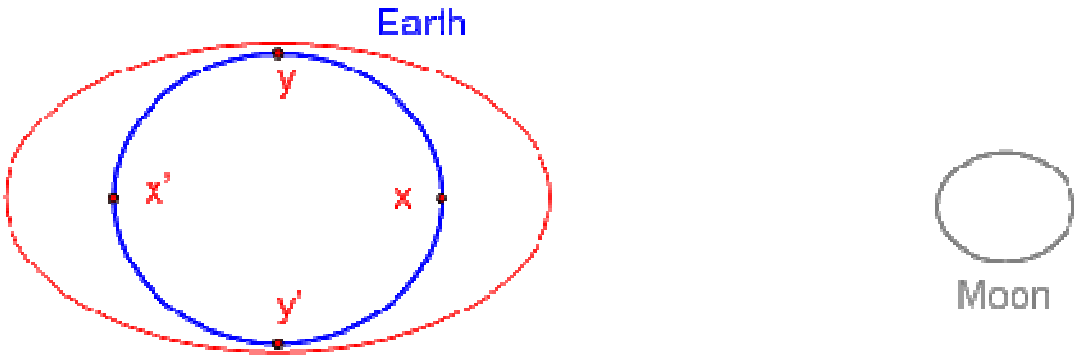

Figure 2-3: Schematic view of water envelope at the Earth surface

Furthermore, centrifugal forces due to the revolution of the Earth-Moon system contribute also to the distortion of the envelope of water.

One other well established observation of the manifestation of the tides is not only the increase and decrease in water levels at the surface of the Earth, but also the horizontal flow of the water back and forth in the same rhythm. Such flows of water are known as *tidal currents* or *tidal streams*. It is a force known as the “tractive force” which is responsible for the ebb and flow of tidal streams.

Every day at any particular location on Earth a semi-diurnal tidal regime can be observed. Such a cycle consists in two raises and two falls of the water level every 24 hours.

The Sun has a similar gravitational effect on Earth and hence on the behavior of the waters at its surface. However, this effect is less important than the one of the Moon due to the much more important distance separating the Sun and the Earth.

When the Sun and the Moon are located on a same line (in other words when the Moon is in a full or new state), the influences of both the Sun and the Moon combine and result in large range tides better known as *spring tides*. When, on the other hand, the Sun and the Moon are located at right angles from each other their interaction considerably decreases the tidal range and *neap tides* are observed. Successive neap tides and spring tides are observed approximately at two-week intervals.

As demonstrated in this part, tides are mostly the consequences of the gravitational and centrifugal forces exerted by the Moon and the Sun (with less importance) on the Earth. However, other factors such as the Coriolis force and the topography of the sea bed are also involved in the tidal process.[10]

2.2 Power in the tides

2.2.1 Available power in a tidal stream

The energy contained in flowing water is its kinetic energy. For a body of mass $m(kg)$ and moving with a velocity $v(m.s^{-1})$, the kinetic energy is given by the following expression:

$$K = \frac{1}{2}mv^2 \qquad \textbf{(2-4)}$$

In order to evaluate the potential power that can be extracted from a tidal flow we need to find the kinetic energy in the stream that goes through a unit area of the stream normal to the stream direction.

As illustrated on figure 1, we first take into account the case of a tidal flow passing through a circular ring that encloses a circular area called A at a velocity v.

If for example the water is moving at a velocity of $2.5\,m.s^{-1}$, we can imagine that a cylinder of water of length $2.5\,m$ will flow through the circular ring each second. As a result, it is a volume of water $V = A \times 2.5$ that will pass through the ring each second. The multiplication of this volume by the water density ρ gives the mass of water flowing through the ring per second$(\dot{m})$.

$$\dot{m} = \rho A v \qquad \textbf{(2-5)}$$

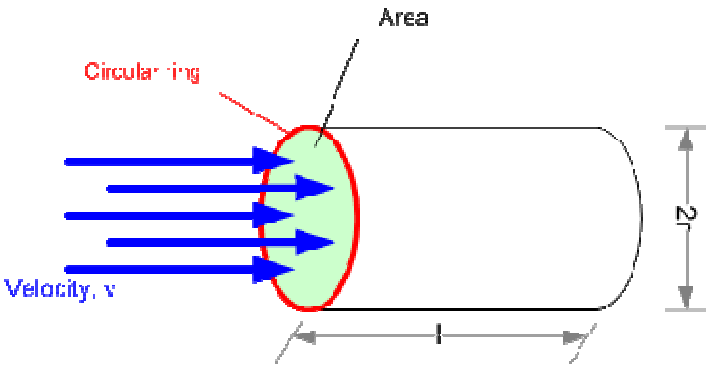

Figure 2-4: Schematic view of tidal flow through circular cylinder

Then, substituting the value of $\dot{m}$ in the expression (dessous) of the kinetic energy we obtain the potential hydraulic power:

$$P_H = \frac{1}{2}\dot{m}v^2 \qquad \textbf{(2-6)}$$

$$P_H = \frac{1}{2}\rho A v^3 \qquad \textbf{(2-7)}$$

From this expression it appears that the power in a water stream is proportional to the water density, the area through which the water is flowing and the cube of the water velocity.[3]

2.2.2 Extracted power

It is important to note that the potential hydraulic power is not the same amount of power that a marine current turbine or other device will extract. This is mainly due to the fact that losses occur in the energy conversion process.

Hence, for any particular tidal device it is necessary to take into account an efficiency factor e which determines the percentage of hydraulic power that the device is able to convert into useful energy. Usually, for wind turbine technologies and tidal power technologies this efficiency factor has a value of 30 to 40%. The power generated by a particular device of the marine current type is then:

$$P_e = \frac{1}{2}\rho e \pi r^2 v^3 \qquad \textbf{(2-8)}$$

Where e is the efficiency factor, r the radius of the rotor, v the free stream velocity and ρ the sea water density [9].

2.3 Tidal power

The production of energy from tidal resources can be divided into two broad categories.

First, electricity can be produced using tidal barrages and lagoons. Tidal barrages use the vertical rise and fall of tides and tidal lagoons use the potential energy of heads of water trapped behind dams [3].

Second, power can be generated using tidal stream devices which exploit the horizontal flow of tidal currents and convert its kinetic energy into electricity.

2.3.1 Tidal barrages and lagoons

A famous example of tidal barrage is the plant of La Rance, France. First tidal power plant worldwide, it was opened in 1966 and still produces electricity. Operated by EDF, the plant has an annual output of about 68MW average power and produces 0.012% of the power consumed by France [3].

Figure 2-5: (a) Aerial view of the La Rance tidal barrage; (b) La Rance's dam

This thesis is mainly concerned with tidal stream devices and a comprehensive review of the technology underneath tidal energy from barrages and lagoons as well as on-going projects can be found in [3; 5; 8; 11; 11; 12].

2.3.2 Tidal stream

Tidal barrages and tidal lagoons technologies present the disadvantages to be costly due to the amount of civil engineering works needed to conceive them and they can be environmentally intrusive. To overcome these problems, interest in tidal stream devices has grown since the early 1990's.

It is possible to extract power from the tidal currents deploying arrays of rotors supported on pontoons tethered to the seabed or fixed to the bottom in appropriate locations. The energy extraction process is then pretty similar to the one of wind energy. In some other cases, different tidal stream processes are used to extract tidal power.

Tidal stream devices are usually classified in four categories as shown on Figure 2-6: The four classic categories of tidal devices.

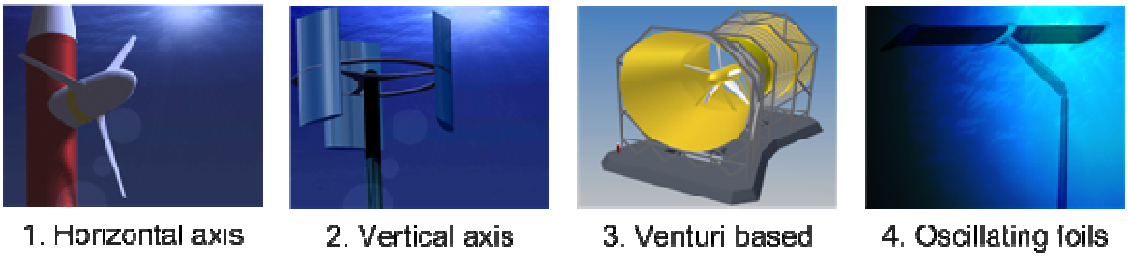

Figure 2-6: The four classic categories of tidal devices

2.4 Tidal stream devices

2.4.1 Horizontal axis marine current turbines (HAMCT)

Horizontal axis marine current turbines and wind turbines share the same principle of operation and energy conversion is performed in the same way for both technologies.

The water flow is parallel to the rotor axis and to the seabed. The linear motion of water is changed into rotational energy used to drive a generator and produce electricity. Water flows above both surfaces of the water turbine blades (Figure 2-7). However, the water is faster over the upper (longer) side of the airfoil shaped blade. This creates a difference of pressure around the blade profile. A zone of lower pressure dominates above the airfoil. The difference of pressure between the top and bottom surfaces generates a lift force. For an aircraft, the lift is the force which causes a plane to rise off the ground. In the case of horizontal axis turbines, the blades are constrained to move in a plane (the turbine's swept area). The lift force leads to a rotation of the blades about the hub (the center of the swept area). Hence, the rotation of the blades drives a generator which produces electricity.

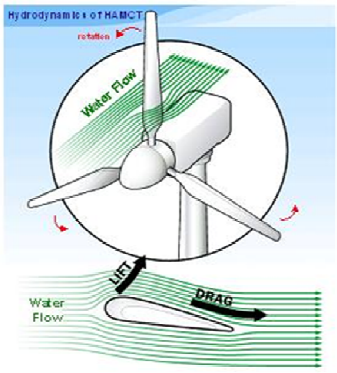

Figure 2-7: Water flow over HAMCT's blades

Deltastream technology enters in this tidal stream devices category. Several other proposals have been made.

At this development stage, Seagen from Marine Current Turbines is the only tidal stream device ever connected and delivering to the national grid. This twin axial-flow rotors device rated at 1.2 MW is currently in commercial operation in Strangford Lough, Northern Ireland. A characteristic of Seagen technology is that the power units and turbines can be raised up the support pile above water level. This allows ease of access for maintenance work using small service vessels.

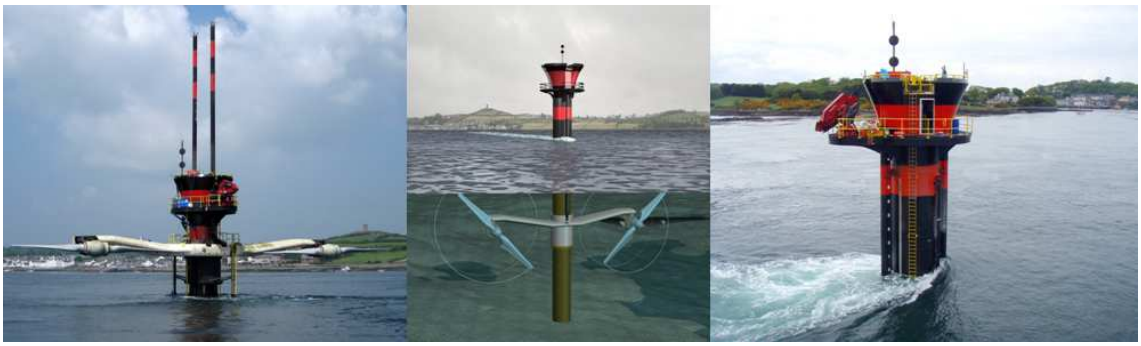

Figure 2-8: The Seagen device (courtesy MCT)

Other technologies such as Verdant Power kinetic hydropower system, SABELLA (hydrohelix energy), tidal stream, tidal generation ltd or Tocardo tidal energy are currently at a development stage [9].

2.4.2 Vertical axis marine current turbines (VAMCT)

The principle of operation of this category of turbines is identical to the one of HAMCT, but in this case the rotor axis is perpendicular to the water flow. VAMCT are equally known as “crossflow turbines”. They present operational advantages due to the fact that gearing and electrical machinery can be maintained above the water level for ease of maintenance and repair [9].

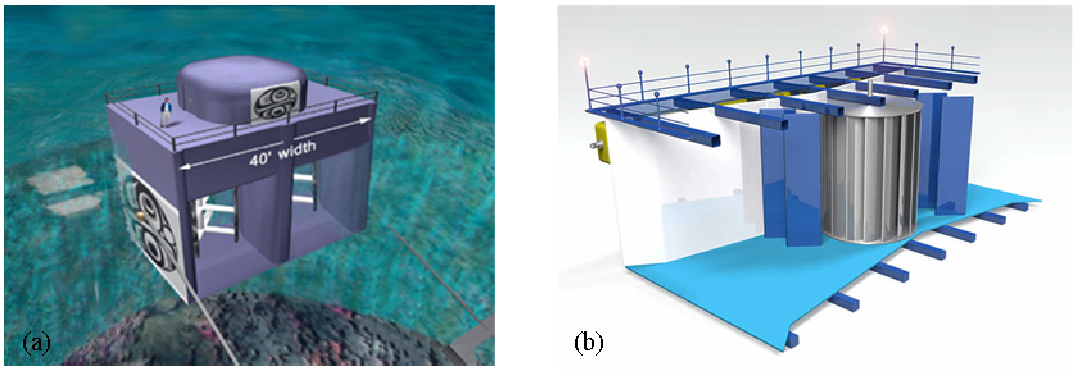

Figure 2-9: (a) Prototype of a VAMCT from Blue Energy, Canada (courtesy Blue Energy); (b) Neptune Proteus NP1000 cutaway showing internal components (Courtesy neptunerenewableenergy.com)

2.4.3 Venturi effect based devices

Ducted horizontal axis turbines may be used to generate electricity. On these devices, a Venturi shaped duct acts as an accelerator of the water flow passing through the turbine swept area. The acceleration of the flow allows to maximize the amount of power generated by a given turbine diameter [9].

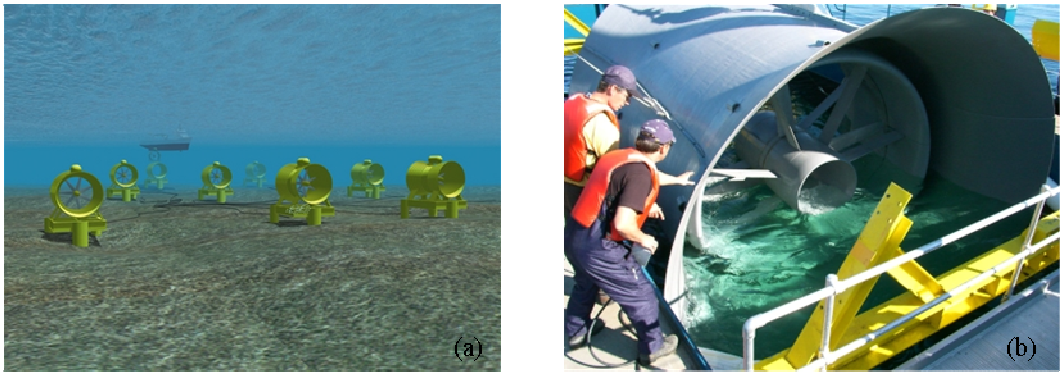

Figure 2-10: (a) Artist view of a Lunar Energy turbines farm (Courtesy Lunar Energy); (b) Maintenance work on a Venturi effect based device

2.4.4 Oscillating foil systems

The concept of hydrofoil systems is different from the one of devices presented above. The hydrofoils oscillate and induce lift and drag forces when placed in the water flow. The oscillation of the device arm activates hydraulic pump systems which in turn drive a generator. Electricity is then generated [9].

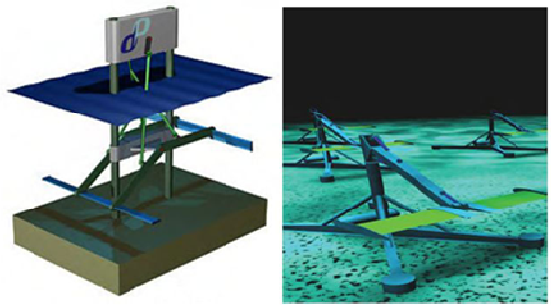

Figure 2-11: (left) Humber prototype design (Courtesy Pulse Generation); (right) Stingray device (Courtesy Engineering Business ltd)

2.5 Tidal stream current status

Tidal energy is an “embryonic technology”. Even though, several projects are undergoing, tidal current turbine industry is not yet established and commercial applications are rare. However, recent developments have led to the creation of the European Marine Energy Centre (EMEC) in Orkney, Scotland. This centre

offers to developers ideal marine conditions for the testing of full-scale grid-connected prototype devices.

2.6 Barriers to development

Several problems faced by the developers slow down the development of tidal current turbine technology. Challenges need to be undertaken to allow the technology to fully develop and reach maturation.

Installation of the devices is a major issue and present challenges to be taken up. The knowledge from other offshore industry has a certain role to play in the resolution of this problem. Due to the nature of the locations where the devices are supposed to be installed the devices must be designed for ease and speed of installation. Foundations and installation must be in a few minutes between tides. Mooring systems can be subject to biofouling and corrosion (threat to survivability of the system).

Easy access to the turbine is essential for maintenance. Ships are needed for routine maintenance and repair of tidal current devices. This makes operations hazardous and difficult. Measures to reduce the frequency and difficulty need to be thought at design stage. Several concepts have been proposed amongst them we can note the rising of the turbine above the water level (such as SeaGen). This allows maintenance from a platform or a ship. Replacement of large parts will be difficult requiring calm waters and good weather.

Electricity transmission is another problem. In some situations, it is necessary to transmit the power to shore over longer distances than usual. Hence, the use of higher voltage transmission is needed. High voltage generators are required. They will prevent the necessary installation of transformers at or below water level. Furthermore, tidal stream devices are often located in area where energy is important and as a result access to the grid is limited. Then, when deploying a device, important upgrade works on the grid network are necessary generating considerable extra costs.

The thrust involved for marine current turbines are much larger than the thrust for wind turbines. This is mainly due to the difference of density between air and water. In order to, resist these thrusts stronger or more materials to build a marine current turbine in comparison to a wind turbine. Again, this means more capital costs to add to the project. Furthermore, several severe problems can be instigated by the flow around the turbine. Blades vibrations can for instance lead to fatigue failure. Much effort needs to be made to realize good design studies and computer simulations before manufacturing and testing.

Although these new technologies face problems of fouling, tethering and power take-off, they present the potential for little visual impact as placed underwater and virtually operate with no noise.[7]

3 DELTASTREAM DEVICE

3.1 Presentation of the concept

Deltastream is a tidal current turbine device developed by Tidal Energy Ltd. Deltastream is a 1 to 2 MW unit which sits on the seabed without the need for an anchoring system. Electricity is generated from three horizontal axis turbines units mounted on a triangular frame. Each side of the triangular frame is 30 meters in length and the rotor diameter of each turbine is initially of 12 m. Each device can generate enough electricity to supply over 1.000 homes.

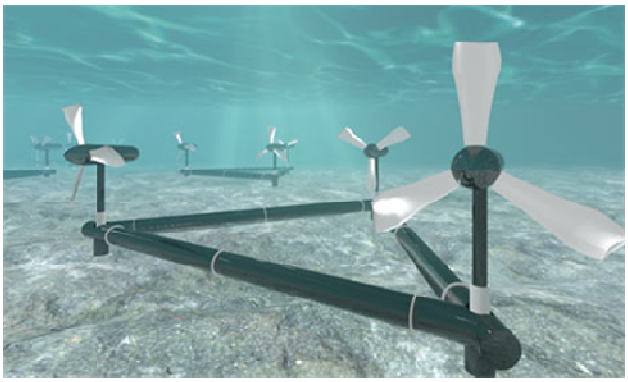

Figure 3-1: Artist view of the Deltastream concept (Courtesy Tidal Energy ltd)

Deltastream is supposed to be deployed for testing in deep water (at least 31.5 m) approximately 1.2km from St Justinian's, off the coast of Ramsey Sound, Pembrokeshire,in Wales.

Deltastream concept offers significant advantages with a high energy yield, ease of manufacture and deployment, and a minimal environmental footprint.

3.2 The installation process

A typical deployment begins with the manufactured part being delivered to a suitable quay. The components are assembled quickly over a matter of days. A floating crane lifts the device on board **(a)**. The crane makes it way to the development location where the mounting chain and grid connection have been

installed. At slack water the crane lowers the assembly **(b)**. Built-in valves systems on the triangular frame help the device to be lowered onto the seabed. Once the device has been installed, it is marked for future recovery **(c)**.

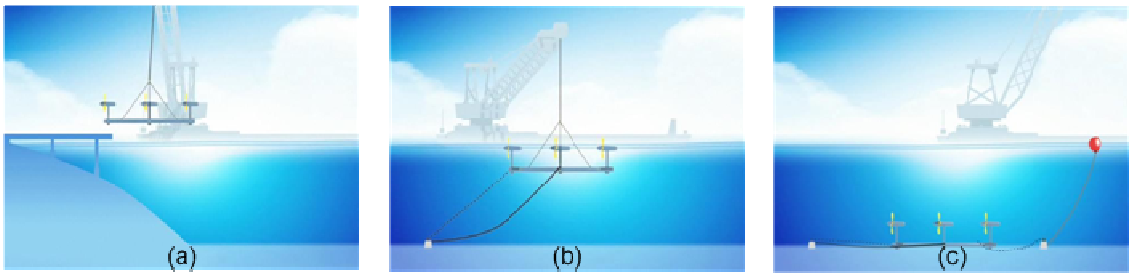

Figure 3-2: (a) Assembly is loaded onboard; (b) Assembly is lowered on the seabed using a crane; (c) device marked for future recovery (Courtesy Tidal Energy Ltd)

Deltastream farms can be quickly deployed and generate large amount of energy.

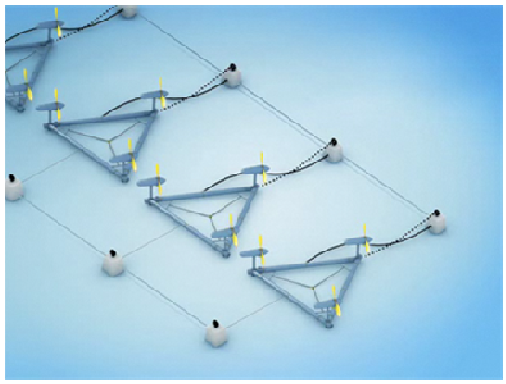

Figure 3-3: Artist view of a Deltastream farm (Courtesy Tidal Energy Ltd)

3.3 Recovery for maintenance

Recovery is straightforward. The unit is lifted from the seafloor. Nacelles can be quickly replaced and a unit can be redeployed with minimum downtime. Deltastream can be deployed at a range of depth including the deep sea where currents are strongest.

3.4 Rotating nacelles

The nacelles maximize the energy transfer, rotating to capture tidal movement in all directions; the slow speed of rotation has a low impact on sea life.

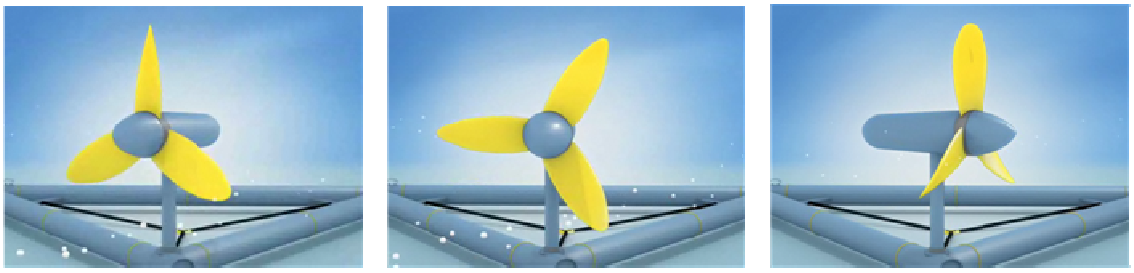

Figure 3-4: Deltastream is equiped with rotating nacelle (Courtesy Tidal Energy Ltd)

The rotation of the nacelle is also of major importance when currents are too strong. Above a certain current velocity, the nacelles adopt a security position. They orient themselves perpendicularly to the flow. This maneuver aims to protect the blades from structural damages due to heavier loads.

3.5 Deltastream's advantages

For now, Deltastream technology is still at a design stage. Even though the device has not yet been tested, the concept is interesting on several points. The key elements which make this technology promising are:

- Low cost and high speed of manufacture
- Delivery
- Installation
- Recovery
- Flexibility to be installed in a range of water depth

(Courtesy Tidal Energy Ltd)

4 OBJECTIVES AND SCOPE OF WORK

After giving a short overview of the current status of marine current turbines technologies and present the Deltastream device, the aim of this study is to evaluate the drag around a proposed shape for the Deltastream turbine's nacelles and to modify its design for minimum drag generation. The commercial CFD packages FLUENT from ANSYS Inc. is employed.

The physics behind the concept of hydrodynamic drag are introduced in the first part of this report as well as a description of the computational method used to carry out the study: computational fluid dynamics (CFD),

In the second part, a validation case of the CFD methodology is presented for the simple case of the flow around a cylinder. Two-dimensionsal numerical simulations are run for various cross-section and side-view nacelle's configurations. The objective of these computations is to evaluate the hydrodynamic characteristics of the original nacelle shape and assess the possibility in drag improvement offered by shape modifications.

Then, an improved three-dimensional model will be proposed based on the two-dimensional results.

5 PHYSICAL APPROACH

5.1 Basic of fluid dynamics

5.1.1 Notion of fluid flow

Fluid motion is an extremely complex phenomenon. When a fluid is at rest or in equilibrium, there is no presence of shear forces and then its study is made easy. However, when the fluid is in motion things are more difficult. Considering the case of a fluid flowing over a solid surface (e.g. a plate), the velocity of the fluid in contact with the plate has to be equal to the plate velocity. This induces the creation of a velocity gradient at right angles to the plate. Shear stresses arise from the change of velocity from layer to layer of fluid flow parallel to the plate. Individual particles of fluid then move. This motion occurs due to the action of forces induced by the differences in elevation or pressure. Inertia and the effects of the shear stresses exerted by the surrounding fluid control this motion.[13]

5.1.2 Properties of fluid flow

In a body of fluid, conditions can vary. These variations can be from point to point, or for any given point from one moment in time to the next. Conditions can be temporally and spatially variable.

When talking about a *uniform* flow, one refers to a particular flow for which the velocity remains constant in magnitude and direction at any point in the fluid. On the contrary, a non-uniform flow is a flow for which velocity varies from point to point.

Furthermore, a steady flow presents variables that can vary from point to point but do not change with time. Temporal variation is present in unsteady flows.

Then from what is said above we can consider four types of flow:

1. Steady uniform flow

2. Steady non-uniform flow
3. Unsteady uniform flow
4. Unsteady non-uniform flow

5.1.3 Shear stress in a moving fluid

Different materials respond to a same amount of applied stress in many different ways. Their behavior in response to the stress depends mainly on the nature of the concerned materials. A classic example to understand this is to imagine that four different materials are dropped on the floor. Each one of the item different in nature will have a completely different reaction to the stress applied. An eraser would simply bounce on the floor, meanwhile clay would stick to it and a cube of salt would break, and finally, a spoon of honey would spread out on the floor. These deformations can be qualified as elastic, plastic, fracture and viscous respectively.

Water is classified in the category of the viscous materials. It responds to an applied stress by flowing. The rate of deformation (the flow) depends upon the intensity of the stress. The equation below is a fundamental relationship which governs the shear stress (τ).

$$\tau = \mu \frac{du}{dz} \qquad \textbf{(5-1)}$$

In this expression, $\frac{du}{dz}$ is the velocity gradient and the coefficient of proportionality μ is called the dynamic viscosity. When a direct proportionality exists between the stress and the velocity gradient, the material is said to be Newtonian. Water is a typical Newtonian fluid. At the molecular level the kinematic viscosity ϑ represents the resistance to applied stress that occurs. It is the ratio between the dynamic viscosity and the mass density.[13; 14; 14]

5.1.4 Reynolds number and turbulence

The effects of three forces regulate the behavior of water in an open tidal channel. These are the inertial, the viscous and the gravitational forces. On one

hand, the viscous force has a stabilizing effect on the fluid behavior. On the other hand, the inertial force has a destabilizing effect. As a result, the fluid's behavior depends highly on the ratio existing between the inertial force and the viscous force.

Generally, the inertial force is function of the fluid density, from this principle and from Newton's first law, it can be stated that the greater the fluid density, the greater the force needed to apply a specific acceleration to a specified volume. These observations are due to British fluid dynamics engineer Osborne Reynolds.

In the nineteenth century, he carried out an experiment in which a reservoir supplied water into a long glass tube within which a streak of dye entered at one end. The rate of water flow was controlled by a valve. The observations of Reynolds revealed that if one increased the velocity, "the streak of dye in the water changed from a coherent and straight line into a complex series of vortices and lateral mixings" [9]. Laminar conditions are represented by the coherent flow where viscous forces are of greater importance than inertial force, flow is "stabilized". At higher velocities, the flow is more chaotic and turbulent conditions are represented. The flow is totally unstable and inertial forces dominate.

Next an expression of each force is given by dimensional analysis.

Newton's laws allow determining the inertial force. Actually, an inertial force exerted on a particle of fluid can be expressed in intensity as the product between the mass of the particle and its acceleration.

The mass of a particle can be obtained by multiplying its mass density to its volume. If we consider that a volume V is the cube of a unit of length characterizing the system, for example L, it is possible to write that:

$$m = \rho L^3 \tag{5-2}$$

The acceleration of the particle is by definition the rate at which its velocity varies with time. Given that, and the fact that we can express the time as the ratio between the characteristic unit of length L and the velocity U, we have:

$$a = \frac{U^2}{L} \tag{5-3}$$

Hence, inertial force can be expressed as:

$$inertial\ force = \ \rho L^2 U^2 \tag{5-4}$$

From the shear stress relation of proportionality, the expression of the viscous force can be deduced:

$$viscous\ force = \frac{\mu U}{L} L^2 = \mu UL \tag{5-5}$$

The gravity force on a particle of water is simply the particle weight expressed as follows:

$$gravity\ force = \ \rho L^3 g \tag{5-6}$$

Flows classification into laminar or turbulent states depending on Reynolds is essential.

The ratio of inertial forces to viscous forces determines whether the flow is laminar or turbulent, and is represented by the Reynolds number (Re). The Reynolds number is then the ratio between equations (5-4) and (5-5). Substituting $\upsilon = \mu/\rho$:

$$Re = \frac{UL}{\upsilon} \tag{5-7}$$

The Reynolds number is dimensionless. For small values of Re, viscous forces are dominant and flow is laminar, but, when Re increases, flow becomes turbulent.

5.2 Mechanism of water flow around an immersed body (Bernoulli's equation)

The hypotheses made to express the Bernoulli's theorem are the following:

- The fluid is inviscid (no viscosity) and incompressible (conservation of fluid volume)
- The flow is laminar and steady

The gross flow over a body immerged in an incompressible fluid is governed by the relationship between velocity and pressure expressed in the Bernoulli's equation.

$$P + \frac{1}{2}\rho v^2 + \rho g z = constant \quad \textbf{(5-8)}$$

The significance of this equation is that it shows how the pressure in a moving fluid decreases as the flow accelerates. In the frame of tidal power devices, it controls flow through ducted devices. However, this equation is very useful to describe the mechanics of a water flow around an immersed body.

The Bernoulli principle can also be expressed as follows:

$$P_{static} + P_{dynamic} = P_{total} \quad \textbf{(5-9)}$$

Or

$$P_{static} + \frac{1}{2}\rho v^2 = P_{total} \quad \textbf{(5-10)}$$

If we consider the case of an immersed body, that means that the static plus the dynamic pressure of the water flow will be constant (P_{total}) as it approaches the body. Considering that the body is stationary and the water flows around it, the water streams along lines, better known as "streamlines". A stream tube is formed by a bundle of streamlines.

At a distance from the body the static pressure is the ambient pressure. The dynamic pressure is due to the relative velocity (constant for all streamlines approaching the body). Hence, the total pressure (P_{total}) is the same for all streamlines and:

$$P_{total} = P_{static} + \frac{1}{2}\rho v^2 \quad \textbf{(5-11)}$$

As the flow approaches the body, the stream tubes split, some of them go above the body and the others go below it. However, one streamline must go straight to the body and stagnate. At that point, known as the stagnation point, the relative velocity has gone to zero, and the static pressure (P_{static}) observed there on the body is the total pressure (P_{total}).

Concerning the streamlines that flow above the body, one may notice that they turn in the upward direction when close to the body. However, at a distance well above the immersed body the streamlines remain straight, and the static pressure in that region must be the same as the ambient. In order for the water stream to be curved upward, the static pressure needs to be higher than ambient to provide the force necessary to turn the water flow. If the static pressure is higher, then the velocity must decrease in this region in order to obey Bernoulli's equation.

On the other hand, has the flow turns to follow the shape of the body (downward curvature at the back of the body) the pressure must go below ambient in order to bend the flow, and as a result the velocity must increase.

Thus Bernoulli's equation shows how the pressure and the velocity must vary in the gross water flow over an immersed body. Supposing an absence of friction the water would simply flow up over the front and down the back of the body, exchanging pressure for velocity as it did at the front. In this particular configuration, the pressure forces on the back of the body would exactly balance those on the front, and there would be no drag produced.

From experience, however, we know that drag is produced. The drag is due in part to friction of the water on the surface of the body, and in part to the way the friction alters the main flow down the back of the body. Its explanation comes about from understanding the action of boundary layers in the flow over an object.

As a result of the water interacting with the vehicle, forces and moments are imposed. These may be defined systematically as the three forces and three moments shown in figure 1, acting about the principal axes of the body.

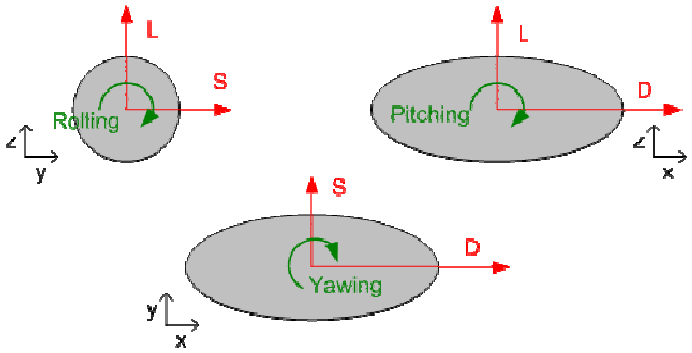

Figure 5-1: Forces and moments on an immersed body

DIRECTION	FORCE	MOMENT
Longitudinal (x-axis, positive rearward)	Drag	Rolling moment
Lateral (y-axis, positive to the right)	Side force	Pitching moment
Vertical (z-axis, positive upward)	Lift	Yawing moment

Figure 5-2: Forces and moments on an immersed body

5.3 Boundary layer theory

When a fluid and a surface are in relative motion equivalence between their velocities exist. This condition is the so-called “no-slip” condition. Far from the surface, the velocity of the fluid quickly increases. The zone where these observations are made is known as the boundary layer. Boundary layer has an

essential role to play in fluid dynamics problems, and particularly when calculating surface drag and viscous forces.

5.3.1 Qualitative description of the boundary layer

A good example we can employ to describe the boundary layer is to consider a flat plate immersed in a moving fluid. The velocity of the fluid when this one is in contact with the plate is zero. This is due to the “no slip” condition previously mentioned. Furthermore, it appears a velocity gradient between the fluid in the free stream (far from the body) and the solid surface. Shear stress τ is defined as:

$$\tau = \mu \frac{\partial u}{\partial y} \qquad \textbf{(5-12)}$$

In this expression, μ is the fluid viscosity and $\frac{\partial u}{\partial y}$ the velocity gradient.

A shear force opposite to the fluid motion is induced by this shear stress acting at the solid surface. Moving along the plate, this force increases due to the increasing of the plate surface affected. Hence, more fluid is retained and the concerned fluid layer goes thicker.

The Reynolds number is based upon the distance from the upstream edge of the plate. At first, the value of the Reynolds is low, and then the flow close to the plate is identified as laminar. As the fluid moves along the plate, the value of the Reynolds increases until a point is reached when the flow changes from laminar to turbulent. In practice, this transition does not occur at a well defined point but in a zone.

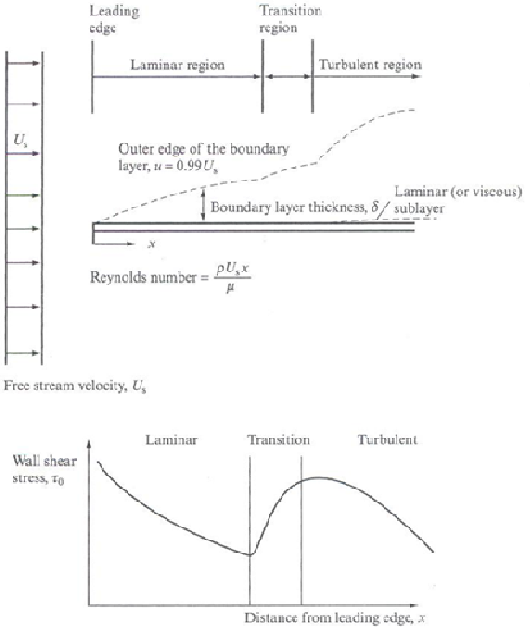

Figure 5-3: Development of the boundary layer along a flat plate

At the edge upstream, there is a large velocity gradient and in consequence a high shear stress. But as we progress along the plate, velocity gradient and shear stress diminish with thickening of the boundary layer. After transition occurs, again the velocity gradient increases together with the shear stress. The thickness of the boundary layer is usually referenced as δ.

Certain factors affect the transition from laminar to turbulent flow regimes. In general, transition occurs for a Reynolds number close to 5×10^5. However, this value is simply an indication and can vary depending on several factors.

For instance, roughness of the solid surface can considerably decrease this value. Furthermore, a pressure gradient dp/dx may have a major influence. In general, if the pressure gradient is positive the transition Reynolds number is reduced; but a negative value of the gradient often means an increase in the Reynolds transition number. Typical velocity profiles through the boundary layer for both flow regimes are presented in the figure below.

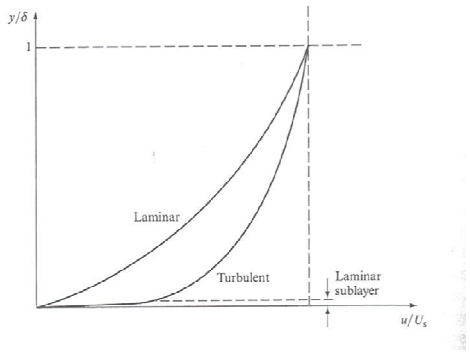

Figure 5-4: Velocity profiles in laminar and turbulent boundary layer regions

The most important study is the one of the turbulent boundary layer. In most engineering problems, the considered flow presents a Reynolds number high enough to ensure transition and that a turbulent boundary layer settles. However, to respect the “no slip” condition, it is essential that the motion of the fluid particles in the near wall region (random and chaotic) disappears. To achieve this, it has been established the existence of a laminar sub layer in the turbulent region. The thickness of this sub layer is small compared with the boundary layer thickness.

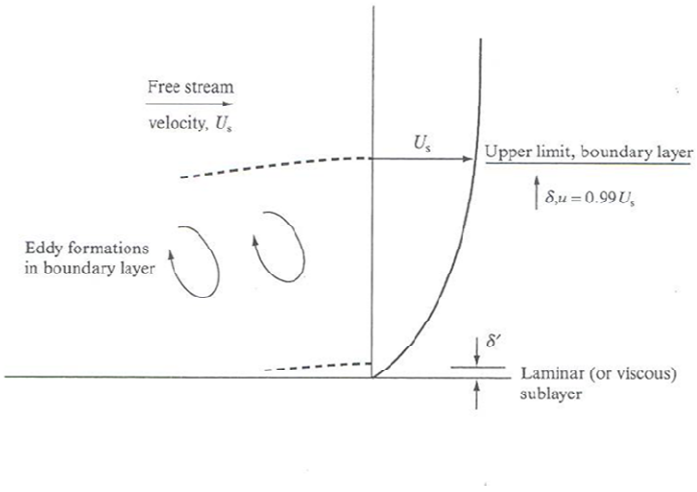

Figure 5-5: Formation of eddy in the boundary layer

This sub layer is linear and tangential to the velocity profile up through the turbulent boundary layer.

In the region very close to the wall the velocity gradient is governed by the fluid velocity. This gradient can be expressed as:

$$\frac{du}{dy} = \frac{\tau_0}{\mu} \tag{5-13}$$

with τ_0 being the shear stress on the wall. After integration of this expression, we obtain:

$$u = \left(\frac{\tau_0}{\mu}\right) y \tag{5-14}$$

And,

$$\frac{u}{\sqrt{\left(\frac{\tau_0}{\rho}\right)}} = \frac{\sqrt{\left(\frac{\tau_0}{\rho}\right)}}{\vartheta} y \tag{5-15}$$

In the equation above ϑ is the fluid kinematic viscosity(μ/ρ). The shear stress velocity is the term $\sqrt{\left(\frac{\tau_0}{\rho}\right)}$. In general it is quoted u^*. Hence,

$$\frac{u}{u^*} = \frac{y}{\vartheta/u^*} \tag{5-16}$$

Laminar sub layer occurs in flows for which the above expression has a value close to 5. The thickness of the laminar sub layer (quoted δ') is then:

$$\delta' = 5\vartheta/u^* \tag{5-17}$$

This shows that for large shear stress flows (u^* large) the sublayer will present a small thickness; and, on the contrary this thickness will grow in the downstream direction while shear stress decreases in this direction.

On top of the laminar sub layer, the flow is turbulent and the equation (first in this section) cannot represent anymore the shear forces in action.

Eddy formations occur in the boundary layer. These eddies move small masses of water up and down through the boundary layer, perpendicularly to the mean stream direction. Because of these eddies, fluid from the higher part of the boundary layer (“high-velocity area”) is dragged down into the lower part of the boundary layer (“slower motion area”). The consequence of this phenomenon is to increase the velocity on the outer part of the laminar sub layer. Slow moving particles of fluid are lifted into the upper levels of the boundary layer. That has the effect of slowing down the main flow velocity and makes the boundary layer thicker. This process is a momentum transfer phenomenon.

To explain this process, the introduction of a new viscosity term is needed. The eddy viscosity ε is injected in the equation seen earlier and the shear stress is expressed as:

$$\tau = (\varepsilon + \mu)\frac{du}{dy} \qquad \textbf{(5-18)}$$

In the turbulent region the fluid velocity can consist in a mean value $\bar{u}$ and deviating components u' and v' (in the main stream direction and normal to it). When this is the case, assumptions may be done that the apparent shear stress needed to duplicate the eddy effects is:

$$\tau = -\rho\bar{u}'\bar{v}' \qquad \textbf{(5-19)}$$

This expression shows that the shear stress in opposition to the fluid motion equals the product of fluid density and the average product of the velocity deviations over a period of time.[2; 13; 15-17]

5.3.2 Prandtl mixing length theory

Prandtl was the first to lay down the basics of boundary layer theory in 1904. He proposed that all viscous effects in fluid flow problems were concentrated within the boundary layer. He developed relations between the apparent shear stress and the mean velocity distribution through the boundary layer in the frame of its mixing length theory.[15; 16]

The mixing length is the distance in which a fluid particle loses its excess of momentum, it is generally quoted l. In practice, the loss of momentum is recognized to be gradual over the mixing length. Considering velocity deviations u' and v' to be equal, it is possible to have:

$$v' = u' = l\frac{du}{dy}, \tag{5-20}$$

And also if we introduce this result in expression (see above):

$$\tau = \rho l^2 \left(\frac{du}{dy}\right)^2 \tag{5-21}$$

Assumption was made by Prandtl that close to the wall l was dependent on the distance from the wall, $l = ky$. In other terms, when $y = 0$ then $l = 0$. From this assumption, we have:

$$\tau = \rho k^2 y^2 \left(\frac{du}{dy}\right)^2 \tag{5-22}$$

In this expression k is a universal constant (around 0.4).

Near to the wall surface the shear stress equals the surface value:

$$\tau_0 = \rho k^2 y^2 \left(\frac{du}{dy}\right)^2 \tag{5-23}$$

Or,

$$du = \frac{\sqrt{(\tau_0/\rho)}}{k}\frac{dy}{y} \tag{5-24}$$

Integration of this expression yields:

$$\frac{u}{u^*} = \left(\frac{1}{k}\right) log_e y + C \tag{5-25}$$

C is integration constant. Experiments determined the form of C as:

$$C = 5.56 - \left(\frac{1}{k}\right) log_e \left(\frac{\vartheta}{u^*}\right) \quad \textbf{(5-26)}$$

Hence, the velocity distribution is such that:

$$\frac{u}{u^*} = \left(\frac{1}{k}\right) log_e \left[y\left(\frac{u^*}{\vartheta}\right)\right] + 5.56 \quad \textbf{(5-27)}$$

As we saw earlier $k = 0.4$. Then,

$$\frac{u}{u^*} = 5.75\ log_{10} \left[y\left(\frac{u^*}{\vartheta}\right)\right] + 5.56 \quad \textbf{(5-28)}$$

This expression applies for $30 < \frac{yu^*}{\vartheta} < 500$. When comparing expression (5-28) with expression (5-16) we notice an obvious change in the velocity profile between the turbulent region of the boundary layer and the laminar sub layer. Even though these profiles are very different in shape they are linked together through the term $\frac{yu^*}{\vartheta}$ usually quoted as y^+ and which is a dimensionless wall distance variable.

Above $y^+ = 500$, a velocity defect law gives a more appropriate description of the velocity profile. This law takes the form:

$$\frac{(U_s - u)}{u^*} = f\left(\frac{y}{\delta}\right) \quad \textbf{(5-29)}$$

In conclusion, there are three zones for the application of velocity distribution equations. These regions are not sharply separated but can merge into each other.

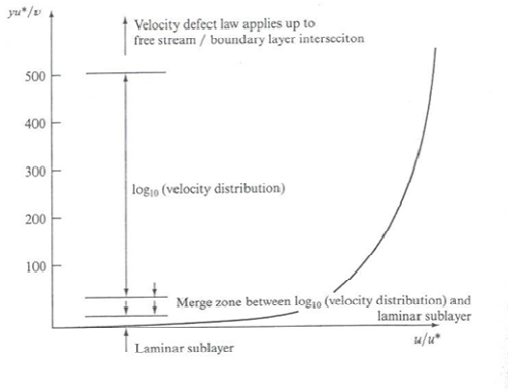

Figure 5-6: Overlap of velocity distributions

5.3.3 Effects of pressure gradients on boundary layer developments

Generally, an immersed body presents a pressure gradient on its surface when placed in a fluid stream.

From what was presented above, it was understood that a laminar boundary layer starts on the leading edge of a body immersed in a flow. If the surface length is sufficiently important the boundary layer will tend to grow and become turbulent. Transition happens when the value of the flow's Reynolds number reaches a critical value downstream. When a sufficiently large pressure gradient exists, separation of the boundary layer occurs.

Then, $\tau_0 = 0$ at the separation point that also means that the velocity gradient $\frac{du}{dy} = 0$.

The flow is reversed along the surface of the body. This reversal of the flow feeds the vortices in the wake (region behind the body). The separation can be delayed by increased turbulence which tends to move the separation point downstream on the body surface. A way to avoid separation to occur is to streamline the body. Appropriate streamlining will delay separation and even prevent it entirely in some cases.

When a pressure gradient $\frac{\partial p}{\partial x}$ exists the flow velocity changes across the surface. In other terms, a $\frac{\partial u}{\partial x}$ term is present. The velocity along a curved surface changes as shown in the figure below.

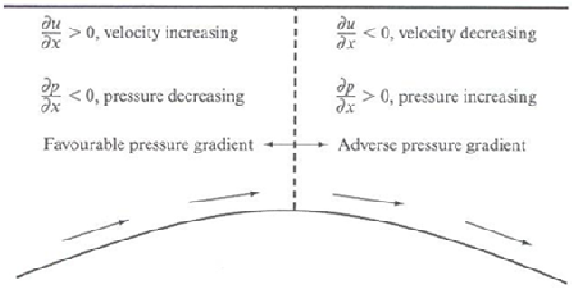

Figure 5-7: Pressure and velocity variation over a curved surface

As we can see when the pressure gradient decreases in the downstream direction, the fluid flow velocity increases and the boundary layer thickness decreases. Then, the pressure gradient is considered to be a favorable pressure gradient.

On the other hand, if pressure increases in the downstream direction, the boundary layer tends to grow thicker and logically the velocity decreases. Then, we talk about an adverse pressure gradient.

It is the action of this adverse pressure gradient combined with the action of the shear forces described in the boundary layer that bring the boundary layer to rest and lead to separation if they can act on a sufficient length on the body surface.

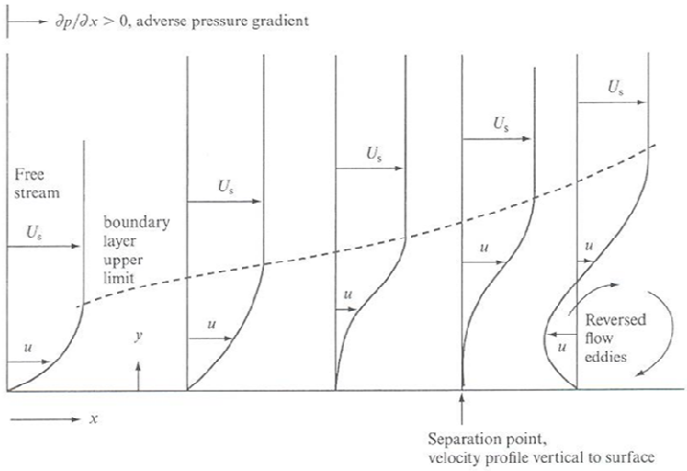

Figure 5-8: Illustration of the effect of an adverse pressure gradient on boundary layer development

5.4 Hydrodynamic drag and drag coefficient

The previous section has introduced the concept of boundary layer. Then, it is now possible to consider the external flows of real fluids, in other words take into account the effects of viscosity. From the potential flow and the boundary layer theories we can consider that an external flow problem consist in two different regimes. Very close to the body's surface, viscous effects are dominant and frictional forces are generated. Outside the boundary layer, viscous effects are neglected but the physical presence of the body has an influence on the velocities and pressures. In this outside part of the flow, ideal flows theory may be used.

Furthermore, a stagnation point exists at the front of the body and a wake is established behind the body. This particular flow region starts from point S (on the figure…). This point S is where boundary layer separation occurs. The wake is further described in the following.

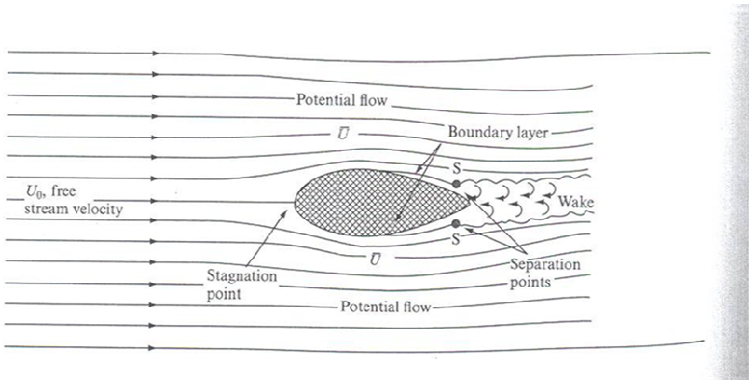

Figure 5-9: Flow regions around an immersed body

As seen earlier, adverse pressure gradients cause separation of the boundary layer to occur. This fact combined to viscous forces on the body surface lead to a reversal of the flow. Hence, the stream detaches itself from the surface. The flow reversal generates a vortex.

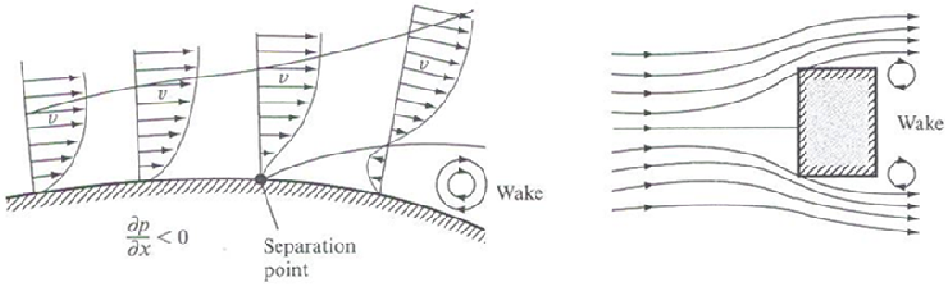

Figure 5-10: Vortex formation in a wake

The wake is then a region of high-turbulence and principally consist of large-scale eddies. It is the nest of important energy dissipation which causes pressure to decrease in the wake. In consequence, the pressure on the front of the body is more important than the one on the rear of the body. As a result, resultant force acting on the body in the direction of the flow appears. This force is due to the pressure difference and is generally known as the *pressure drag*. However, the non-uniformity of the pressure distribution on the body is not the only source of drag. Frictional drag can also apply on the whole surface of an immersed body. This frictional drag is defined the force on the body that acts in the direction of the flow and which is due to fluid shear stress at the surface.

The total drag force (or profile drag) on the body is then the result of two contributions:

$$Profile\ Drag = Pressure\ drag + Friction\ drag$$

The shape of the body and its orientation in the flow dictate the respective contributions of pressure drag and frictional drag.

A mathematical formulation of the two types of drag can be given as the following will demonstrate it.

$p_s$is defined as the fluid pressure which acts on d_s a surface element. The action of p_s is normal to the surface and the pressure force on this part of the body is $p_s d_s$. This force can be also expressed using two components normal and parallel to the direction of the flow. The parallel component is identified as the drag.

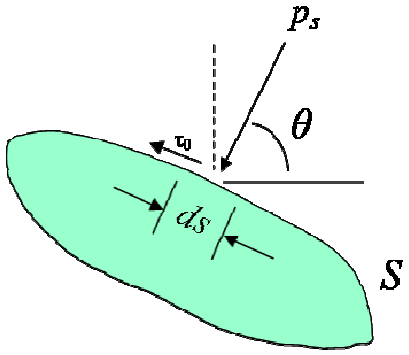

Figure 5-11: Mathematical formulation of the 2 types of drag

The drag is then $p_s \cos\theta d_s$. The pressure drag can be found by integrating the drag component around the total contour of the body. Pressure drag is then,

$$D_p = \oint p_s \cos\theta d_s \qquad \textbf{(5-30)}$$

As the pressure force on the body is defined by $p_s d_s$, the friction force on the body due to a shear stress at the surface S can be expressed as $\tau_0 d_s$. This is a tangential force. Its component in direction of the flow is $\tau_0 \sin\theta d_s$.

The same operation of integration around the body allows obtaining the friction drag:

$$D_f = \oint \tau_0 \sin\theta d_s \qquad \textbf{(5-31)}$$

Hence, it is possible to calculate each contribution to the total drag. However, the pressure distribution around the body is required as well as the shear distribution on the surface. The determination of these parameters is very complicated and to simply the task it is preferred to measure the profile drag by experiments (force component in a wind tunnel).

A general formulation of the profile drag is proportional to the projected area of the body on a plane perpendicular to the relative motion, the density of the fluid, and finally the velocity of the fluid free stream U_0. The profile drag D is given by the expression below:

$$D = \frac{1}{2} C_D \rho U_0^2 A \qquad \textbf{(5-32)}$$

In this formulation, C_D is known as the drag coefficient. It is a dimensionless parameter. The lower the drag coefficient is, the more the body presents an aerodynamic or hydrodynamic profile.

Drag coefficient

A dimensional analysis on the drag coefficient leads to the following result (Douglas and al., 2009). The drag coefficient cannot be considered to be a numerical constant. Actually, it is a proportionality coefficient with a numerical value dependent on a series of dimensionless groups.

$$C_D = f(Re, Fr, We, Ma) \qquad \textbf{(5-33)}$$

In expression (5-33), Re stands for Reynolds number, Fr for Froude number, We for Weber number and Ma for Mach number. The relative importance of each of these groups in the value of the drag coefficient depends entirely on the significance of the kind of forces represented by them. For instance, when

viscous effects are considerable Re will predominate. Or, when the presence of gravity waves is significant Fr will predominate.

However, even if the drag coefficient values depend on Re number and other parameters, the first important they depend on is the shape of the considered body and its position in the flow.[14; 18]

5.5 Flow past a cylinder

The variations in the flow pattern around an immersed body and the changes in drag coefficient values (with variation of Reynolds) are illustrated using the example of a thin cylinder of infinite length that has been positioned in a fluid flow. In that case, the Reynolds is directly proportional to the fluid velocity. As a result the variations observed depending on the values taken by the Reynolds number are logically dependent on the velocity. We place ourselves in a two-dimensional case.

For very small Reynolds values ($Re < 0.5$), the flow pattern is identical to what is observed in the case of an ideal flow. At such small Reynolds numbers, the inertia effects are insignificant. The pressure recovery is almost total. As a result, pressure drag is almost zero and the skin friction is the only important contribution to profile drag.

When the Reynolds increases ($2 < Re < 30$), separation of the boundary layer is observed as well as the formation of eddies. The boundary layer separation is located at the points referenced S on the figure... below. There are two eddies symmetric to each other and which rotate in opposite motions. Their position behind the cylinder does not change and closure of the main stream behind them is observed.

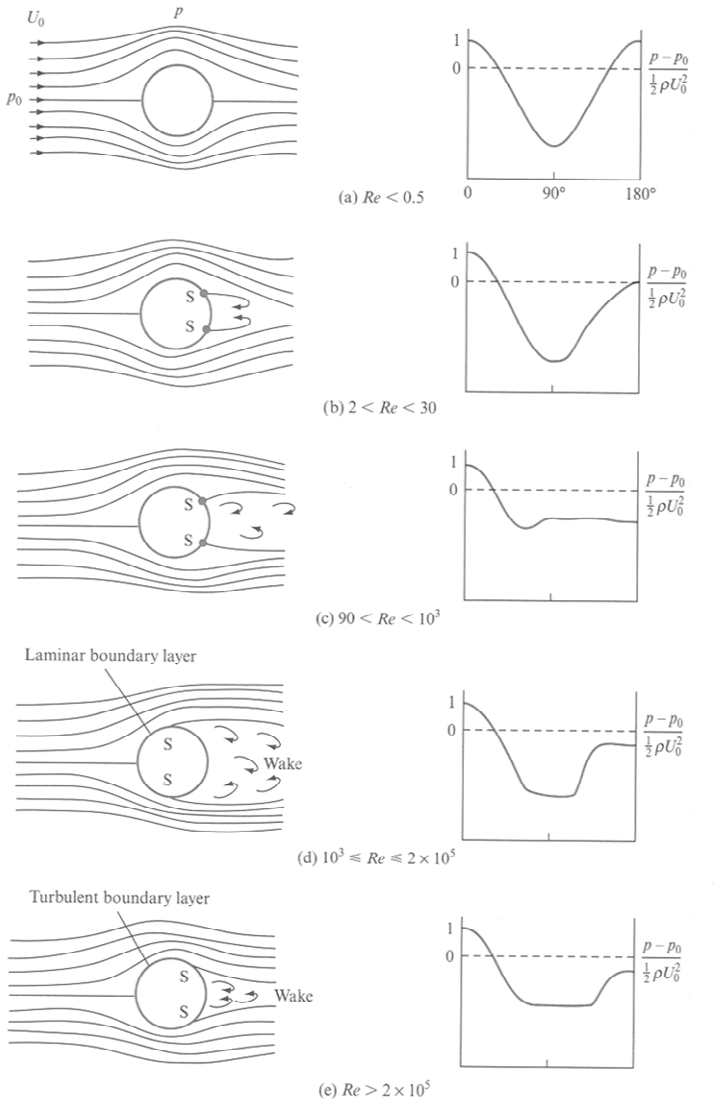

Figure 5-12: Flow past a cylinder

If the Reynolds number increases even more, eddies tend to elongate and start to operate oscillations until $Re = 90$. Eddies break away from the cylinder in an alternate manner first from one side of the cylinder and then from the other side repeatedly, it is like eddies being washed away from the rear of the cylinder by the flow. This break away depends on the turbulence level of the free stream. The intensity of this process increases with higher values of Reynolds number. The shedding of eddies from alternate sides of the cylinder becomes continuous. Two distinct rows of vortices are then created in the wake. This is a so-called *vortex street* or von Kármán vortex street. In that configuration, the contribution of pressure drag to profile drag is about 75%.

At even higher values of Reynolds, these vortices tend to vanish due to important rates of shear. Instead, a highly turbulent wake takes place. That considerably increases the value of the drag coefficient. At this level, profile drag is nearly entirely due to pressure drag.

Until the Reynolds number reaches a value of 2×10^5, the boundary layer on the cylinder surface remains laminar. The boundary layer changes to turbulent at around this value of Reynolds. This phenomenon causes the separation to happen further back at the rear of the cylinder, and this lead to a sudden drop in the value of the drag coefficient.

When the Reynolds number exceeds 10^7 the value of the drag coefficient seems to be independent of the Reynolds. However, not enough experimental data are available for such high Reynolds values.[13; 14]

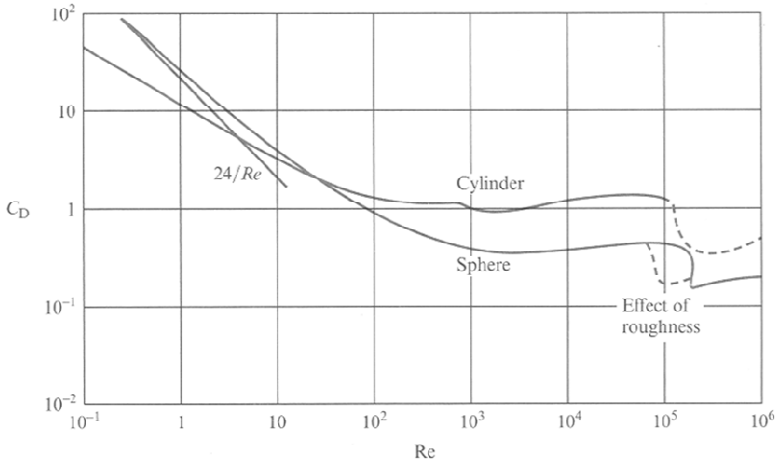

Figure 5-13: Drag coefficient for a cylinder and a sphere

6 COMPUTATIONAL FLUID DYNAMICS

The aim of this section is to present *Computational Fluid Dynamics* better known as CFD. CFD is a set of computational methods used to numerically simulate fluid flows and is part of the world of *Computer-Assisted Engineering*.

6.1 The role of CFD in the development of an engineering project

The life cycle of an engineering product or system can be divided into three main stages.

First of all, the specifications and geometrical definitions of the product must be covered by a definition phase.

Then, engineering teams operate calculations and experiments to assess the physical behavior of the product or system. For instance, when dealing with an aircraft engineers may be interested in predicting the behavior of air flows around various structural components such as the wings, or rotating blades.

When this simulation and analysis phase is completed and gives satisfactory results, the manufacturing cycle can be launched. This stage mainly consists in the simulation of fabrication processes and verifications that what was specified during the two previous stages can be tolerably and realistically manufactured.

Nowadays with the development of computers any engineering project development is supported by the use of numerical methodologies. Engineers tend to computerize the whole production cycle right from the start at the definition stage. The product is not anymore designed on drawing boards but can be conceived, visualized and infinitely modified directly on a computer monitor. The experimental investigations on the physics of a system usually carried out on prototypes or material models are too expensive and time-consuming. Hence, they have been gradually replaced by the use of cheaper and equally efficient numerical methods. Computers allow engineers to create a

virtual environment where they can visualize the whole product with tremendous realism and assess its physical behavior before any part of it materially exists.

Each stage of this virtual prototyping is supported by specific software tools. Three families of software systems are currently the most important on the market. These can be listed as CAD (*Computer-Assisted Design*), CAE (*Computer-Assisted Engineering*), and CAM (*Computer-Assisted Manufacturing*).

In order to support the definition phase, engineers use CAD software such as *CATIA* or *AutoCAD* to "model" a system. The geometry of the system can be comprehensively defined and created using CAD.

The model obtained is then transmitted to CAE software tools that support the simulation and analysis phase and are used to predict the physical behavior of the system. Depending upon the physical effects that are to be simulated, the engineers can rely on various branches of CAE such as:

- CSM (*Computational Solid Mechanics*) designed to study all forms of mechanical and thermal effects applied to the model (*deformations, vibrations, heat conduction, thermal stresses, etc*.).
- CFD (Computational Fluid Dynamics) designed to analyze fluid flows and main focus of this study.
- Other areas such as acoustics and electromagnetics benefit from CAE with software tools like CAA (*Computational Aero-Acoustics*) or CEM (*Computational Electromagnetics*).
- CAM software support the manufacturing cycle phase. Many processes are simulated on computers including Stamping, Molding or Welding.

Hence, with the exponential growth of computer performances in terms of speed and memory, virtual prototyping has become the privileged alternative to binding material experimental investigations for industrial manufacturers.

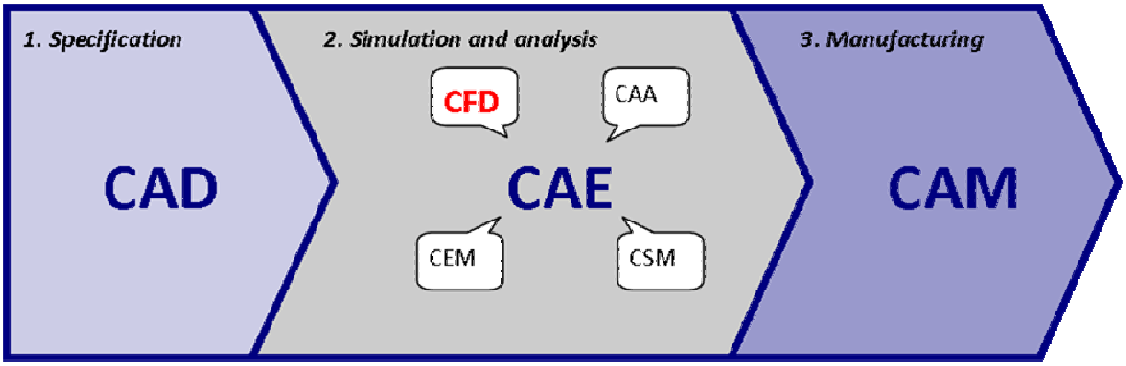

Figure 6-1: Virtual prototyping

CFD is part of this revolution and allowed various fields of the industry to achieve tremendous progress since its appearance in the 1970's. Amongst those fields of engineering which benefited and still benefit the most from CFD we can quote aeronautics, turbo-machinery and automotive. However, CFD tends to be more and more present in any engineering sector dealing with fluids and is not anymore exclusive to these branches of engineering. Chemical, bio-medical, sport, civil and environmental engineering are other examples of engineering domains where CFD is wisely applied.[19]

After the presentation of the role undertaken by CFD in the production cycle of an engineering system, the following will go further in details in the presentation of CFD and its underlying physical principles.

6.2 Presentation of CFD

CFD found its origins in three fields that are Engineering (especially fluid dynamics), Computer Science and Mathematics. For a long time it was used mainly in high-technologies research and development scheme in aeronautics and astronautics and CFD users tend to create their own CFD programs writing computer codes to solve their problems. Nowadays, with the evolution in computer power and costs, CFD has become a very common alternative tool used by engineers at the early design stages of a project. Furthermore, several commercial CFD software packages are now available to CFD users. Skills in programming are no longer essential to realise a CFD study.

The aim of a CFD analysis is to predict the behaviour of a given fluid for a particular fluid flow problem. The CFD study provides the user with data concerning the fluid properties at any given point in space and time. The CFD simulation is based on the numerical resolution of the equations governing the fluid flow problem. In fluid dynamics, governing equations are often found in the form of non-linear partial differential equations. These equations are mathematical expressions of the physical phenomenon happening in reality. It is very complex and sometimes even impossible to come up with the exact solution to these equations. The goal of CFD is to translate these mathematical expressions into simplified expressions that can be dealt with by a computer. Then iterative methods are employed to find approximated solutions to the mathematical expressions. The results provided by CFD analysis are then approximations that tend to be as close as possible of an exact solution. [19; 20]

6.3 Advantages of CFD

The interest in CFD of different areas of engineering can be easily explained by the fact that this methodology presents several advantages.

First of all, CFD completes the traditional experimental and analytical approaches in dealing with fluid flow problems. It provides an alternative way of simulating real fluid flows. When compared to experimental-based approaches, CFD offers the possibility to engineers to considerably reduce the time and cost in designing the product. Moreover, CFD makes the resolution of a range of complex flow problems possible where analytical approaches are often facing limitations.

The recent evolutions in computer power performance alongside the decreasing prices of computer hardware have favoured the role of CFD as the perfect complement to experiments and analysis of flow problems.

Second, CFD uses a virtual environment to simulate fluids behaviour. It is then possible to simulate flow conditions that would be impossible to recreate in

experiments otherwise. That is the case for large scale scenarios such as a tsunami or a nuclear accident for example.

Third advantage of CFD is its ability to provide engineers with more detailed, visualised and comprehensive information in comparison with analytical and experimental fluid dynamics.

The fundamentals of CFD lies on the in depth study of the governing equations of a fluid motion. The CFD methodology leads to numerical solutions of the governing equations and allows the study of various approximations to these equations. This makes it possible to focus on specific terms corresponding to characteristic processes (convection, diffusion…).

Finally, another big advantage of CFD is the possibility for engineers to evaluate different alternative designs at early development stages for a range of dimensionless parameters predominant in fluid dynamics (Reynolds number, Mach number…). CFD reduces the need for expensive experimental set-ups and prototype developments. It contributes to lead engineers towards an optimal design of their product quicker and at lesser cost. However the time when CFD will replace experiments has not come yet but is surely a viable alternative to experimental testing.[20]

6.4 The governing equations of CFD

Conservation laws in physics state that a measurable quantity characteristic of a physical system remains constant when the system evolves. In other terms, there is no creation or destruction of this quantity. Conservation laws form the bases of any CFD analysis.

The physical phenomena of fluid motion can be entirely described studying the conservation of the following quantities:

- Mass
- Momentum
- Energy

These conservation laws can be mathematically expressed under the form of non-linear partial differential equations. The developments that lead to these expressions can be found in the literature [2,13,14,17,20].

In the case of an unsteady compressible viscous flow and in three dimensions, the governing equations are the following.

6.4.1 Continuity equation (mass conservation)

The continuity equation mathematically expresses the conservation of fluid mass.

$$\frac{\partial \rho}{\partial t} + \nabla \cdot (\rho U) = 0 \qquad \textbf{(6-1)}$$

6.4.2 Momentum equation

The momentum equation mathematically translates the fact that the rate of change of momentum is equal to the sum of the forces acting on a fluid particle.

x-component:

$$\frac{\partial (\rho u)}{\partial t} + \nabla \cdot (\rho u U) = -\frac{\partial p}{\partial x} + \frac{\partial \tau_{xx}}{\partial x} + \frac{\partial \tau_{yx}}{\partial y} + \frac{\partial \tau_{zx}}{\partial z} + \rho f_x \qquad \textbf{(6-2)}$$

y-component:

$$\frac{\partial (\rho v)}{\partial t} + \nabla \cdot (\rho v U) = -\frac{\partial p}{\partial y} + \frac{\partial \tau_{xy}}{\partial x} + \frac{\partial \tau_{yy}}{\partial y} + \frac{\partial \tau_{zy}}{\partial z} + \rho f_y \qquad \textbf{(6-3)}$$

z-component:

$$\frac{\partial (\rho w)}{\partial t} + \nabla \cdot (\rho w U) = -\frac{\partial p}{\partial z} + \frac{\partial \tau_{xz}}{\partial x} + \frac{\partial \tau_{yz}}{\partial y} + \frac{\partial \tau_{zz}}{\partial z} + \rho f_z \qquad \textbf{(6-4)}$$

6.4.3 Energy equation

The equation for the conservation of energy comes from the first principle of thermodynamics that states that the rate of change of energy is equal to the sum of the net rate of heat added and the net rate of work done.

$$\frac{\partial}{\partial t}\left(\rho\left(e+\frac{U^2}{2}\right)\right)+\nabla\cdot\left(\rho U\left(e+\frac{U^2}{2}\right)\right)$$
$$=\rho\dot{q}+\frac{\partial}{\partial x}\left(k\frac{\partial T}{\partial x}\right)+\frac{\partial}{\partial y}\left(k\frac{\partial T}{\partial y}\right)+\frac{\partial}{\partial z}\left(k\frac{\partial T}{\partial z}\right)-\frac{\partial(up)}{\partial x}-\frac{\partial(vp)}{\partial y}$$
$$-\frac{\partial(wp)}{\partial z}+\frac{\partial(u\tau_{xx})}{\partial x}+\frac{\partial\left(u\tau_{yx}\right)}{\partial y}+\frac{\partial(u\tau_{zx})}{\partial z}+\frac{\partial\left(u\tau_{xy}\right)}{\partial x} \quad \textbf{(6-5)}$$
$$+\frac{\partial\left(u\tau_{yy}\right)}{\partial y}+\frac{\partial\left(u\tau_{zy}\right)}{\partial z}+\frac{\partial(u\tau_{xz})}{\partial x}+\frac{\partial\left(u\tau_{yz}\right)}{\partial y}+\frac{\partial(u\tau_{zz})}{\partial z}+\rho fU$$

In all expressions above, ρ represents the fluid density, U the fluid velocity with components (u,v,w), p the pressure, T the temperature, e the internal energy per unit mass, $f=\left(f_x,f_y,f_z\right)$ a body force, k the thermal conductivity, $\dot{q}$ the rate of volumetric addition per unit mass and τ_{nn} the viscous stresses.

Put together, these equations form a system of five transport equations most commonly known as the Navier-Stokes equations and are known since the 1850's. [19-21]

6.4.4 Turbulence

All flows are turbulent in nature. Engineers have to deal with turbulence in any fluid related engineering problem. It is possible to use models in CFD to deal with turbulent flow problems.

6.5 CFD methodology

The aim of a CFD simulation is to virtually visualize a whole engineering system with realism and to assess its physical behaviour before any part of the system

ever exists. All CFD jobs consist in successive operations leading in the end to a numerical solution to a physical fluid flow problem.

The structure of a CFD analysis is always formed by three major elements:

- Pre-processor
- Solver
- Post-processor

These elements are interconnected as demonstrated in the figure below.

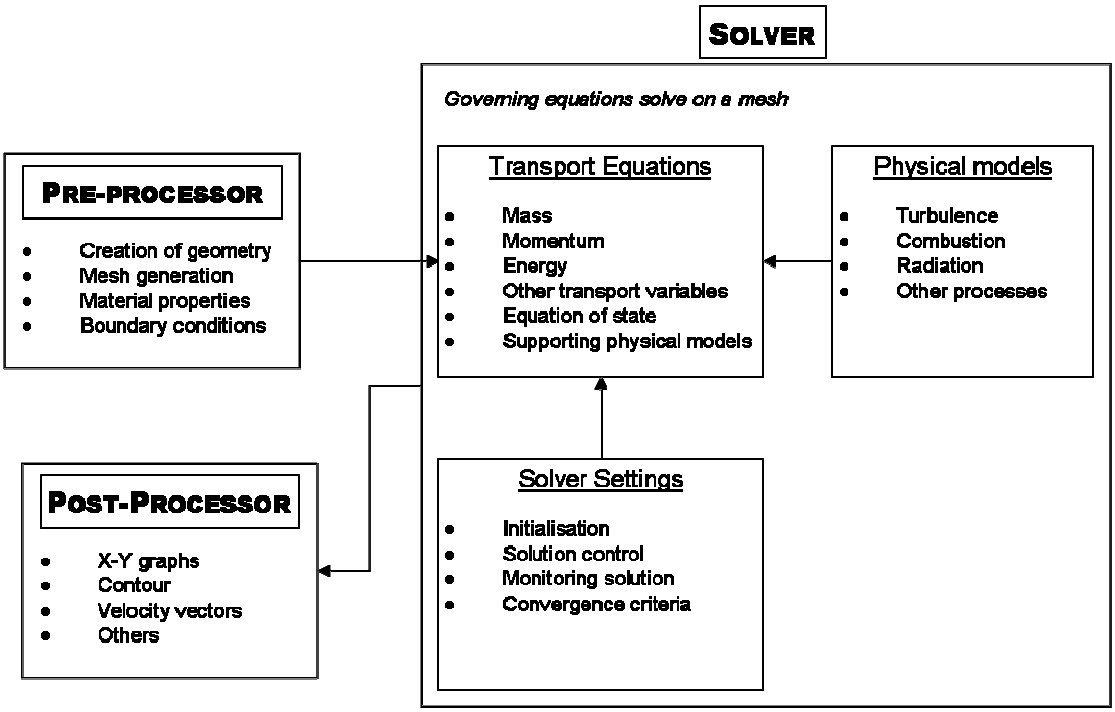

Figure 6-2: Inter-connectivity of CFD analysis elements

6.5.1 Definition of the mathematical model

First of all, the CFD users need to define an appropriate mathematical model which approximates the reality to be simulated. Hence, the physics of the problem at hand have to be defined.

The full equations of fluid mechanics, the so-called Navier-Stokes equations, have been presented in the previous section. These equations are extremely complex and their analytical resolution is close to impossible. This is due to the

fact that they form a set of non-linear partial differential equations. The non-linearity property leads to the existence of phenomena such as turbulence or unsteadiness of the flow. These phenomena lead to non-unique solutions. On top of that even more complex phenomena may be added to the basic flow study. Multispecies and multiphase flows or chemical reactions can be present in a fluid flow problem. They can generate potential subsidiary effects like condensation or evaporation. When this is the case, the analytical resolution of the system of equations is even more complex.

As a result, appropriate modeling assumptions and simplifications need to be defined in order to translate these equations into a mathematical model. This model will consist in a set of partial differential equations. Laws characterizing the type of fluid and the dependence of certain parameters on other flow quantities complete the mathematical problem. For example, viscosity may change depending on temperature and pressure and this has to be specified. Finally, laws defining various quantities linked to the description of additional physics and other reactions can be added to the mathematical model when necessary.

6.5.2 Discretization process (mesh generation)

The second stage undertaken in any CFD simulation is a discretization process. This consists in the translation of geometrical and mathematical models into numbers understandable by the computer. There are two phases in the discretization process.

First, the space is discretized. This is done by distributing points in the flow domain and on the solid surfaces of a model. The points replace the continuity of the real space and form what is called a mesh or a grid. The difficulty of the grid generation process depends on the complexity of the considered geometries. Grid generation can reveal to be extremely delicate and time consuming. However, it is an essential stage in the set up of any CFD analysis. Often, the results of a CFD study and their accuracy entirely depend on the mesh properties and its quality. Indeed, in the end, the object of a CFD

simulation is to provide the user with the numerical values of the flow variables of interest at the positions of the mesh nodes (or points). By definition, no CFD analysis exists without a grid.

There are two approaches to mesh the model of a fluid flow problem. A mesh can be either structured or unstructured. In simple cases, straightforward geometries, it is possible to employ a structured mesh. This type of mesh present an arrangement of rectangular cells regularly distributed on the domain. In more complex geometries, it is sometimes difficult to use a structured meshing approach. It is then common practice to use triangular cells for a more flexible mesh generation.

In some cases, both structured and unstructured approach can be used forming what is better known as a hybrid mesh. The use of this particular type of meshing technique is mostly governed by the problem geometry that can alternate simple and intricate shapes.

In general, the number of cells in a mesh goes together with the accuracy of the CFD solution. Plus the number of cells is important, more the solution is accurate. However, although a large number of meshing elements will often warrantee a good CFD solution, there are some limitations in terms of computational costs and calculation times that can lead engineers to sometimes tend towards the best compromised.

Secondly, after having discretized space, the mathematical model equations are transformed. All mathematical operators are changed into arithmetic operations on the mesh node values. In order to do so, several methods are available such as the finite difference method, the finite volume or finite element methods. The aim of this second step in the discretization process is to obtain a set of algebraic relations between neighboring mesh point values, one relation for each mesh point, better known as a numerical scheme.

6.5.3 Convergence

In the third step of the CFD analysis the numerical scheme is analyzed to detect the possible errors generated by the discretization process. The properties of stability and accuracy need to be highlighted to ensure convergence, and then the validity of the numerical scheme.

In order for the CFD solution to be successful it is essential to prove the convergence of the iterative process and grid independence.

The assessment of convergence is carried out by monitoring the inequalities that are emphasized at each step of the numerical calculations of the algebraic equations. These inequalities are often quoted as residuals. A converged solution is then observed when the residuals present values below a certain threshold, the convergence criteria, which is defined inside the solver controlling parameters of the iterative process.

6.5.4 Verification and validation

In order to be trusted, any CFD analysis should go through the process of validation and verification. This means that the obtained have to be compared to experimental data or data available in literature in order to assess their accuracy and that they are realistically possible.

6.5.5 Resolution

In the fourth step of any CFD simulation the numerical scheme is solved in order to obtain the mesh point values for the main flow variables. At this stage, iterative methods are employed. These methods lead to the solution of the equations after successive approximations. They are different from direct methods. The most frequently employed iterative methods are the finite element method, the finite volume method or the finite difference method.

6.5.6 Post-processing

That is the final stage. The CFD user visualizes and interprets the predicted flow data. Fluid flow animations, contour plot diagram or vectors diagram can be generated using various tools in computer graphics design.

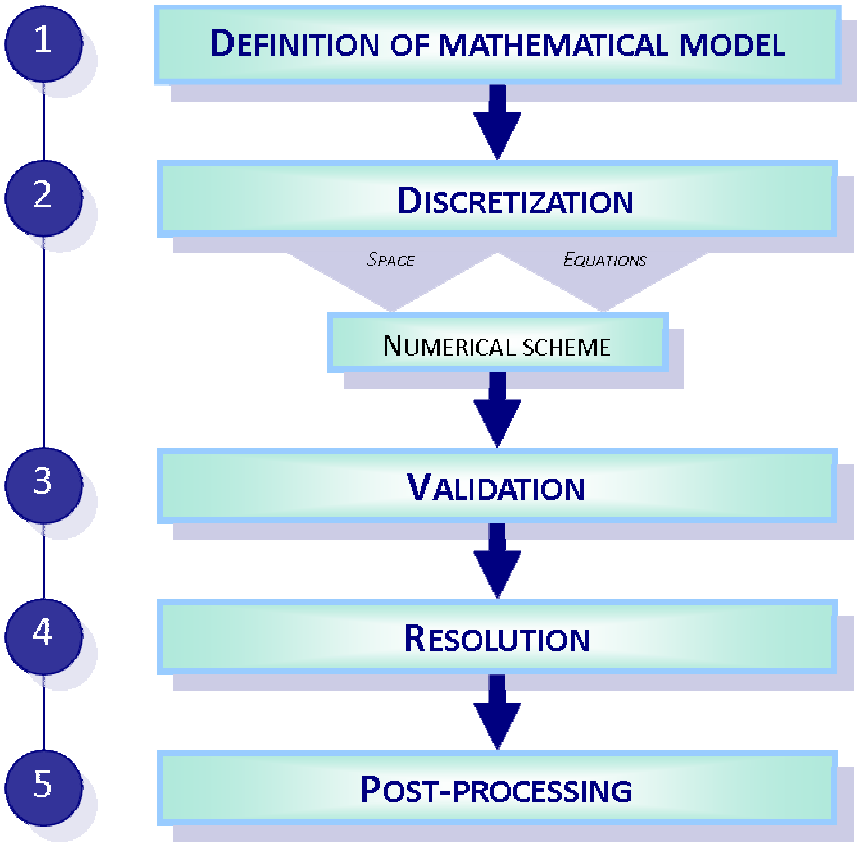

Figure 6-3: The different steps of a CFD analysis

7 VALIDATION CASE STUDY: FLOW PAST A CYLINDER

In this section, numerical calculations are carried out for a two-dimensional circular cylinder and the results are compared to those available in literature for a similar problem. In addition, a grid and time dependency study will determine the validity of the numerical scheme and its applicability to solve the problem at hand.

7.1 Literature review

The flow around a circular cylinder is a classical problem in fluid mechanics. It is of particular interest in offshore and subsea engineering as several systems present a similar geometrical configuration such as marine risers or platform legs. Very often, the flow conditions for these engineering applications correspond to very high Reynolds number flows, typically values ranging from $O(10^6)$ to $O(10^7)$.

Trying to recreate the conditions of such flows experimentally is very complex and costs a lot in terms of human skills, efficient measuring equipment and appropriate facilities. Then, CFD is the best alternative to these expensive experiments. Engineering design can rely on the essential hydrodynamic quantities provided by a CFD study.

There are a few numerical simulations that have been performed for the prediction of very high Reynolds number flows around a circular cylinder (i.e. for Re greater than 10^6). This is mainly due to the complexity of the flow. The high demand in terms of computational resources makes the Direct Numerical Simulation (DNS) of flows at this range of Reynolds currently impossible [22].

There are a few articles dealing with this subject in the open literature. The studies of Catalano et al. (2003)[23], Singh and Mittal (2005)[24] and Ong et al. (2009)[22] are interesting for us.

In 2003, Catalano et al. used both 3D Large Eddy Simulation (LES) with wall modeling and URANS employing the standard k-ε model from Launder and Spalding (1972)[25] using wall functions. The study has been carried out for Reynolds numbers ranging from 0.5×10^6 to 4×10^6. In this region, the drag coefficient recovers from a brutal drop in its values also known as the drag crisis. The numerical results of Catalano et al. highlighted a delayed boundary layer separation and reduced drag coefficients right after the drag crisis. Their conclusion was that the LES results gave more accurate results than the URANS results at $Re \sim 1 \times 10^6$. Nevertheless, it was also observed that LES results were less accurate in comparison to the experimental data for higher Reynolds number. The reason for that was identified to be an insufficient grid resolution.

In 2005, the studies performed by Singh and Mittal[24] used a 2D LES method for a wide range of Reynolds number from 100 to 1×10^7. The objective of the study was to look for an eventual relationship between the drag crisis and the instability of the separated shear layer. Their calculations highlighted the sudden drop in drag coefficient values close to the critical Reynolds number. The primary concern of the study is the flow in the subcritical regime ($300 < Re < 3 \times 10^5$) but some results are also presented concerning the flow beyond the supercritical regime, typically Reynolds numbers greater than 10^6.

In 2009, Ong et al.[22] computed the flow around a two-dimensional smooth circular cylinder for very high Reynolds numbers. The range of Reynolds numbers covered the supercritical and upper-transition flow regime. The numerical calculations have been carried out based on three values of Reynolds number ($Re = 1 \times 10^6$, 2×10^6 and 3.6×10^6). The 2D URANS with a standard high Reynolds k-ε model was used. The objective of the study was to evaluate whether this model could be applicable for engineering design within the concerned flow regimes. Comparing their results with published experimental and numerical results, the authors showed that even if the k-ε model yields to less accurate predictions of flows with strong turbulence, it can provide satisfactory results for engineering design purposes for this range of

Reynolds numbers. The study is presented to be reliable and useful as an engineering assessment tool for design work.

Nowadays, the standard k-ε model is part of most commercial CFD codes. Its use together with wall functions is known to be less expensive than LES and DNS in terms of computational resources.

The objective of this section is to assess whether or not a high Reynolds k-ε turbulence model could be used for closure in the different simulations to be undertaken in our study. The results obtained for the simple case of a 2D circular cylinder are compared to data available in the literature particularly those reported by Catalano et al. (2003), Singh and Mittal (2005) and Ong et al. (2009).

The U-RANS equations [19; 20] are used for conservation of mass and momentum. These equations are given by:

$$\frac{\partial \bar{u}}{\partial x} + \frac{\partial \bar{v}}{\partial y} = 0 \qquad \textbf{(7-1)}$$

$$\frac{\partial \bar{u}}{\partial t} + \frac{\partial (\overline{uu})}{\partial x} + \frac{\partial (\overline{vu})}{\partial y} \qquad \textbf{(7-2)}$$

$$= -\frac{1}{\rho}\frac{\partial \bar{p}}{\partial x} + \nu\left(\frac{\partial^2 \bar{u}}{\partial x^2} + \frac{\partial^2 \bar{u}}{\partial y^2}\right) + \frac{\partial}{\partial x}\left[\nu \frac{\partial \bar{u}}{\partial x}\right] + \frac{\partial}{\partial y}\left[\nu \frac{\partial \bar{v}}{\partial x}\right]$$

$$- \left[\frac{\partial \left(\overline{u'u'}\right)}{\partial x} + \frac{\partial \left(\overline{u'v'}\right)}{\partial y}\right]$$

$$\frac{\partial \bar{v}}{\partial t} + \frac{\partial(\overline{vu})}{\partial x} + \frac{\partial(\overline{vv})}{\partial y} \qquad \textbf{(7-3)}$$
$$= -\frac{1}{\rho}\frac{\partial \bar{p}}{\partial x} + \nu\left(\frac{\partial^2 \bar{v}}{\partial x^2} + \frac{\partial^2 \bar{v}}{\partial y^2}\right) + \frac{\partial}{\partial x}\left[\nu\frac{\partial \bar{u}}{\partial y}\right] + \frac{\partial}{\partial y}\left[\nu\frac{\partial \bar{v}}{\partial y}\right]$$
$$-\left[\frac{\partial\left(\overline{u'v'}\right)}{\partial x} + \frac{\partial\left(\overline{v'v'}\right)}{\partial y}\right]$$

Where $\bar{u}$ and $\bar{v}$ are the mean velocities components. $\overline{u'u'}$, $\overline{u'v'}$ and $\overline{v'v'}$ are the Reynolds stress components with u' and v' being the turbulent fluctuations. $\bar{p}$ is the mean dynamic pressure and ρ the density of the fluid.

The mathematical formulation of the k-ε model is given as follows [19; 20; 20; 22; 26]:

$$(\rho U_i k) = \frac{\partial}{\partial x_i}\left(\left(\mu + \frac{\mu_t}{\sigma_k}\right)\frac{\partial k}{\partial x_i}\right) + P_k - \rho\varepsilon \qquad \textbf{(7-4)}$$

$$\frac{\partial}{\partial x_i}(\rho U_i \varepsilon) = \frac{\partial}{\partial x_i}\left(\left(\mu + \frac{\mu_t}{\sigma_\varepsilon}\right)\frac{\partial \varepsilon}{\partial x_i}\right) + C_{\varepsilon 1}P_k\frac{\varepsilon}{k} - \rho C_{\varepsilon 2}\frac{\varepsilon^2}{k} \qquad \textbf{(7-5)}$$

The following standard model coefficients are adopted:

$$C_\mu = 0.09\,;\ \sigma_k = 1.00\,;\ \sigma_\varepsilon = 1.30\,;\ C_{\varepsilon 1} = 1.44\,;\ C_{\varepsilon 2} = 1.92 \qquad \textbf{(7-6)}$$

7.2 Model Description

The flow around a circular cylinder of 2 meters diameter (D) is considered. This diameter has been taken in the close neighborhood of the dimensions of the nacelle's cross section (height 2.2 meters excluding the appendix box). This cylinder is placed in a two-dimensional rectangular computational domain which dimensions are 54 meters × 28 meters (27D × 14D) as illustrated in figure (Figure 7-1).

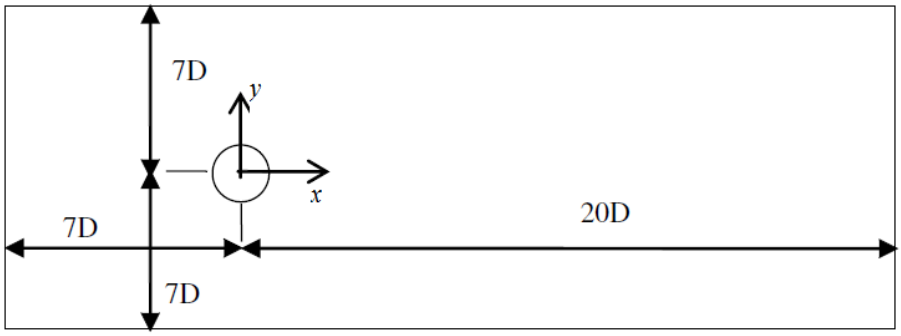

Figure 7-1: Validation case model geometry

This computational domain is similar to the one used by Ong et al. (2009)[22].

7.3 Boundary conditions

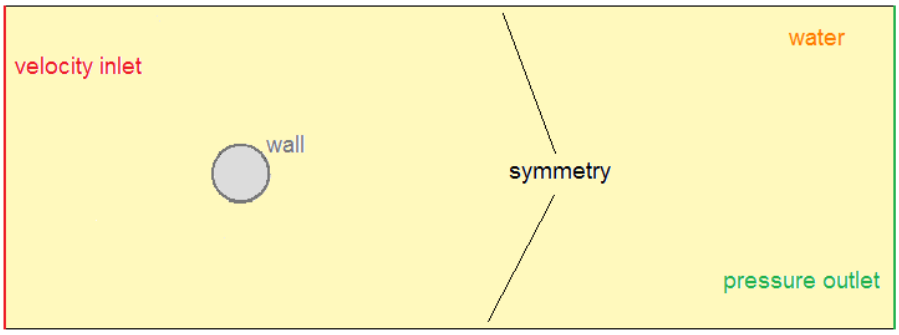

Figure 7-2: Boundary conditions for validation case

The boundary conditions used for the simulations are presented on the figure above.

Uniform flow is specified at the *velocity inlet* on the left of the domain with $U = 3\,m.s^{-1}$. Tutar and Holdø (2001)[27] have proposed values for the free stream inlet turbulence values for kinetic energy and turbulent dissipation based on a turbulent intensity of 0.8% and a non-dimensional turbulent length-scale $(L/D)$of 0.0045. We use the same values in this study, adjusting the turbulent length scale to the value of D in our problem and we then use 0.009.

Along the outflow boundary is defined as pressure outlet meanwhile the upper and lower boundaries are defined as symmetries in order to guarantee a traction-free velocity-pressure along them.

The cylinder surface is defined as a wall with no slip condition which mean that the velocity at the cylinder surface equals zero.

Standard wall functions are applied along with the turbulence k-ε model due to the high Reynolds number.

7.4 Meshing

In order to realize the grid independency study, four meshes have been created. Each of these meshes presents a different number of nodal points and a boundary layer with parameters y plus of 80, distance of the first node from the wall 0.00107 meters and thickness 0.03684 meters. These parameters were retained after different trials. Figure 7-3 references the different meshes and their properties.

Mesh	Nodes	Cd	Cl
M1	26103	0.5670	-0.0022
M2	35945	0.5732	-0.0032
M3	44440	0.5774	0.0005
M4	63525	0.5804	0.0006

Figure 7-3: Mesh independence study

A grid convergence study is performed for the flow at Reynolds Re = 4×10^6. The grid convergence study for the drag and lift coefficient with respect to the number of nodes are shown on Figure 7-4 and Figure 7-5.

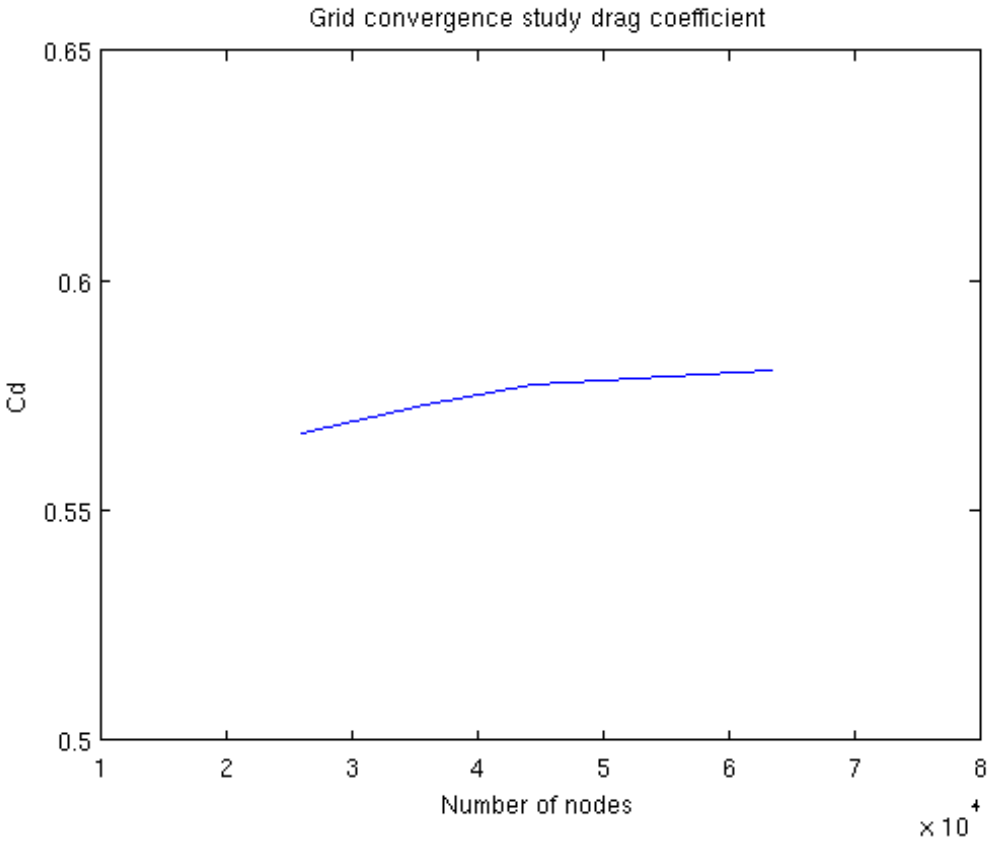

Figure 7-4: Grid convergence study drag coefficient

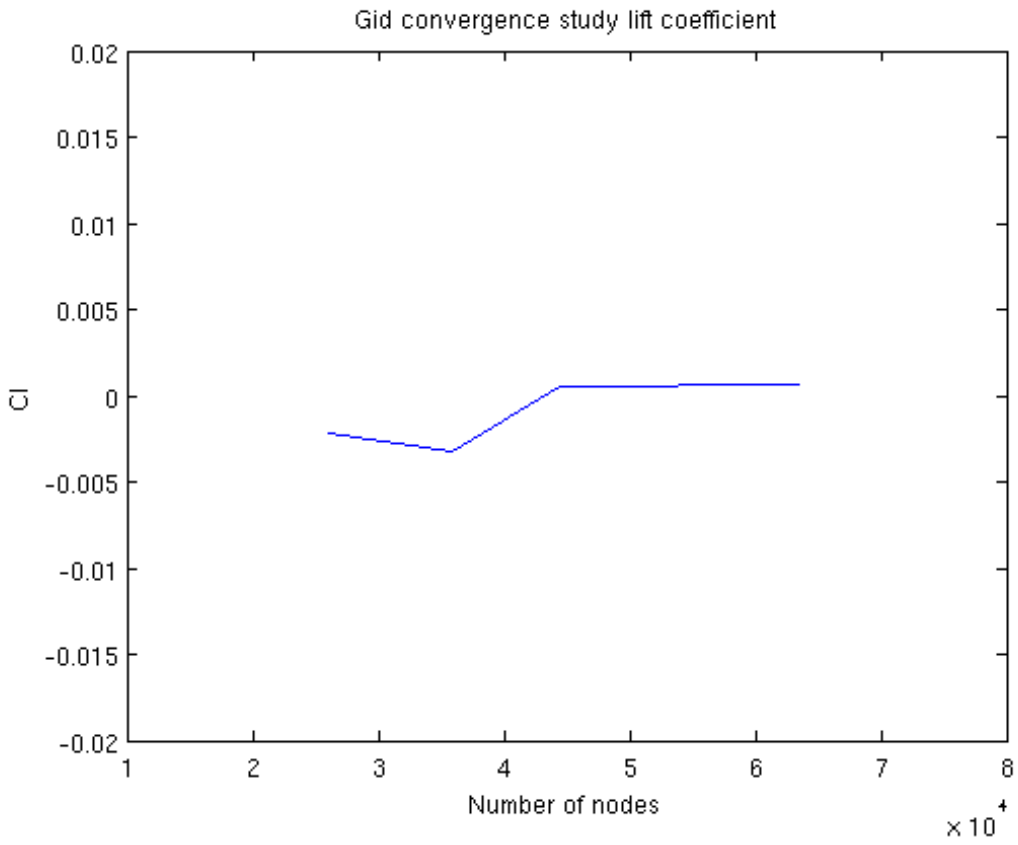

Figure 7-5: Grid convergence study lift coefficient

From the two graphics above it appears that meshes M3 (44440 nodes) and M4 (63525 nodes) give very close time-averaged drag and lift coefficients. As a result, mesh M3 is giving sufficient grid resolution. Mesh M3 is presented in Figure 7-6 and Figure 7-7.

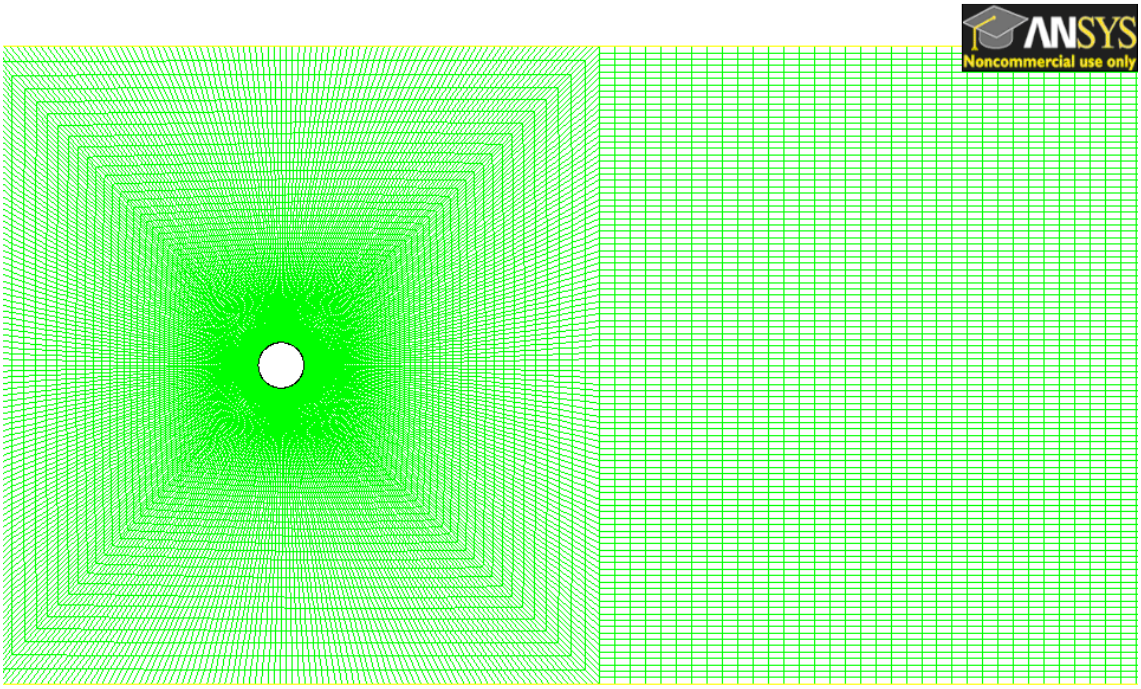

Figure 7-6: Validation case mesh

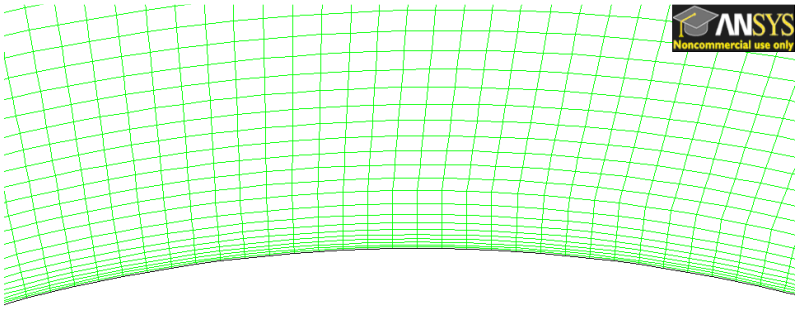

Figure 7-7: Mesh close to the cylinder surface

7.5 Results

Figure 7-8 and Figure 7-9 presents the drag coefficient and lift coefficient history for the validation case study. The drag coefficient value $C_d = 0.57$ is in range with the value available in literature at similar Reynolds number (around 6.10^6)[22-24; 28]. A comparison is proposed on Figure 7-10.

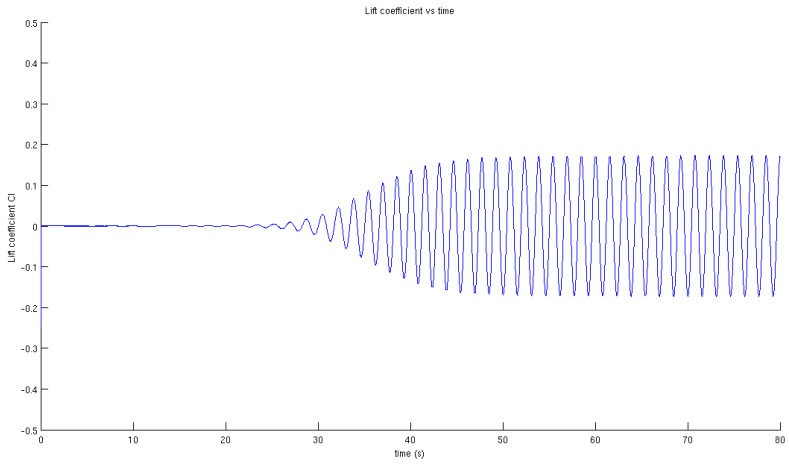

Figure 7-8: Lift coefficient versus time for validation case

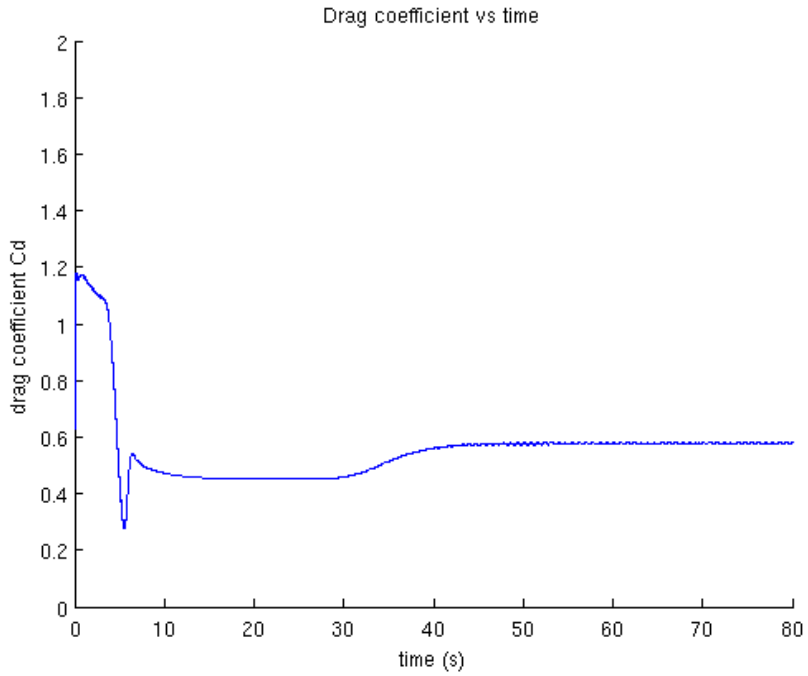

Figure 7-9: Drag coefficient versus time for validation case

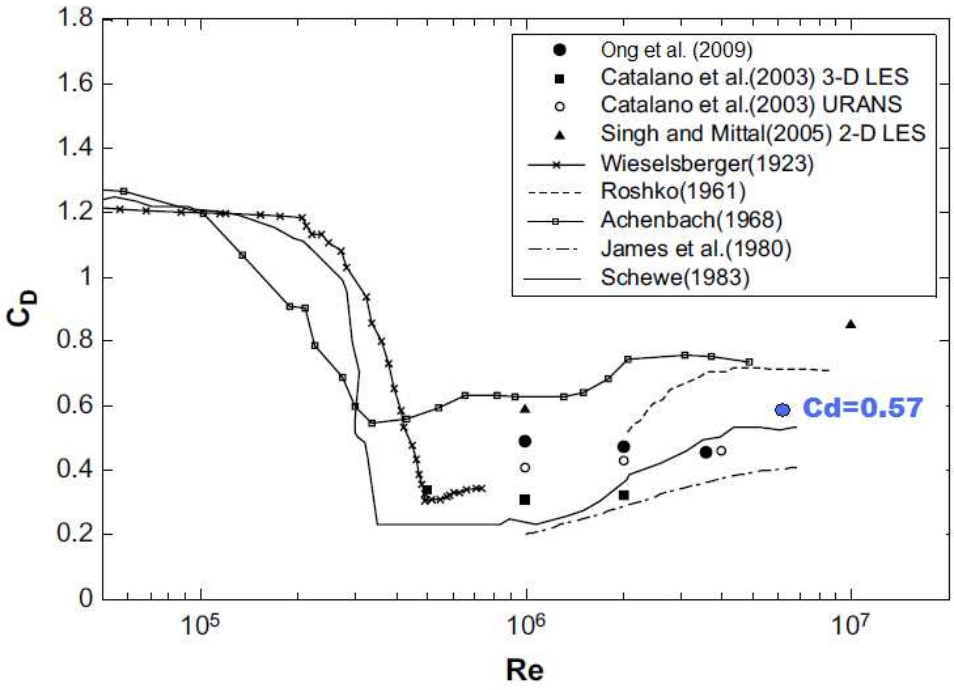

Figure 7-10: Time averaged drag coefficient vs Re number

8 2D CROSS SECTION UNSTEADY SIMULATIONS

8.1 Methodology

A series of simulations have been launched to evaluate the drag coefficients of various cross section shapes (front view) for the Deltastream nacelles. The stream velocity is taken equal to 3 m/s. The drag coefficients have been investigated employing 2D unsteady RANS (Reynolds-Average Navier-Stokes) equations coupled to a standard k-ε turbulence model with standard wall function.

The reference drag coefficient value is the drag coefficient value found for the cross section of the proposed nacelle shape. This drag coefficient is referred as $C_{d_{ref}}$. In order to assess the reduction in drag coefficient values relatively to the shape of reference, a percentage of improvement is defined such as:

$$\%\ of\ improvement = \frac{\Delta C_d}{C_{d_{ref}}}$$

In the expression above ΔC_d is the difference between the calculated coefficient and the coefficient of reference.

Many different shapes have been tested. The aim of these different trials is not to come up with an accurate shape proposal and drag coefficient value but more to be able to propose an idea of profile for which drag reduction is significant. In this report the shapes that have been retained are the ones presenting the most interest. The post-processing of the results obtained is available in the Appendix.

8.2 Original cross section and reference drag coefficient value

The figure below shows the cross section of the proposed nacelle shape.

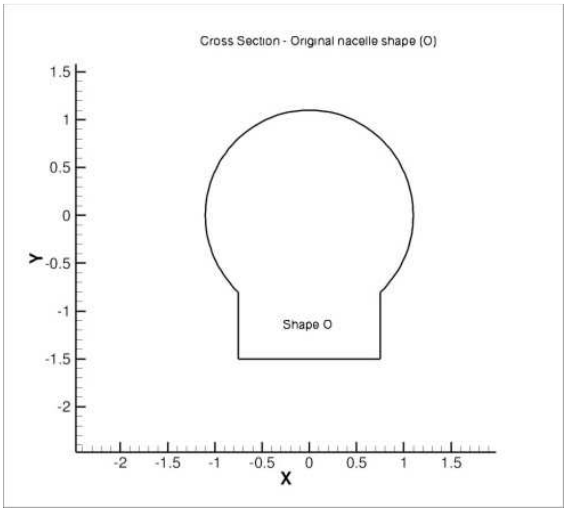

Figure 8-1: Original nacelle's cross section

The main body of the nacelle presents a cylindrical section. Underneath this main structure the presence of a rectangular appendix can be noticed. For similar Reynolds numbers (in the order of 10^6), numerical simulations of flow around a smooth circular cylinder indicate that for such profiles drag coefficients with values of between 0.36 and 0.50 are usually found. In our case, the presence of the appendix makes us expect much higher values due to the break in the structure smoothness and the sharp corners on the bottom of the nacelle.

The value of the drag coefficient for this case was found equal to $C_{d_{ref}} = 1.0305$

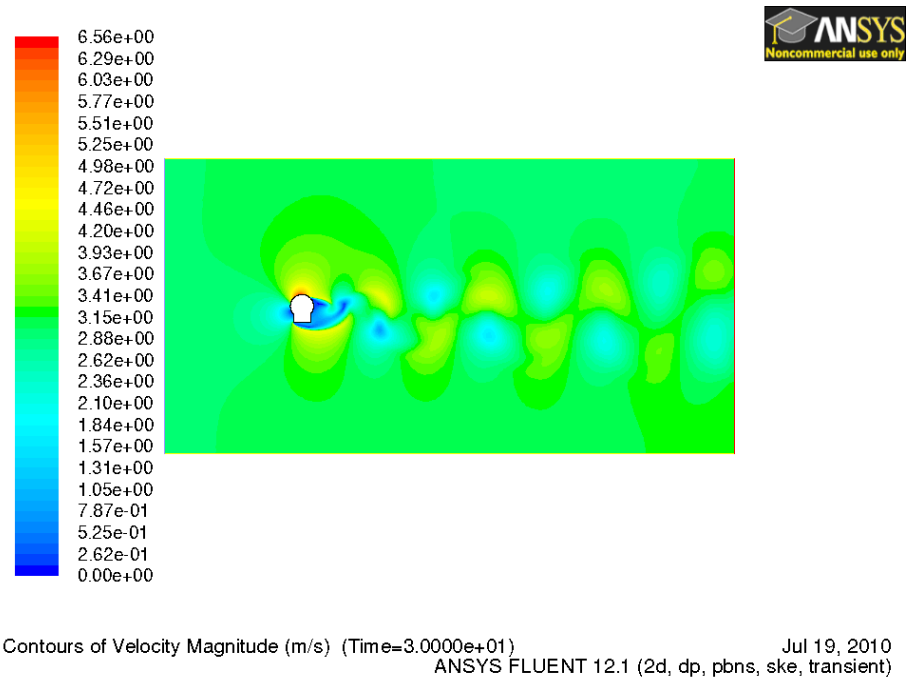

.

Figure 8-2: Contour of velocity magnitude for nacelle's original cross section

This value of drag coefficient is relatively high. In an attempt to reduce this value, it has been chosen to run simulations on a pretty similar profile, but this time the main body of the nacelle does not present a cylindrical cross section but an elliptical one. Indeed, literature shows that drag coefficient for elliptic bodies are lower than drag coefficient for cylindrical bodies. As a result, the drag force applied on elliptical body is less important in magnitude than the one applied on cylindrical shapes.

8.3 Elliptical cross section

The figure below presents the first cross section shape investigated. This shape is referenced as shape A and the corresponding drag coefficient will be quoted C_{d_A} in the following. The main body of the nacelle is given an elliptical shape; however, the shape of the appendix underneath remains the same.

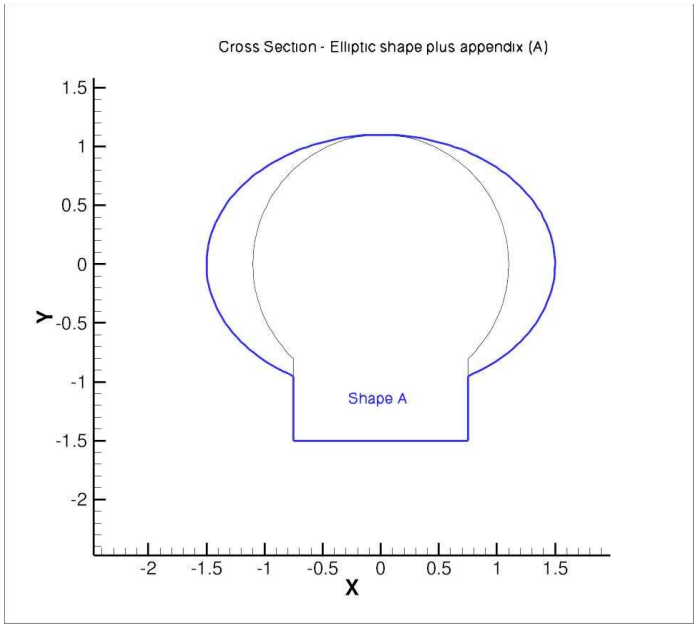

Figure 8-3: Elliptical cross section

This modification shows a considerable improvement in the value of the drag coefficient which is found to be equal to $C_{d_A} = 0.6457$.

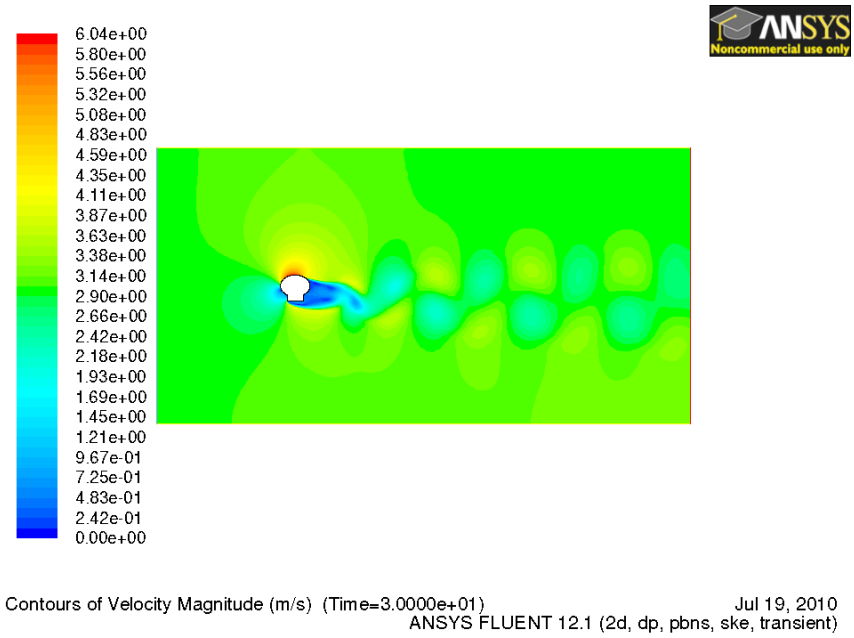

Figure 8-4: Velocity magnitude for elliptical shape

8.4 Cross sections without appendix

Next, the sharp angled appendix underneath the main nacelle's body does not appear in the following proposed shapes. Instead the main body shape and size are extended to provide a substitute to this appendix and more smoothness in the lines of the structure. The expected effect is a decrease in the value of the drag coefficient. Numerical simulations are then carried out for shapes (B), (D), and (F). These shapes are presented in the figures below.

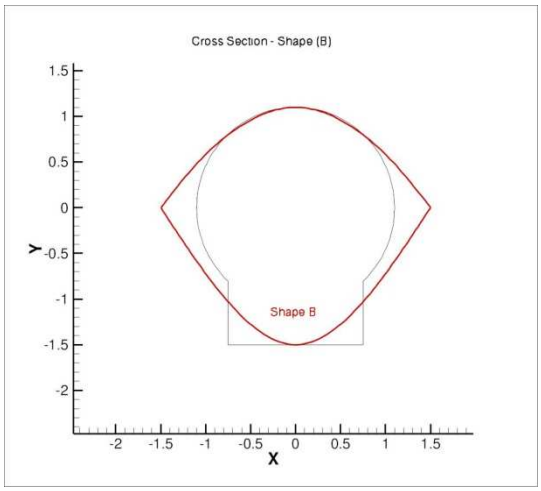

Figure 8-5: Shape B cross section

For shape (B) the drag coefficient $C_{d_B} = 0.4816$. This shape is not symmetric.

For shape (D) the drag coefficient was evaluated to $C_{d_D} = 0.4854$. This shape presents a fineness ratio of roughly 2:1. The fineness ratio is generally used in aeronautics to describe the shape of streamlined bodies. It consists in the ratio of the total length of the body also known as chord to its maximum width. Furthermore, we can note that the shape is symmetric.

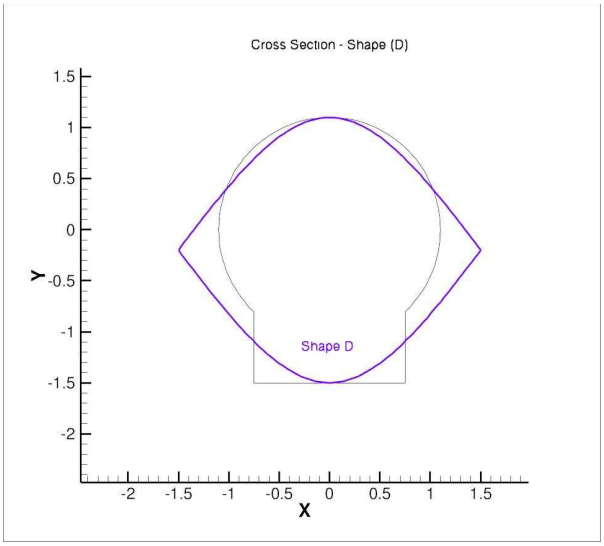

Figure 8-6: Shape D cross section

Finally, a last shape has been chosen to be given an elliptical section presenting a fineness ratio similar to the one of shape (D). The numerical simulations ran for shape (F) gave a drag coefficient value $C_{d_F} = 0.2056$.

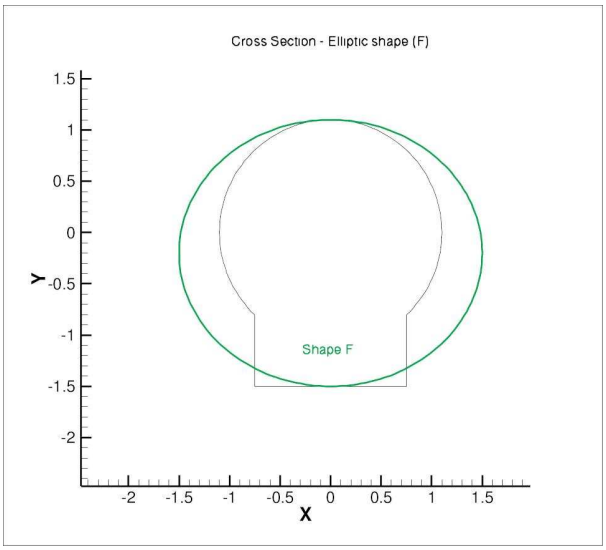

Figure 8-7: Shape F (elliptic section)

8.5 Results

The figure below (Figure 8-8: Comparison of drag coefficients for various cross section shapes and percentage of improvementpresents a summary of the drag

coefficients obtained with the computations as well as the value of the percentage of improvement for each studied shape.

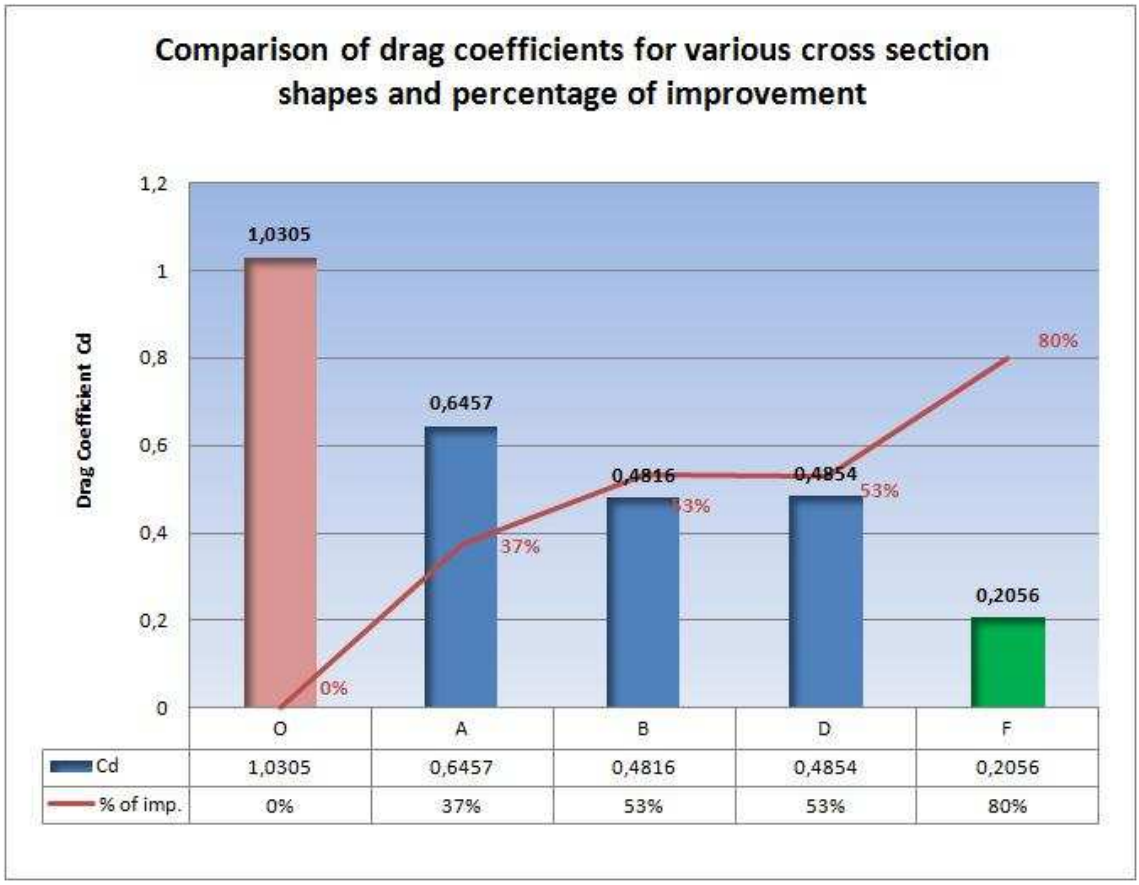

Figure 8-8: Comparison of drag coefficients for various cross section shapes and percentage of improvement

8.6 Conclusions

From what has been said above, we can notice that a really important improvement is made when dealing with the last two shapes. It is quite clear that the appendix present underneath the nacelle structure for both the original cross section and the elliptical cross section is the reason of such high drag coefficients. This is mainly due to the fact that the surface of nacelle opposed to the flow is quite large and then a lot of resistance occurs. This appendix is meant to host part of the vital components of the water current turbine such as

the generator or gearbox. An effort has been made in the design of the other shapes in order to suppress this appendix while trying to conserve as much room in the nacelle as with the appendix not to face any problems with the hosting of the internal turbine components. The results are interesting for shape B and D. However, even though the drag improvement is quite significant the nature of this shapes and the presence of very sharp cut edges does not allow the streamlines flowing around the body to take a smooth path around the nacelle and gradually behind the shape to insure minimal drag. Furthermore, these shapes will probably be very difficult to manufacture. Then, shape B and D cannot be retained as possible shapes for the nacelle's cross section design.

The last body (F) presents an elliptic shape. The appendix is not present anymore as with shape O and A. However, the capacity of hosting internal equipments remains the same as for the original cross section. The drag improvement is the best with this proposed shape. Manufacturing an elliptic box should not be as complicated as manufacturing the intricate geometries presented above. Then, in an effort of reducing drag on the nacelle when it is in a safe position (perpendicular to the tidal flow) we should tend to develop an elliptic shape for the cross section. The elliptic shape without appendix looks like the optimum solution with a drag reduction of about 80%, however if the appendix cannot be suppress a good compromise would be to adopt an elliptic shape on top of the appendix like shown in shape A. In that case, even if the drag is still important we can still observe a net decrease of its value of about 37%. However, the counterpart in decreasing the drag is the probability of an increase in the lift values.

9 2D SIDE VIEW UNSTEADY SIMULATIONS

9.1 Methodology

A series of simulations have been launched to evaluate the drag coefficients of various shapes for the longitudinal section for the Deltastream nacelles. The stream velocity is taken equal to 3 m/s. The drag coefficients have been investigated employing 2D unsteady RANS (Reynolds-Average Navier-Stokes) equations coupled to a standard k-ε turbulence model with standard wall function.

The reference drag coefficient value is the drag coefficient value found for the original nacelle longitudinal shape shown on the figure below.

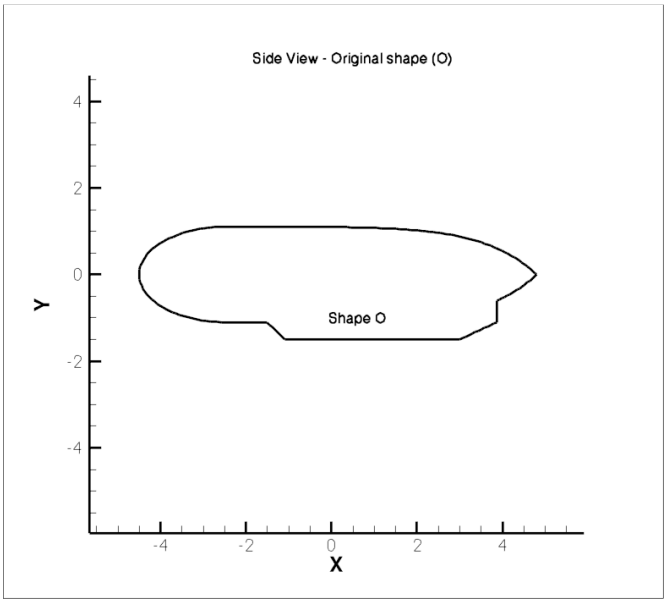

Figure 9-1: Original nacelle longitudinal shape

This drag coefficient is referred as $C_{d_{ref}}$. In order to assess the reduction in drag coefficient values relatively to the shape of reference, a percentage of improvement is defined such as:

$$\%\ of\ improvement = \frac{\Delta C_d}{C_{d_{ref}}}$$

In the expression above ΔC_d is the difference between the calculated coefficient and the coefficient of reference.

Many different shapes have been tested. The aim of these different trials is not to come up with an accurate shape proposal and drag coefficient value but more to be able to propose an idea of profile for which drag reduction is significant. In this report the shapes that have been retained are the ones presenting the most interest.

9.2 Original longitudinal section and reference drag coefficient value

The calculations have shown that $C_{d_{ref}} = 0.1318$. The drag on this structure could possibly be reduced by giving more smoothness to the shape of the nacelle. In other terms, several discontinuities and sharp angles can be eliminated to avoid brutal changes in the pattern of the streamlines surrounding the bodies. However, the value of drag coefficient is already pretty good.

Modifications are made at several points of the structure. These changes are made in an effort to give more smoothness to the profile. Five profiles are then proposed and CFD calculations are carried out to evaluate the drag coefficient for each of them.

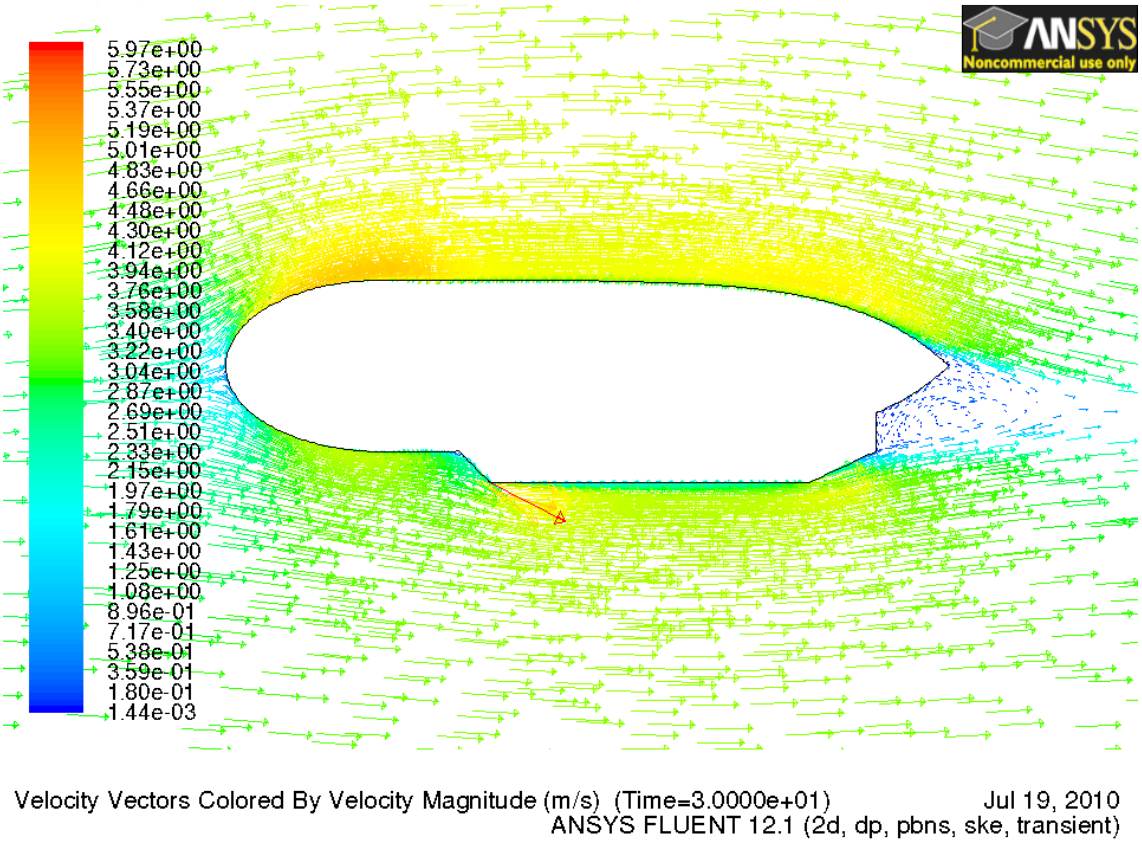

Figure 9-2: Original nacelle vectors velocity magnitude

Most of the modifications on these longitudinal shapes are made on the appendix underneath the main body of the nacelle. Sharp edges of the appendix as they can be seen on Figure 9-2: Original nacelle vectors velocity magnitude are given more rounded forms in an effort to make the contours of the nacelle smoother. That way we want to avoid breaks in the nacelle profile and consequently avoid brutal disruptions of the streamlines path along the nacelle body. This is of course in an effort to diminish drag. In total, five shapes are under study referenced as shape I, II, III, IV and a longitudinal elliptical shape.

9.3 Longitudinal shape I

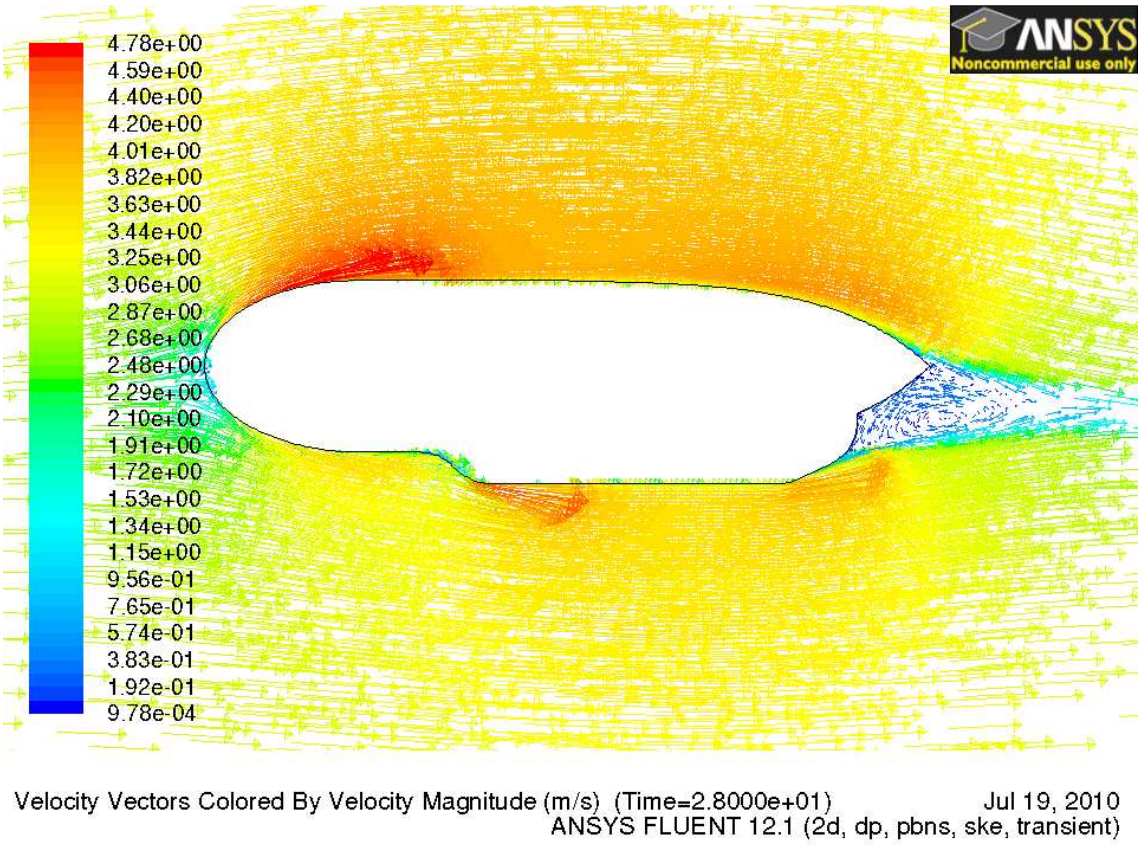

Figure 9-3: Shape I vectors velocity magnitude

The drag coefficient for this shape is $C_{d_I} = 0.1058$.

9.4 Longitudinal shape II

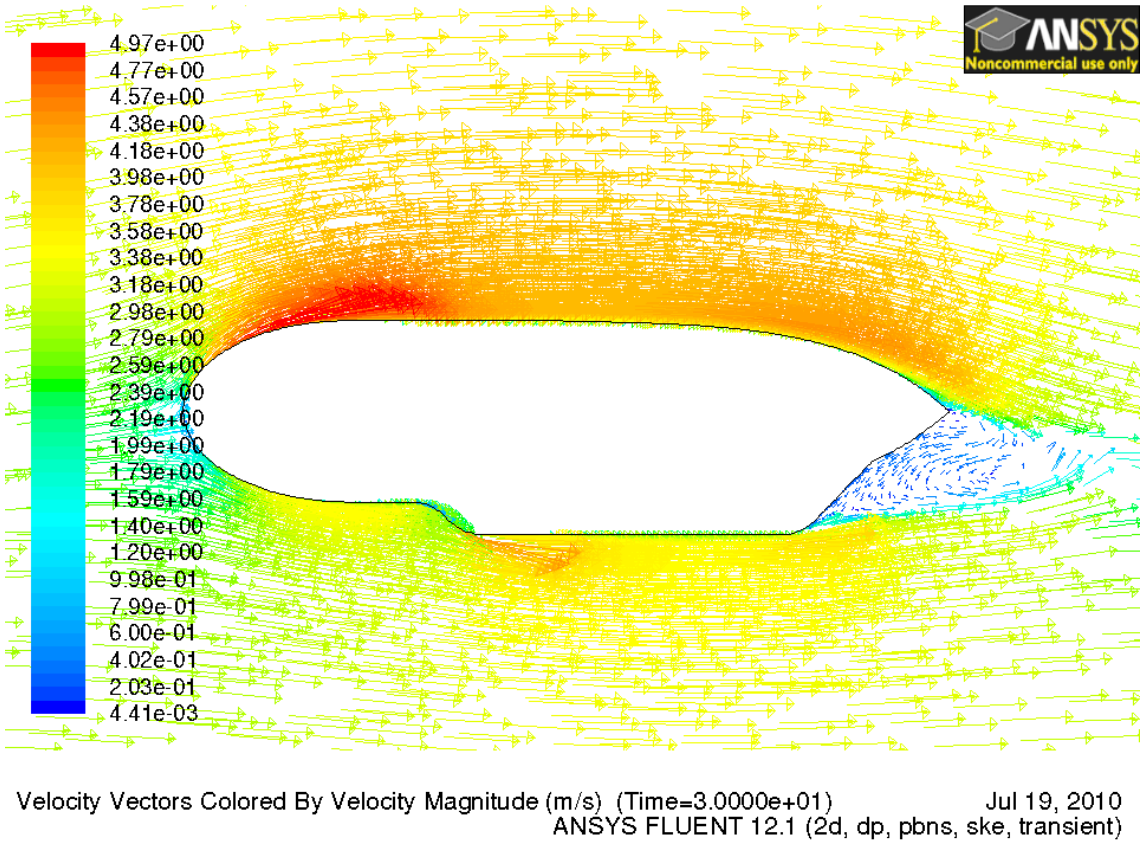

Figure 9-4: Shape II vectors velocity magnitude

The drag coefficient for this shape is $C_{d_{II}} = 0.1640$.

9.5 Longitudinal shape III

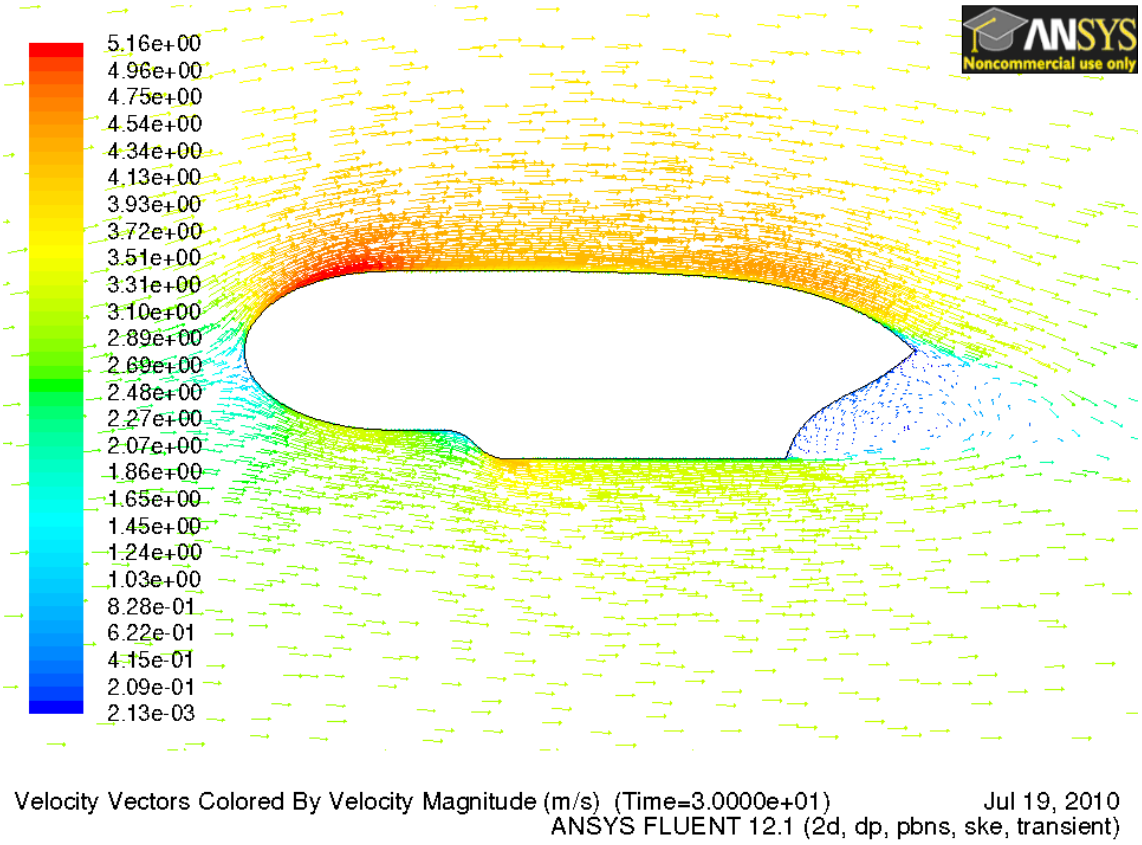

Figure 9-5: Shape III vectors velocity magnitude

The drag coefficient in that case is $C_{d_{III}} = 0.2122$.

9.6 Longitudinal shape IV

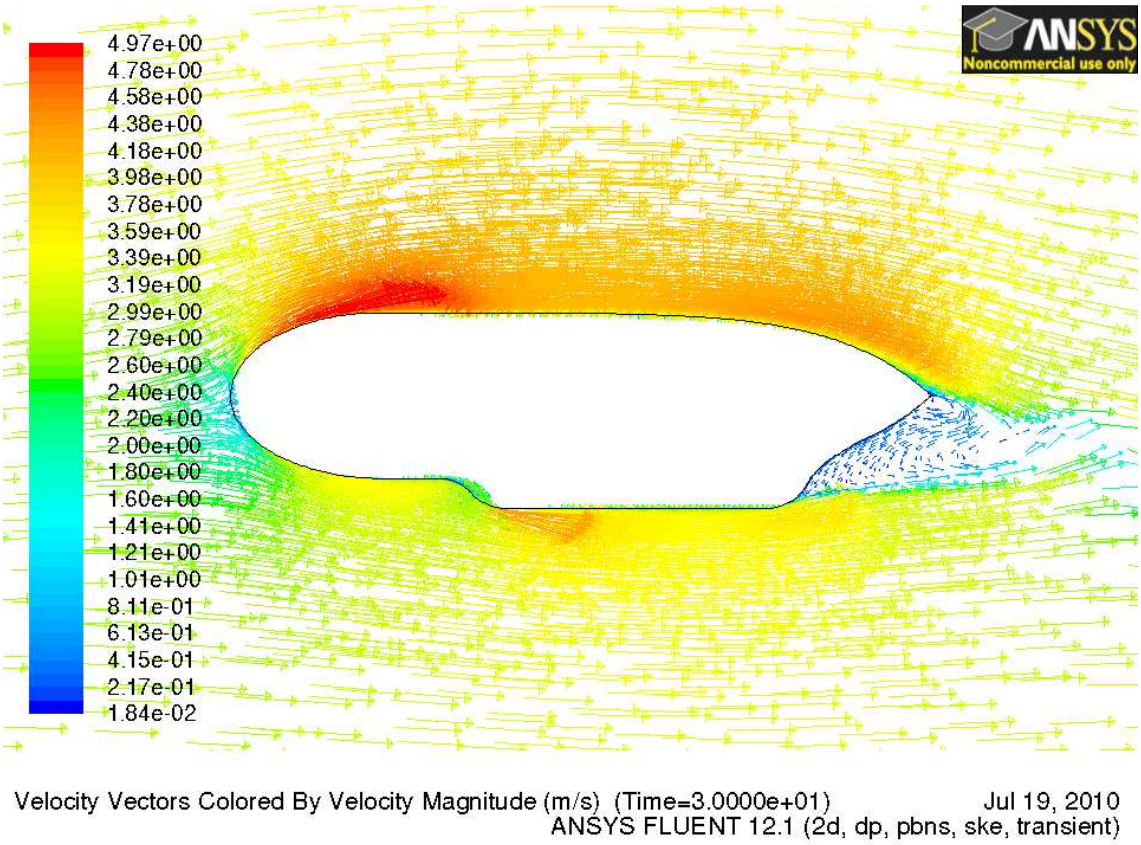

Figure 9-6: Shape IV vectors velocity magnitude

The drag coefficient for this shape is $C_{d_{IV}} = 0.1639$.

9.7 Longitudinal elliptical shape

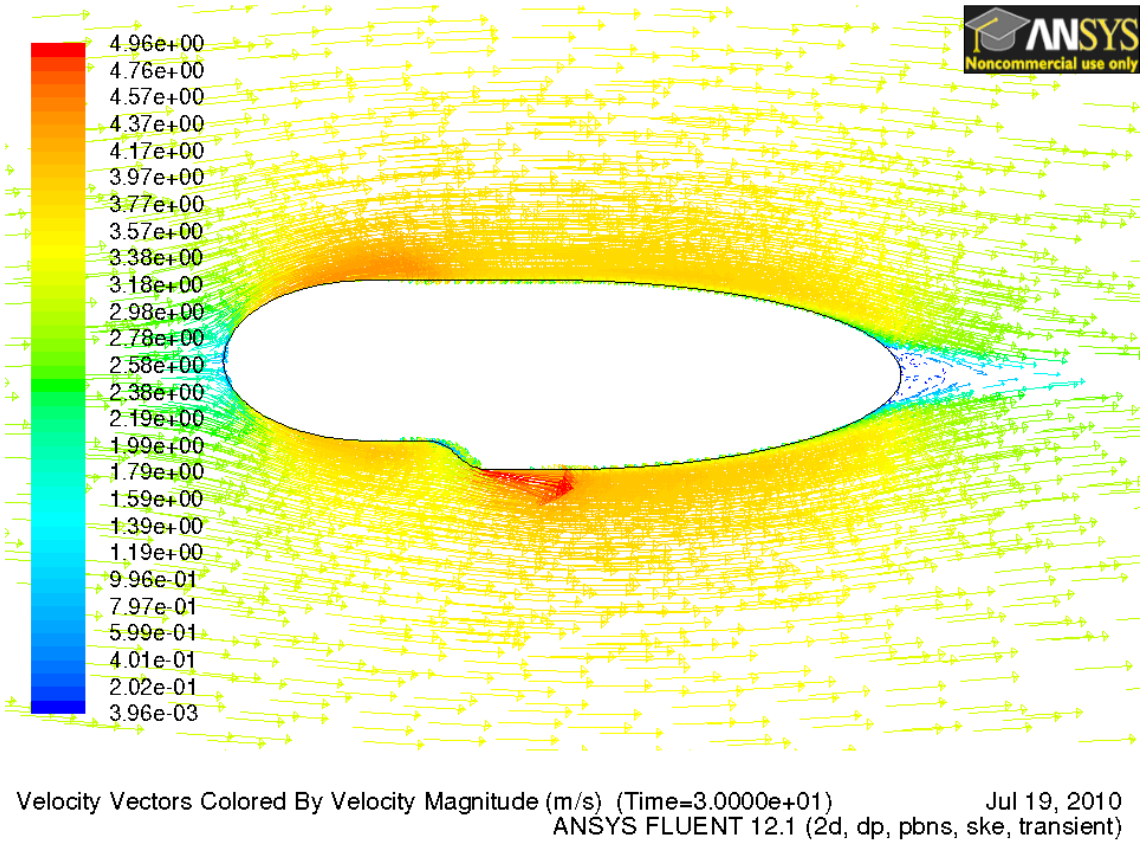

Figure 9-7: Elliptical shape vectors velocity magnitude

The drag coefficient for this shape is $C_{d_{ell}} = 0.0661$.

9.8 Results

Figure 9-8 presents a summary of the drag coefficients obtained with the computations as well as the value of the percentage of improvement for each studied shape.

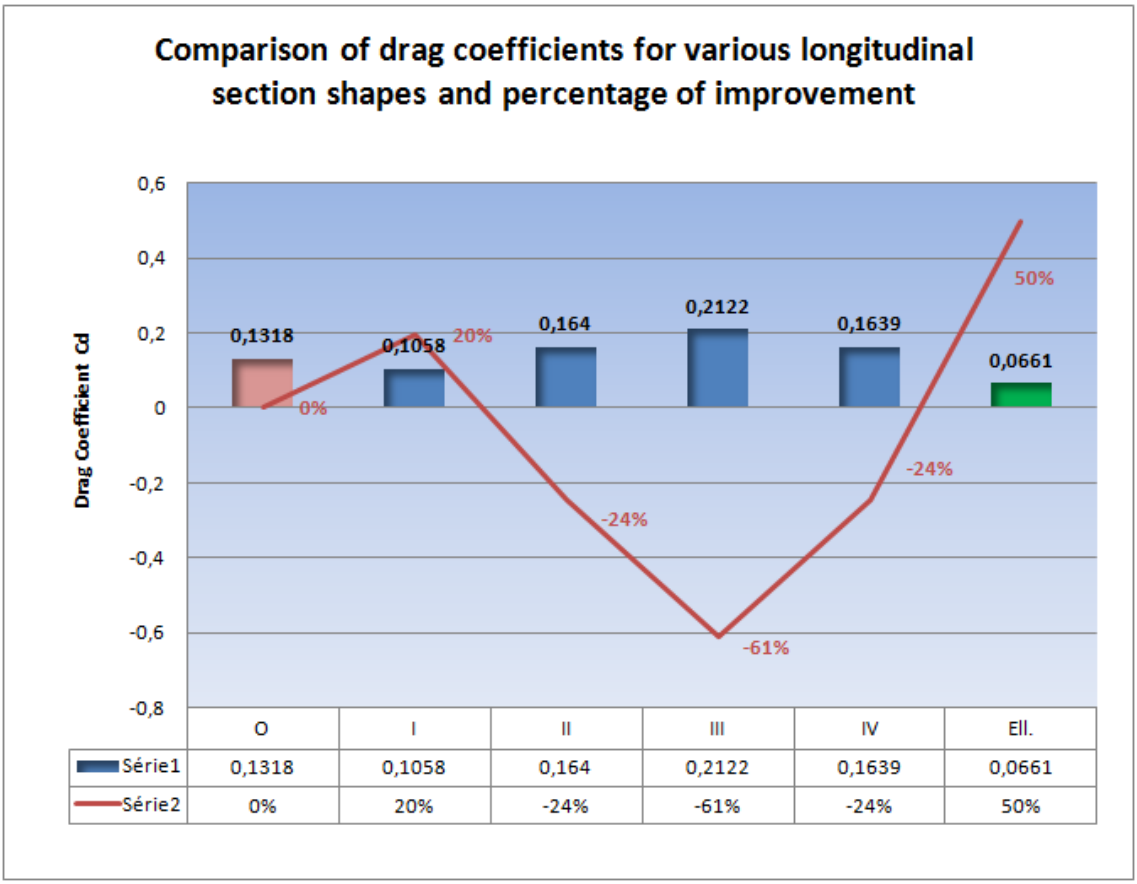

Figure 9-8: Comparison of drag coefficients for various longitudinal section shapes and percentage of improvement

9.9 Conclusions

Contrarily to the previous section where all proposed shapes presented a value of drag coefficient lower than the drag coefficient value of reference, these alternative shapes do not all contribute to reduce the drag coefficient value except for shape I and for the longitudinal elliptical shape. Furthermore, it is interesting to notice that the drag coefficient of reference is not very high, and in

that case the original longitudinal shape is somehow quite acceptable. The gain in drag reduction made by applying shape I is of about 20%. This is not really significant (represents a gain of about 0.03 less). Furthermore, the appendix box used in the original nacelle is probably much easier to manufacture than the one involved in shape I. This is mainly due to the fact that the profile of the appendix in the first case is quite straightforward, while for shape I the rounded forms can make it more difficult to realize and as a matter of fact more expensive. Finally, the remark is the same for the last shape. The elliptical shape looks like a good solution to reduce the drag coefficient value. However, such a profile will be probably difficult to manufacture.

In other terms, the ideal profile amongst the ones proposed would probably be the elliptical longitudinal shape but reality is that for ease of manufacture and costs saving the original shape is probably the best proposal in that case.

10 CONCLUSIONS AND FURTHER WORK

10.1 Three-dimensional model proposal

From the results obtained in the two-dimensional studies of the cross section and the longitudinal section we can propose a three –dimensional model which consists in the combination of the two best highlighted options. The original nacelle model is shown in Figure 10-1: Original nacelle model.

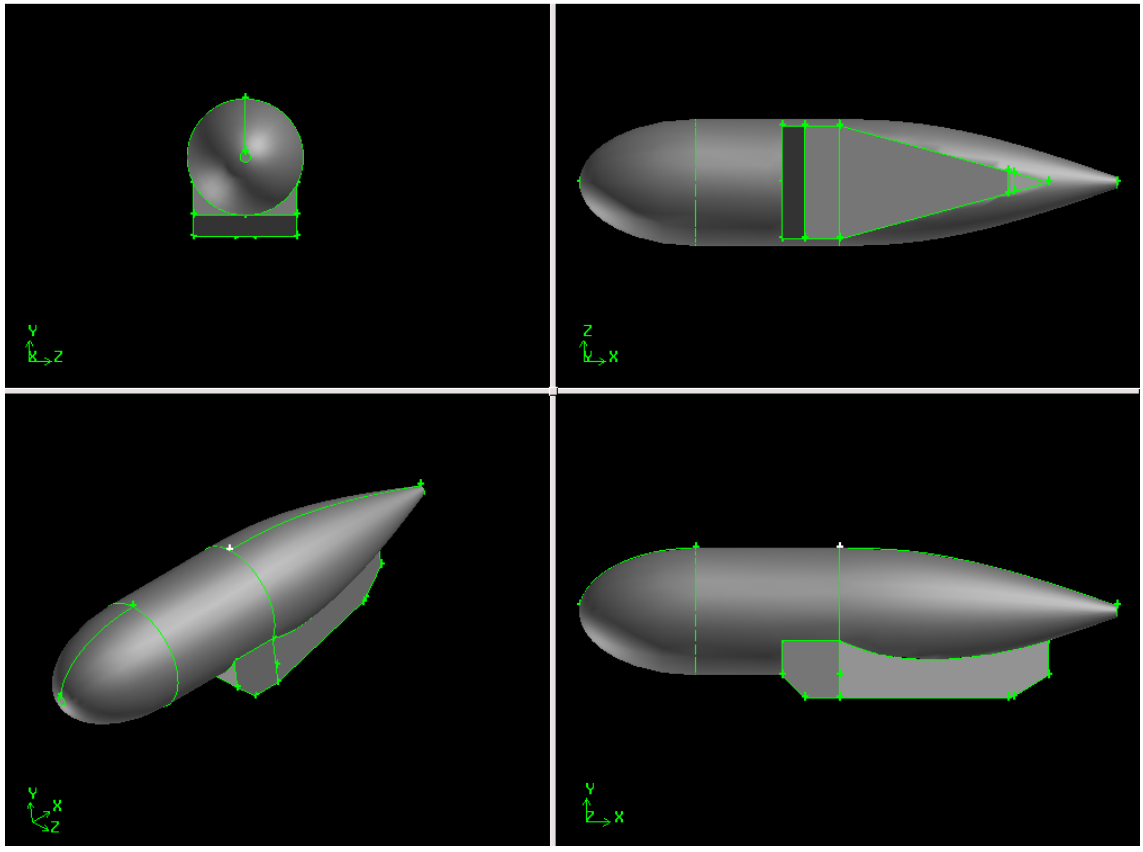

Figure 10-1: Original nacelle model

The proposed alternative nacelle shape for drag reduction is presented in Figure 10-2.

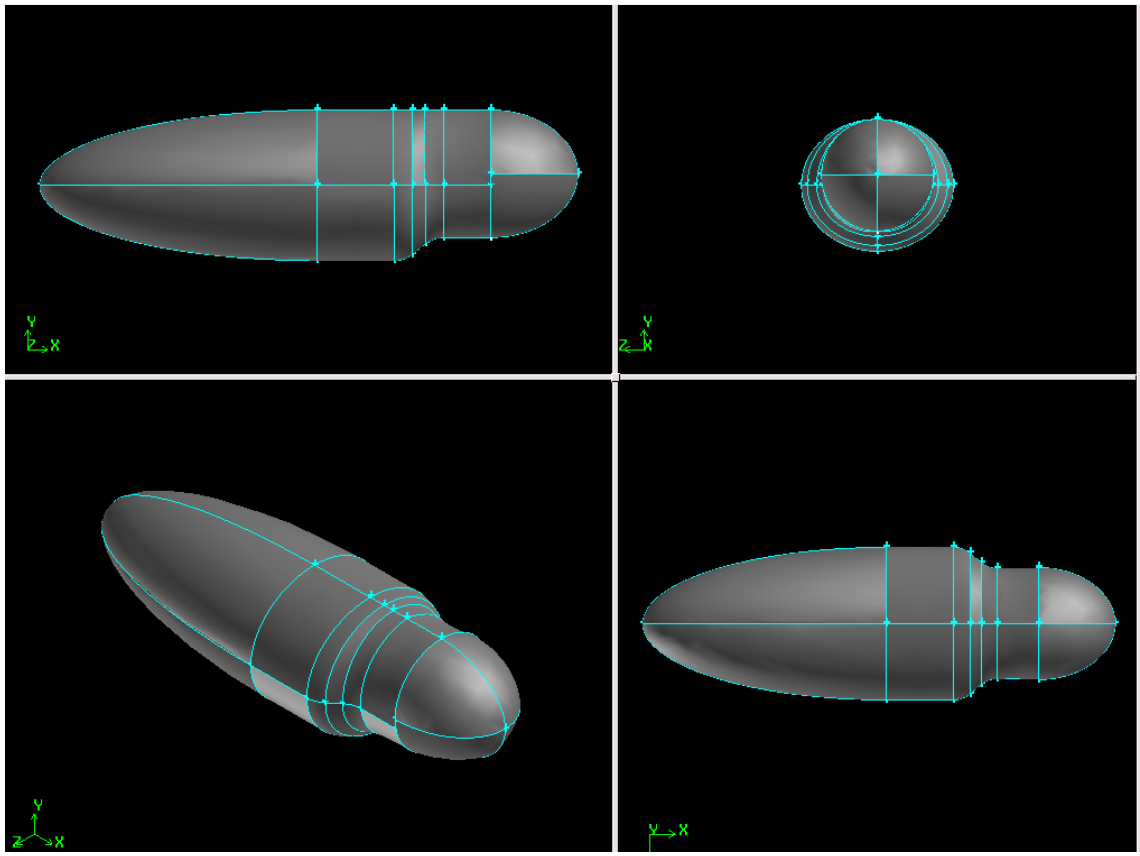

Figure 10-2: Alternative nacelle shape

10.2 Conclusions

The aim of this study was not to carry out a detailed analysis of the hydrodynamic properties of the Deltastream's turbines nacelles. It was also not to come up with a detailed design and in depth study of an alternative nacelle shape. Instead, the aim of this project was to assess the possibilities in drag coefficient values reduction by applying some shape modifications on the cross section and the longitudinal section of the nacelle.

The study showed that for the cross section of the nacelle it was possible to obtain quite good results in terms of drag coefficient reduction by modifying the original shape to a more elliptical body and by suppressing the underneath appendix hosting turbine's internal components. However, in the case of the longitudinal section the results in drag reduction were not as good and even

though the last shape was offering a much less important drag coefficient value, it does not look like the difference is significant between the original shape and a modified one.

The real interest of this study is to look at the cross section. Indeed, when tidal currents are too strong, the Deltatream turbine's nacelles rotate and place themselves in a so-called "security position" orientating perpendicularly to the tidal flow. The reason of this positioning is to prevent the blades from high hydrodynamic loads when not in operation. However, even if the blades are well protected using this method, this position offers more surface of material opposing to the tidal stream. The structure is not anchored on to the seabed and is just put down onto the bottom. Then there is a chance for the tidal device to be dragged on to the seafloor due to resistance of the structure to the water flow. In the event of any problem of this sort, downtimes in power production and extra costs for recovery and repairs are inevitable. Then, even though this "security position" ensures the safety of the blades it does not necessarily warrantee the integrity of the whole device. The point of modifying the cross section shape of the nacelle is to reduce the potential loads on the structure and avoid this undesirable situation. The results arising from our study showed that the appendix underneath the nacelle greatly contributes to high drag coefficient values as well as the cylindrical shape of the nacelle's cross section. When modifying this cylindrical shape to a more elliptical one and conserving the appendix better results were obtained. But even better results were obtained when removing the appendix and giving the nacelle a completely elliptical cross section while ensuring that the same volume was available in order to host the internal components of the water turbine. Other shapes were investigated but not retained due to their intricate geometry and the difficulty to be faced in their manufacturing.

10.3 Further work

This study can be taken as a basis for a more in depth analysis of the hydrodynamics of the nacelle and a more complete investigation on potential drag improvements.

Particularly, three dimensional CFD analyses can be undertaken to evaluate the drag on the nacelle. The obtain results would be probably more accurate in three-dimension than in two-dimension. First, two-dimensional CFD tends to over-predicted drag and then the nacelle will be taken as a whole in a three-dimensional analysis instead of being a cut in a plane like in two-dimension.

Moreover, this three-dimensional model can be submitted to different flow conditions, such as different flow velocities and angles of attack.

A particular interesting matter would be to consider the blades interaction with the nacelle. In operation, while the blades are rotating the tidal flow behaviour is considerably modified. As a result, the drag of the nacelle when Deltastream is in operation is probably much different than the drag highlighted in our study. A study with the blades in operation could provide information on the drag of the overall water turbine and determine whether or not a modification of the nacelle shape is greatly needed.

REFERENCES

1. Department of trade and industry (2007), Meeting the energy challenge: a white paper on energy, .

2. White, F. (2002), *Fluid Mechanics,* Fifth ed, McGraw-Hill, USA.

3. Boyle, G. (2004), *Renewable Energy Power for a Sustainable Future,* 2nd edition ed, Oxford University Press, Oxford, UK.

4. Manwell, J., McGowan, J. and Rogers, A. (2002), *Wind energy explained: Theory, Design and application,* Wiley-Blackwell.

5. Lemonis, G. (2004), "Wave and Tidal Energy Conversion", in Cutler J. Cleveland (ed.) *Encyclopedia of Energy,* Elsevier, New York, pp. 385-396.

6. Mustoe, J. (1984), *An atlas of renewable energy resources in the United Kingdom and North America,* John Wiley & Sons.

7. Owen, A. (2008), "Tidal Current Energy: Origins and Challenges", in Trevor M. Letcher (ed.) *Future Energy,* Elsevier, Oxford, pp. 111-128.

8. Charlier, R. H. (2003), "A “sleeper” awakes: tidal current power", *Renewable and Sustainable Energy Reviews,* vol. 7, no. 6, pp. 515-529.

9. Hardisty, J. (2009), *The analysis of tidal stream power,* Elsevier.

10. Bryden, I. G. (2004), "Tidal Energy", in Cutler J. Cleveland (ed.) *Encyclopedia of Energy,* Elsevier, New York, pp. 139-150.

11. Baker, C. (1991), "Tidal power", *Energy Policy,* vol. 19, no. 8, pp. 792-797.

12. Bryden, I. G. (2001), "Tidal Power Systems", in Robert A. Meyers (ed.) *Encyclopedia of Physical Science and Technology,* Academic Press, New York, pp. 751-761.

13. Hughes, F. and Brighton, J. (1999), *Fluid Dynamics, third edition,* McGraw Hill.

14. Douglas, J., Gasionek, J., Swaffield, J. and Jack, L. (2005), *Fluid mechanics, fifth edition,* Pearson Prentice Hall.

15. Prandtl, L. and Tietjens, O. G. (1934), *Applied Hydro- and Aeromechanics,* First edition ed, McGraw-Hill Book Company, inc, New York, USA.

16. Prandtl, L. and Tietjens, O. G. (1934), *Fundamentals of Hydro- and Aeromechanics,* First edition ed, McGraw-Hill Book Company, New York, USA.

17. Triton, D. J. (1982), *Physical fluid dynamics,* Van Nostrand Reinhold.

18. Hoerner, S. (1951), *Aerodynamic drag : Practical Data on aerodynamic drag evaluated and presented by Sighard F. Hoerner,* First edition ed, Hoerner S., Dayton, Ohio, USA.

19. Hirsch, C. (2007), *Numerical computationof external and internal flows Vol.1: The fundamentals of computational fluid dynamics,* Butterworth-Heinemann.

20. Tu, J., Heng Yeoh, G. and Liu, C. (2008), *Computational Fluid Dynamics : A practical Approach,* 1st edition ed, Elsevier, United States of America.

21. Shaw, C. T. (1992), *Using computational fluid dynamics,* Prentice Hall.

22. Ong, M. C., Utnes, T., Holmedal, L. E., Myrhaug, D. and Pettersen, B. (2009), "Numerical simulation of flow around a smooth circular cylinder at very high Reynolds numbers", *Marine Structures,* vol. 22, no. 2, pp. 142-153.

23. Catalano, P., Wang, M., Iaccarino, G. and Moin, P. (2003), "Numerical simulation of the flow around a circular cylinder at high Reynolds numbers", *International Journal of Heat and Fluid Flow,* vol. 24, no. 4, pp. 463-469.

24. Singh, S.P. and Mittal, S., (2005), *Flow past a cylinder: shear layer instability and drag crisis*, - John Wiley & Sons, Ltd.

25. Launder, B. E. and Spalding, D. B. (1972), *Mathematical models of turbulence,* Academic Press, London.

26. Launder, B. E. and Spalding, D. B. (1974), "The numerical computation of turbulent flows", *Comp. Meth. Appl. Mechanical engineering,* vol. Vol.3.

27. Tutar, M. and Holdø, A.E., (2001), *Computational modelling of flow around a circular cylinder in sub-critical flow regime with various turbulence models*, - John Wiley & Sons, Ltd.

28. Roshko, A. (1960), Experiments on the flow past a circular cylinder at very high Reynolds number, GALCIT/P-497, Guggenheim Aeronautics Laboratory (California Institute of Technology), Pasadena, California, USA.

APPENDICES.

Appendix A 2D cross section study

A.1 Original shape

A.1.1 Drag coefficient history

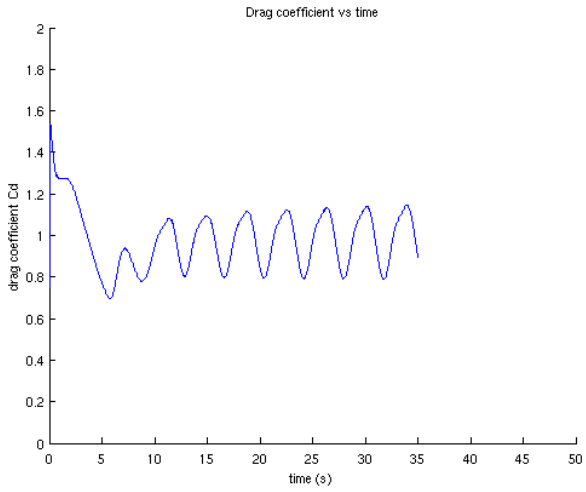

A.1.2 Lift coefficient history

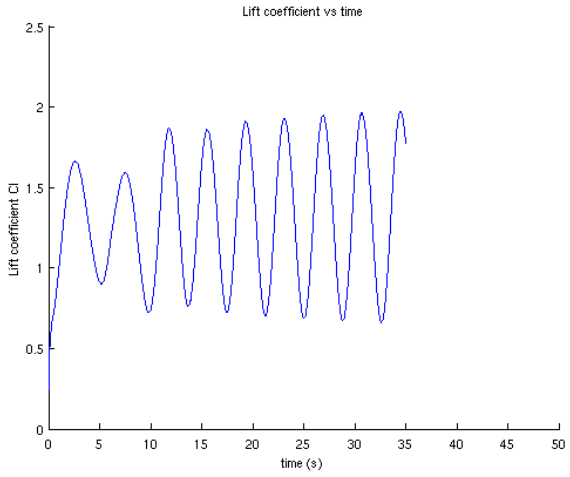

A.1.3 Pressure coefficient

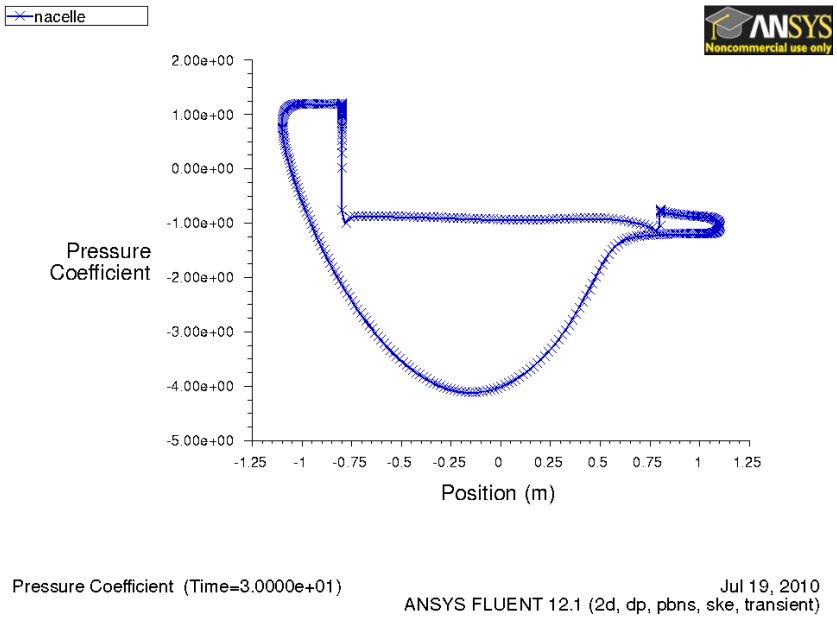

A.1.4 Skin friction coefficient

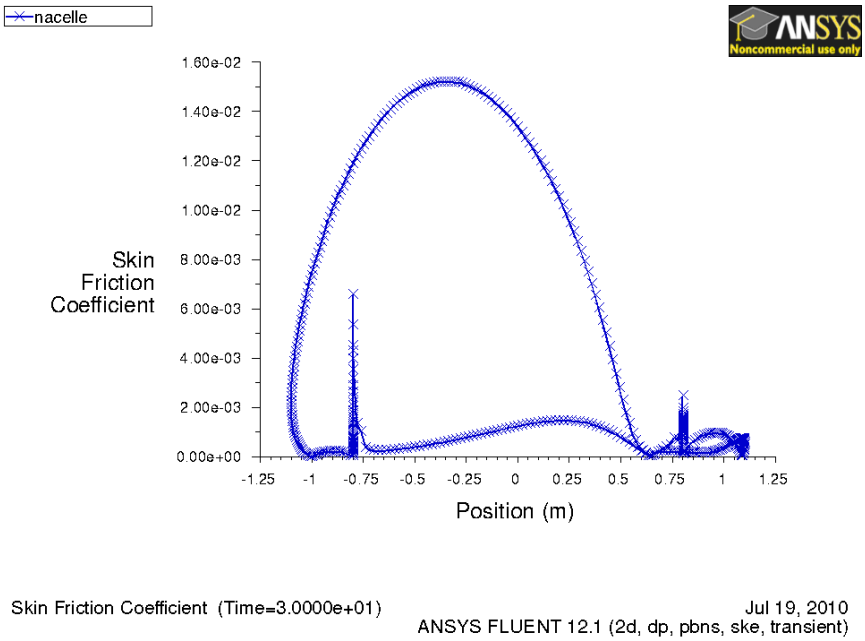

A.1.5 Contour of static pressure

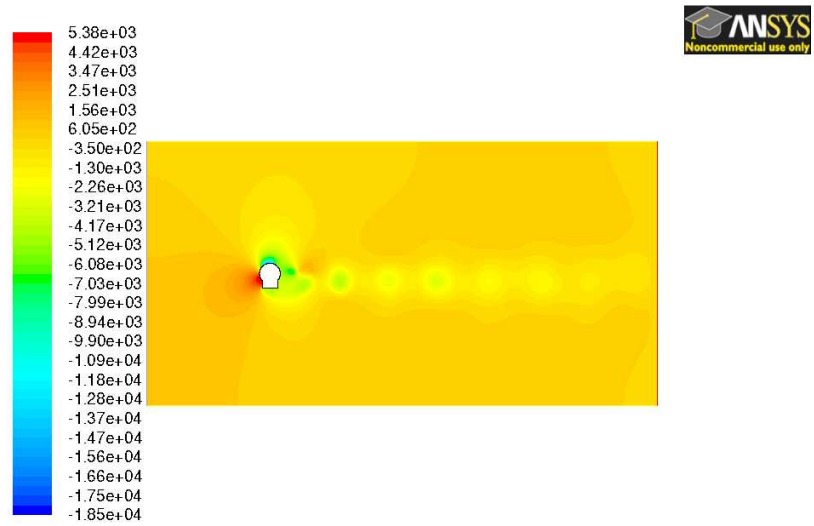

Contours of Static Pressure (pascal) (Time=3.0000e+01) Jul 19, 2010
ANSYS FLUENT 12.1 (2d, dp, pbns, ske, transient)

A.1.6 Turbulence intensity

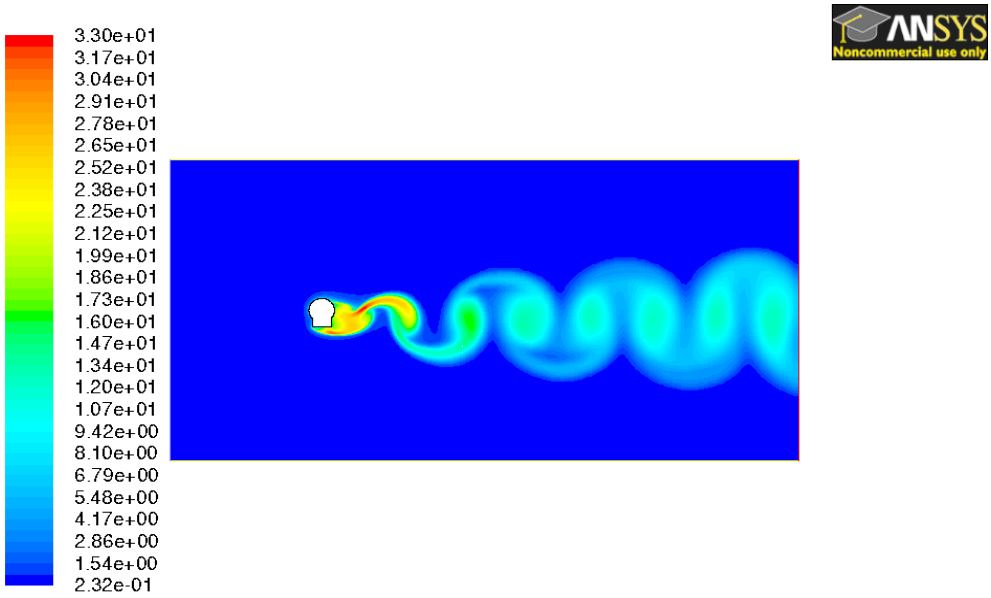

Contours of Turbulent Intensity (%) (Time=3.0000e+01) Jul 19, 2010
ANSYS FLUENT 12.1 (2d, dp, pbns, ske, transient)

A.1.7 Velocity vectors

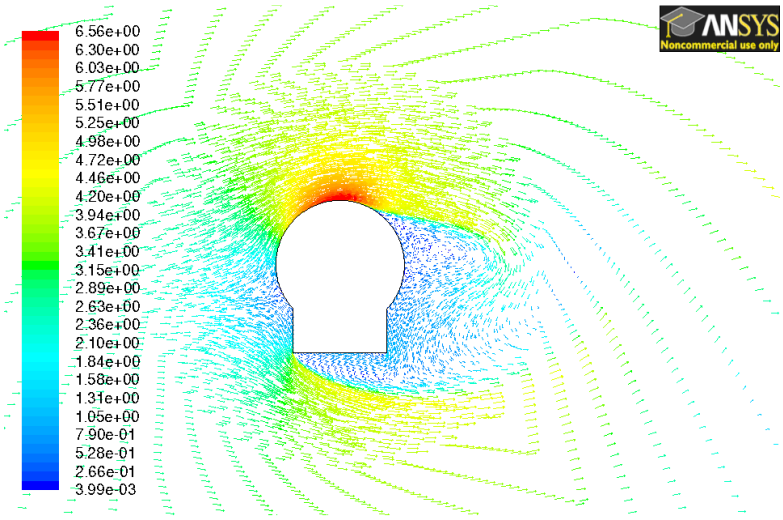

Velocity Vectors Colored By Velocity Magnitude (m/s) (Time=3.0000e+01) Jul 19, 2010
ANSYS FLUENT 12.1 (2d, dp, pbns, ske, transient)

A.1.8 Contours of velocity magnitude

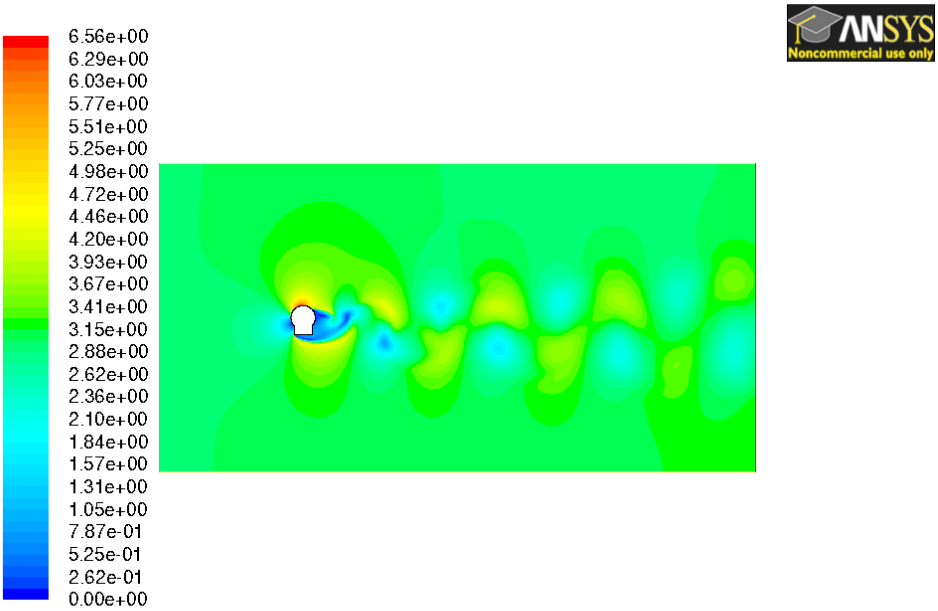

Contours of Velocity Magnitude (m/s) (Time=3.0000e+01) Jul 19, 2010
ANSYS FLUENT 12.1 (2d, dp, pbns, ske, transient)

A.2 Elliptical cross section

A.2.1 Drag coefficient history

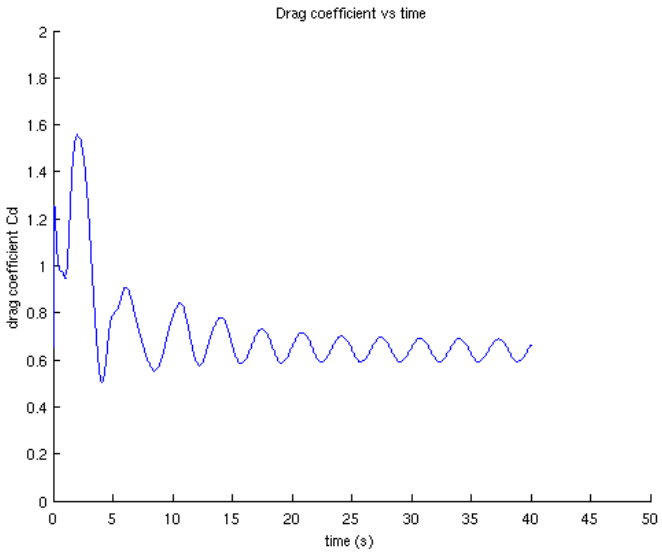

A.2.2 Lift coefficient history

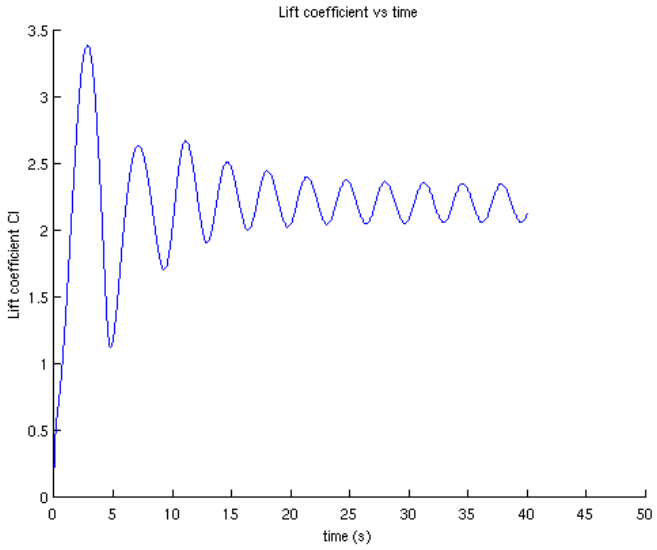

A.2.3 Pressure coefficient

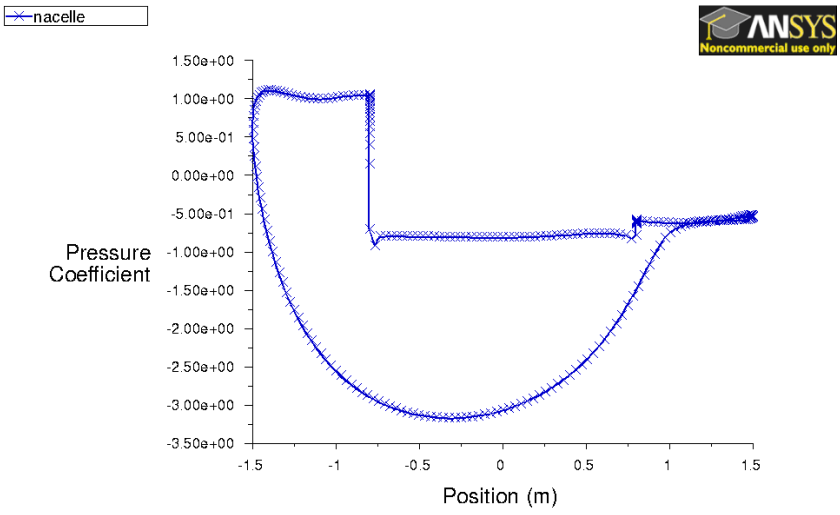

A.2.4 Skin friction coefficient

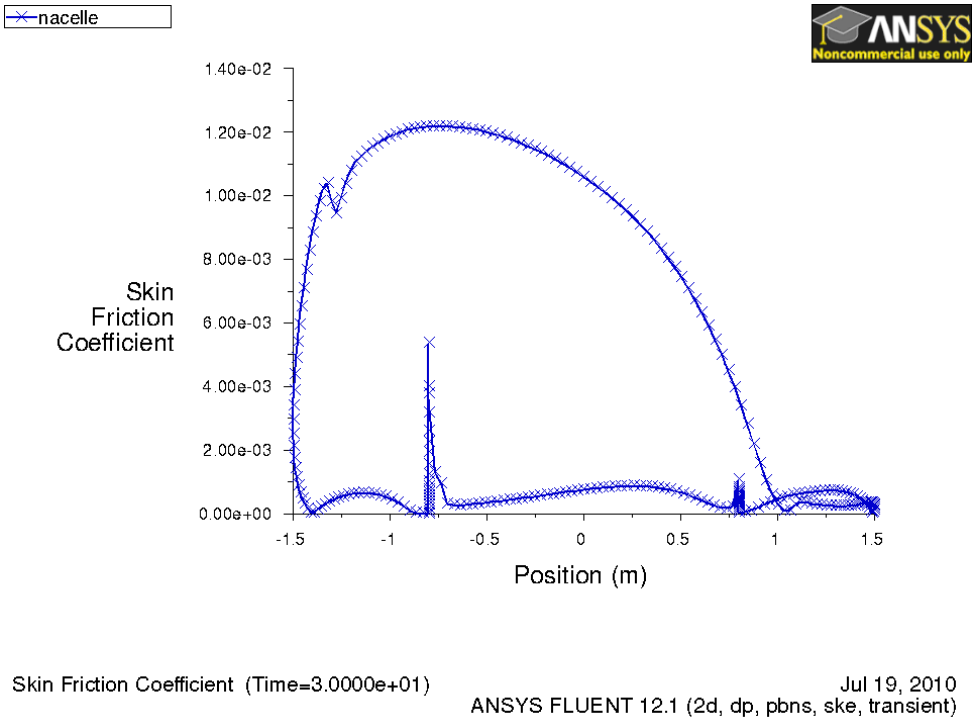

A.2.5 Contour of static pressure

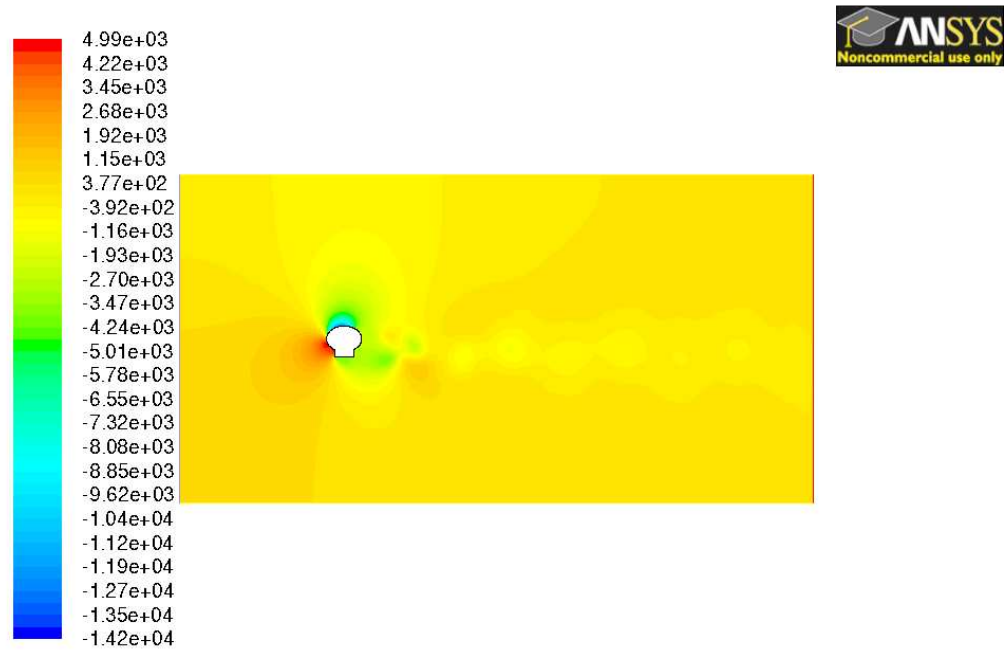

Contours of Static Pressure (pascal) (Time=3.0000e+01) Jul 19, 2010
ANSYS FLUENT 12.1 (2d, dp, pbns, ske, transient)

A.2.6 Turbulence intensity

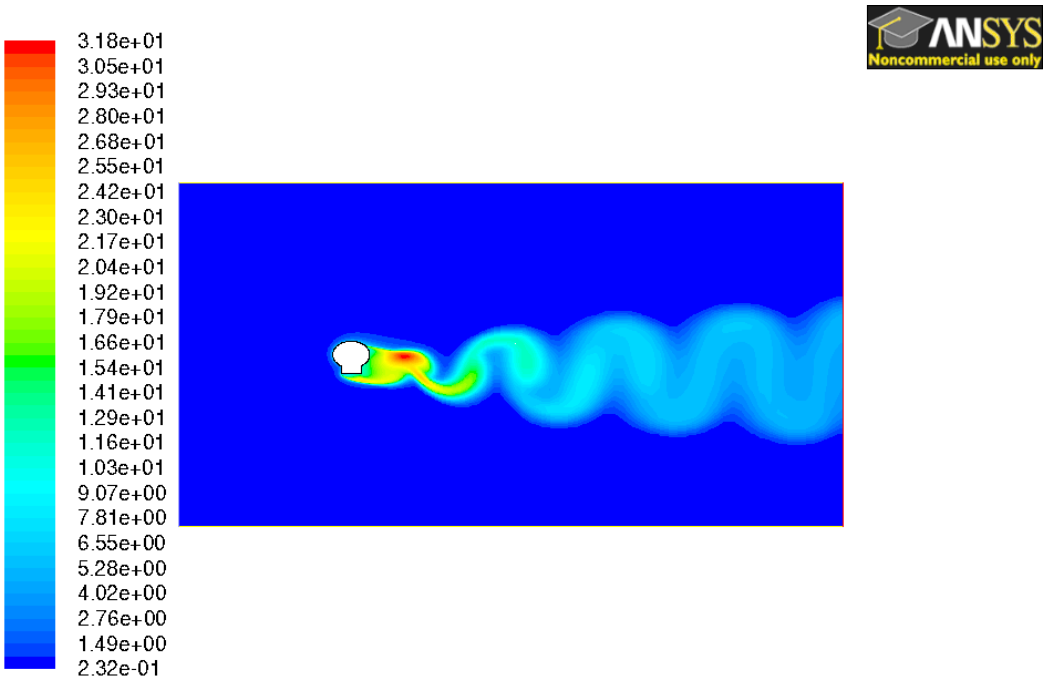

Contours of Turbulent Intensity (%) (Time=3.0000e+01) Jul 19, 2010
ANSYS FLUENT 12.1 (2d, dp, pbns, ske, transient)

A.2.7 Velocity vectors

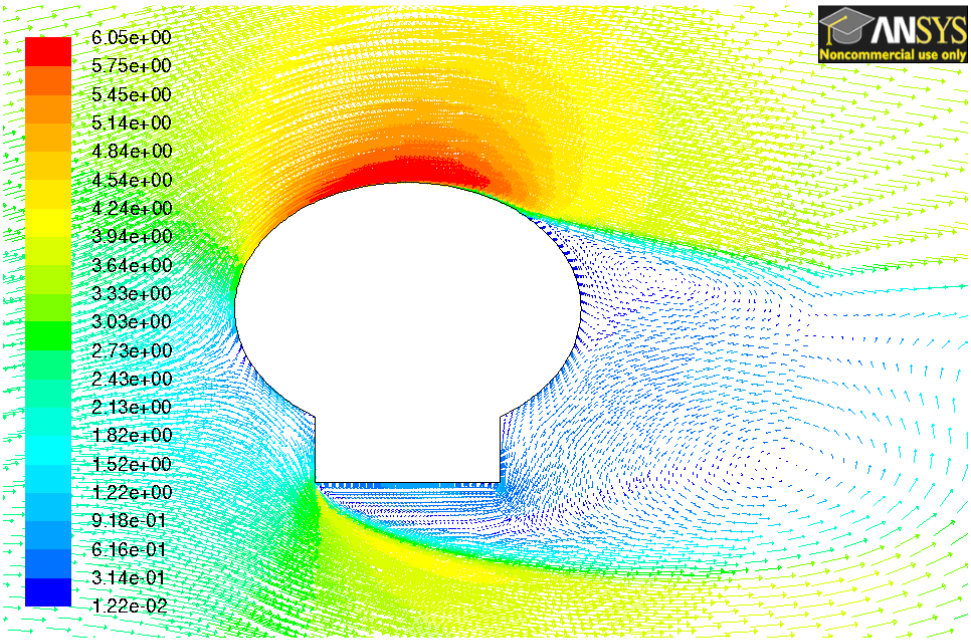

Velocity Vectors Colored By Velocity Magnitude (m/s) (Time=3.0000e+01) Jul 19, 2010
ANSYS FLUENT 12.1 (2d, dp, pbns, ske, transient)

A.2.8 Contours of velocity magnitude

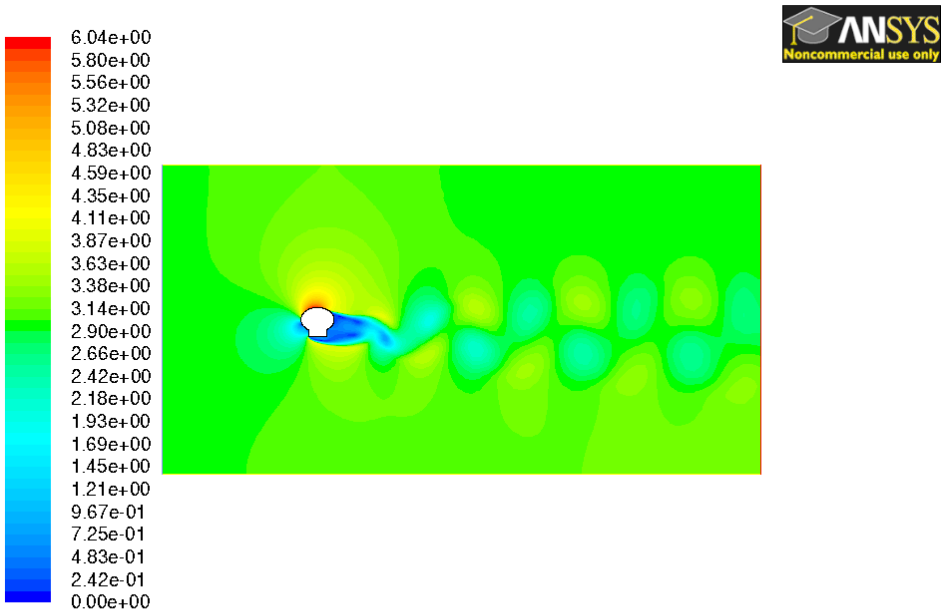

Contours of Velocity Magnitude (m/s) (Time=3.0000e+01) Jul 19, 2010
ANSYS FLUENT 12.1 (2d, dp, pbns, ske, transient)

A.3 Cross section shape B

A.3.1 Drag coefficient history

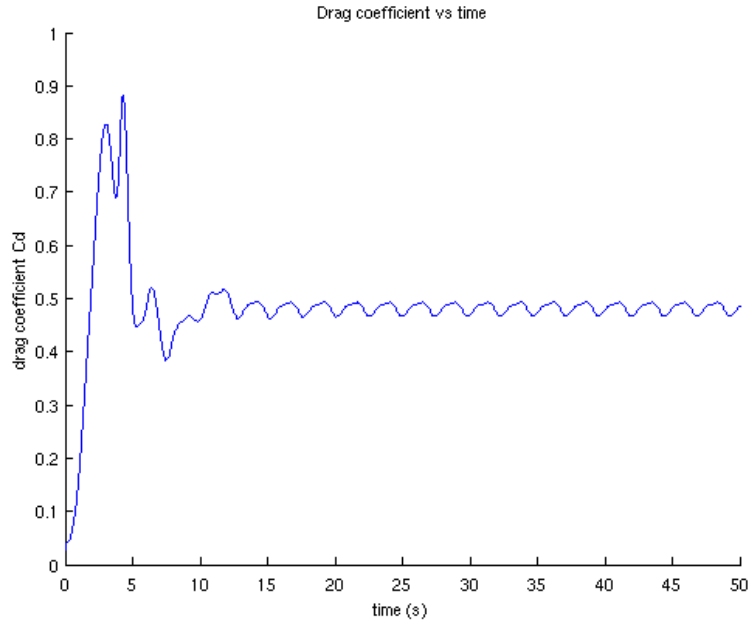

A.3.2 Lift coefficient history

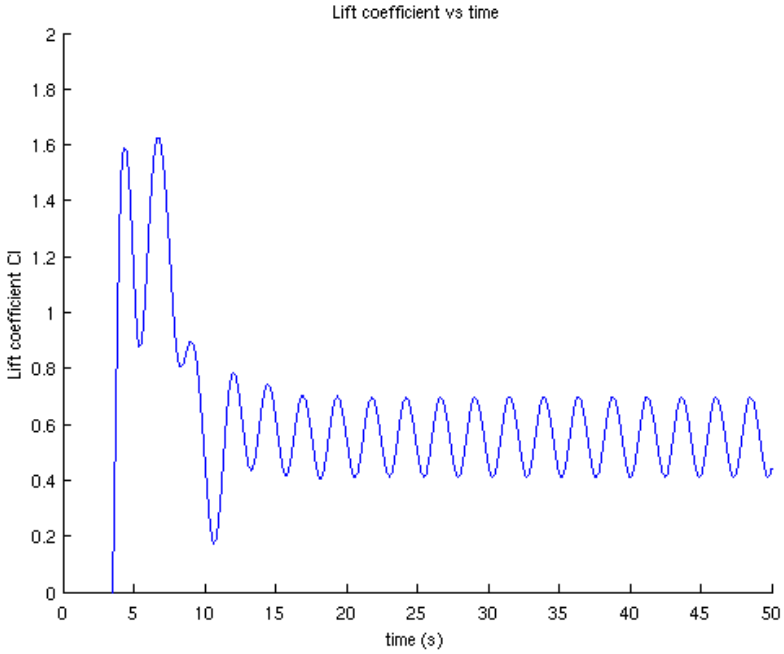

A.3.3 Pressure coefficient

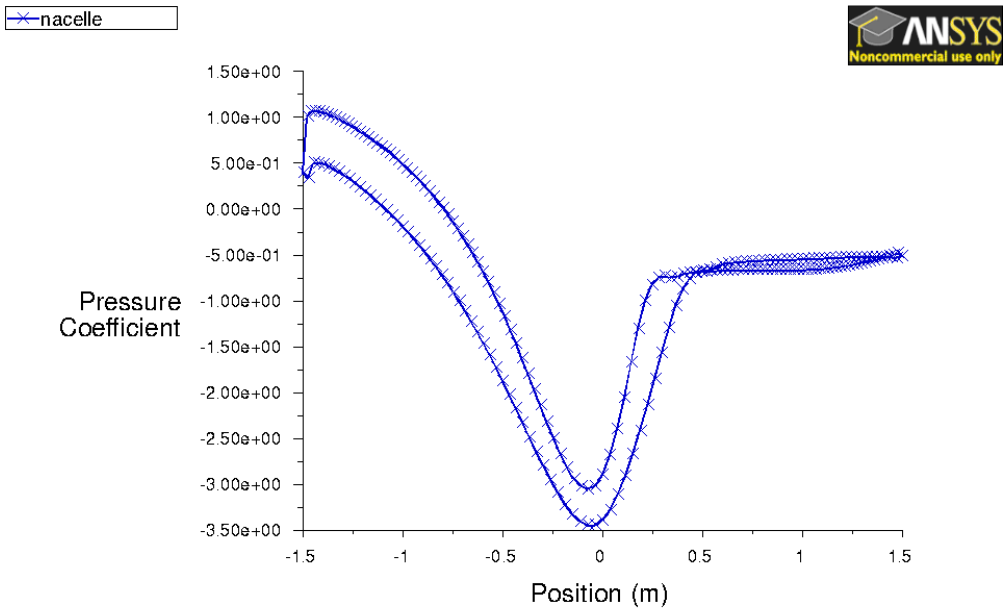

A.3.4 Skin friction coefficient

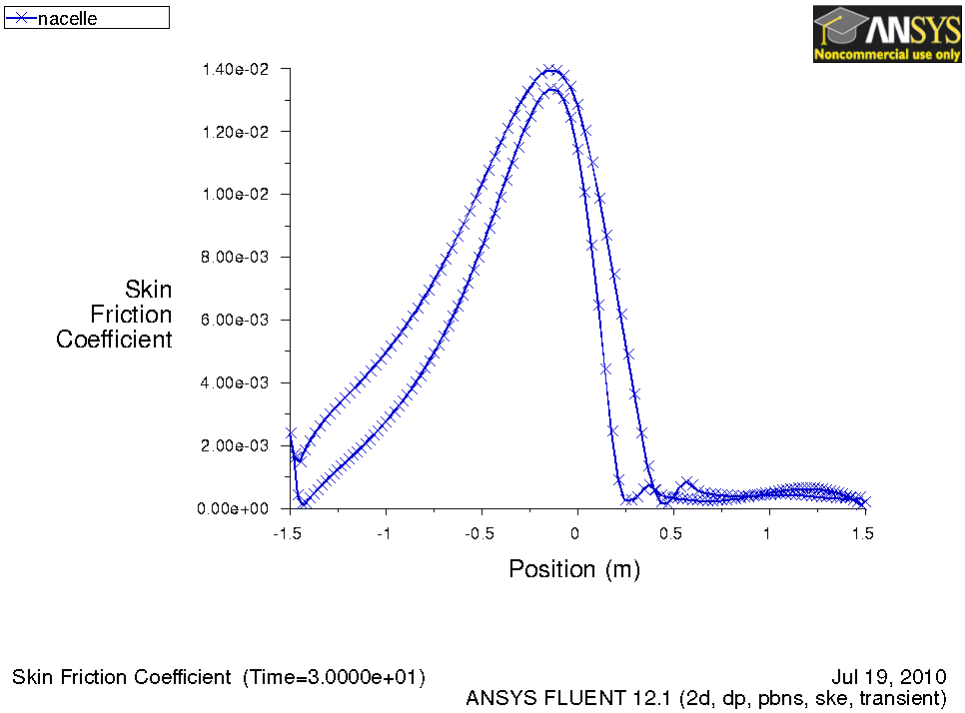

A.3.5 Contour of static pressure

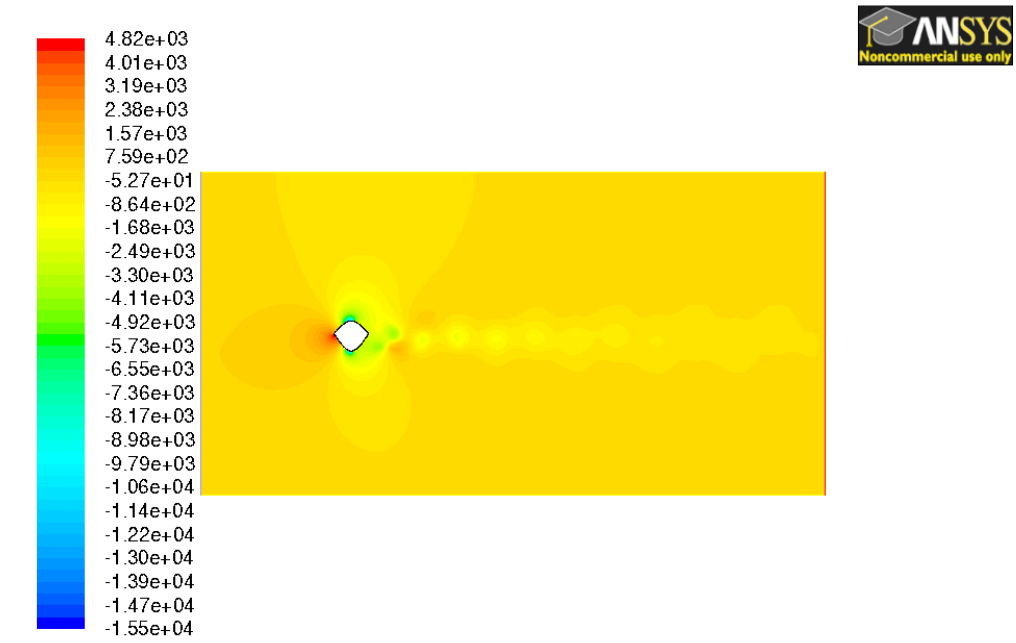

Contours of Static Pressure (pascal) (Time=3.0000e+01) Jul 19, 2010
ANSYS FLUENT 12.1 (2d, dp, pbns, ske, transient)

A.3.6 Turbulence intensity

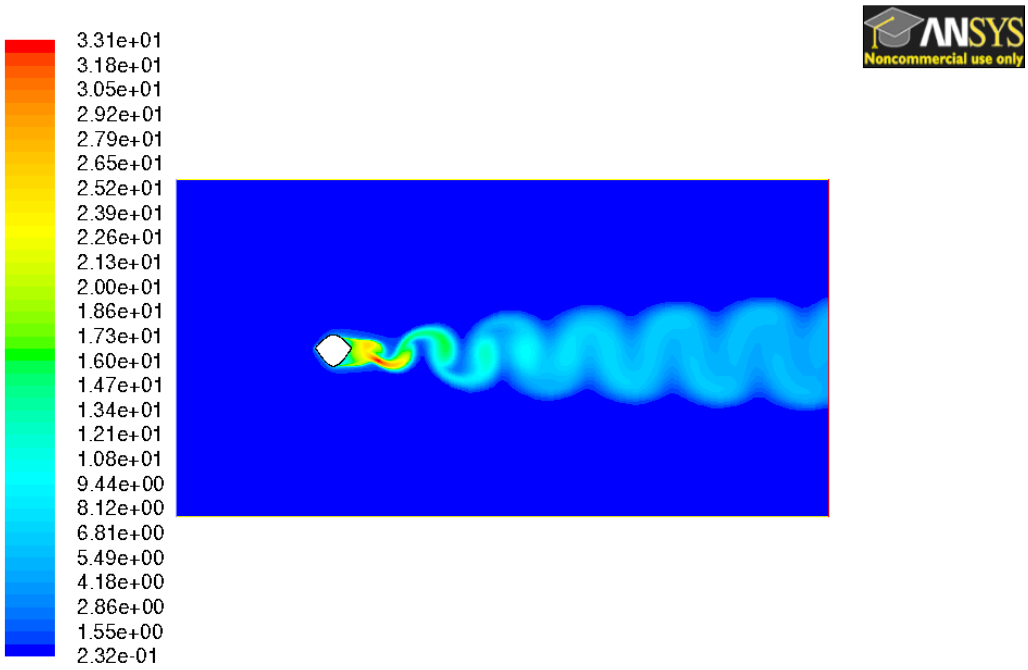

Contours of Turbulent Intensity (%) (Time=3.0000e+01) Jul 19, 2010
ANSYS FLUENT 12.1 (2d, dp, pbns, ske, transient)

A.3.7 Velocity vectors

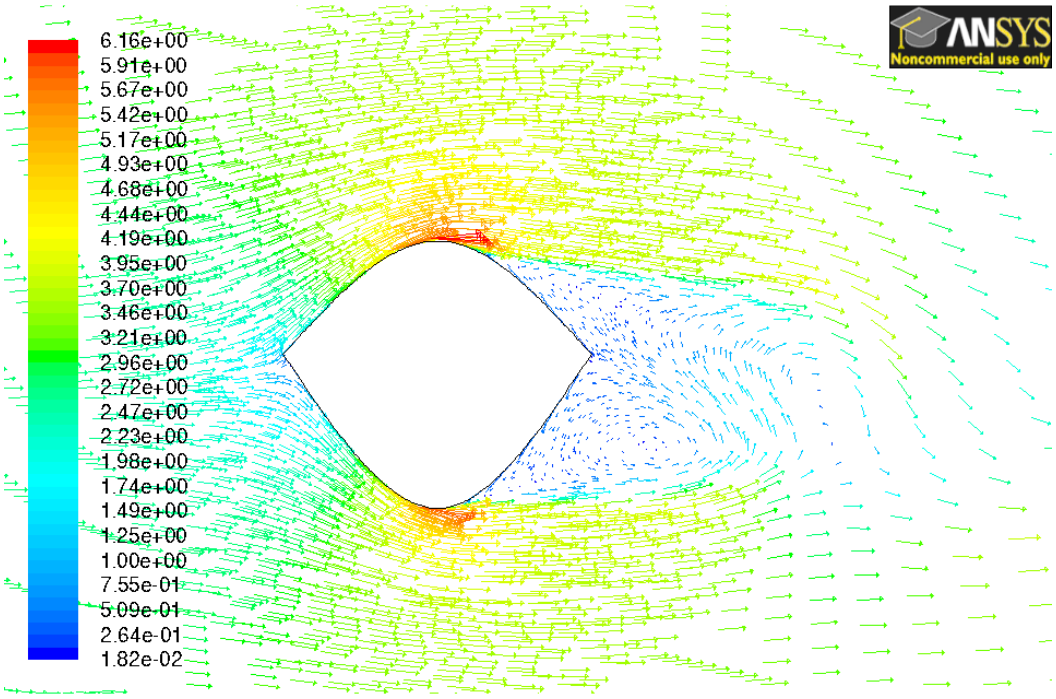

Velocity Vectors Colored By Velocity Magnitude (m/s) (Time=3.0000e+01) Jul 19, 2010
ANSYS FLUENT 12.1 (2d, dp, pbns, ske, transient)

A.3.8 Contours of velocity magnitude

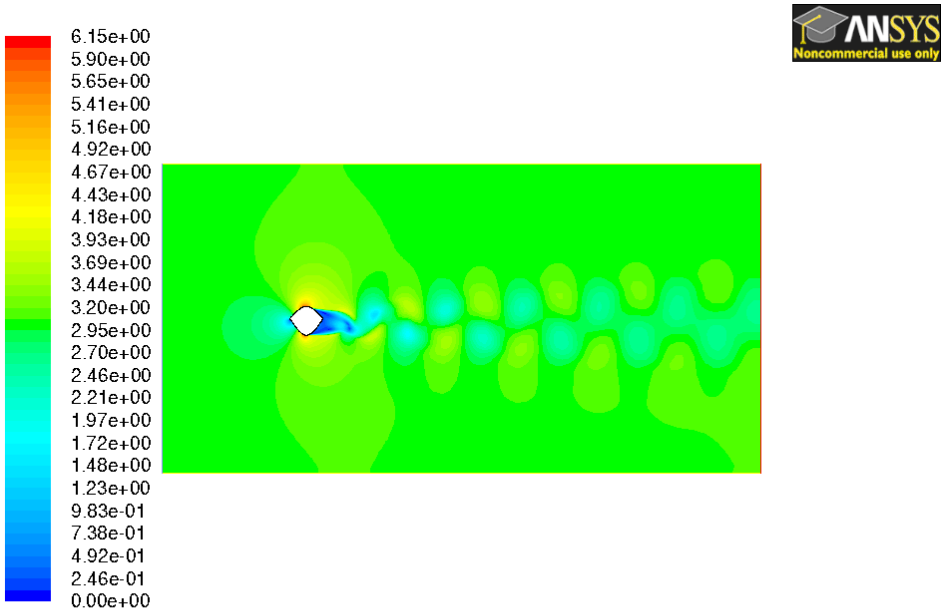

Contours of Velocity Magnitude (m/s) (Time=3.0000e+01) Jul 19, 2010
ANSYS FLUENT 12.1 (2d, dp, pbns, ske, transient)

A.4 Cross section shape D

A.4.1 Drag coefficient history

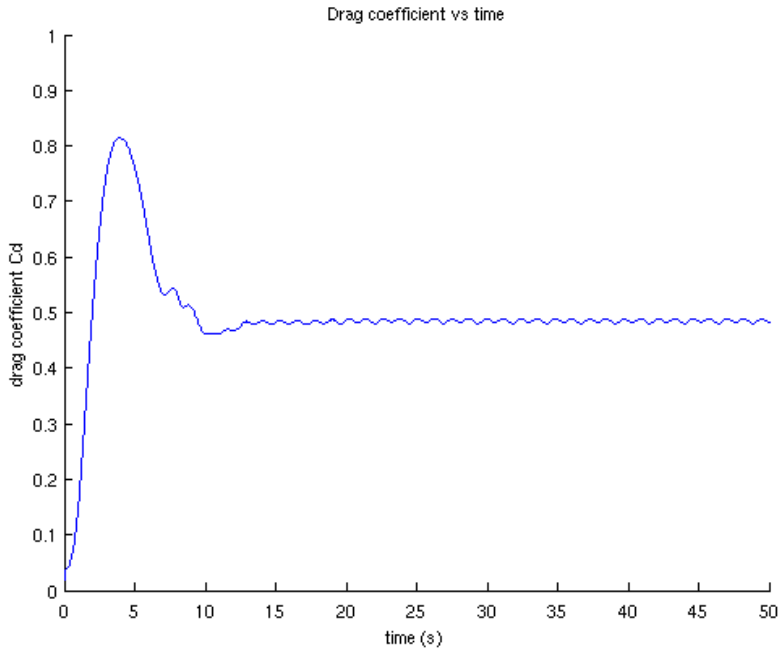

A.4.2 Lift coefficient history

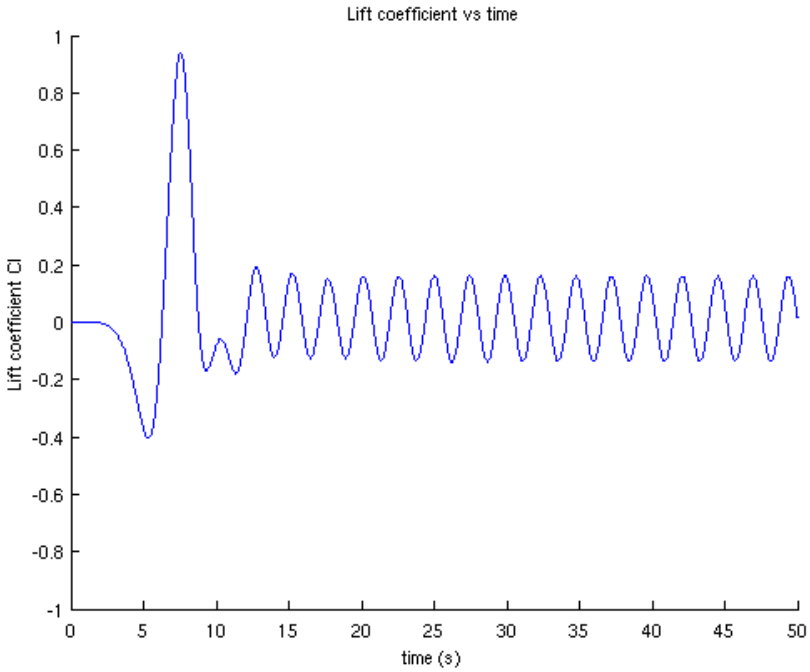

A.4.3 Pressure coefficient

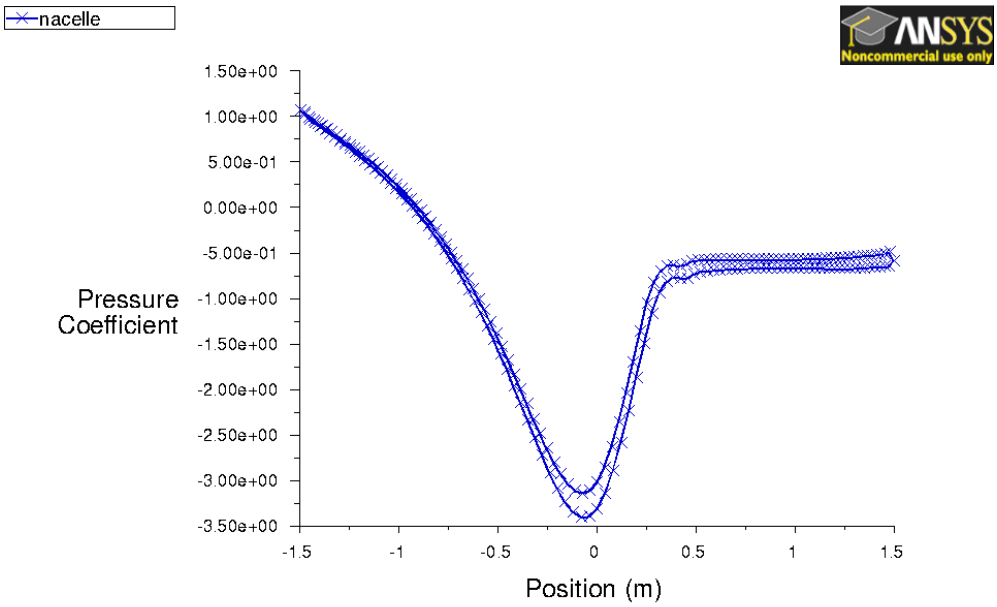

Pressure Coefficient (Time=3.0000e+01)

Jul 19, 2010
ANSYS FLUENT 12.1 (2d, dp, pbns, ske, transient)

A.4.4 Skin friction coefficient

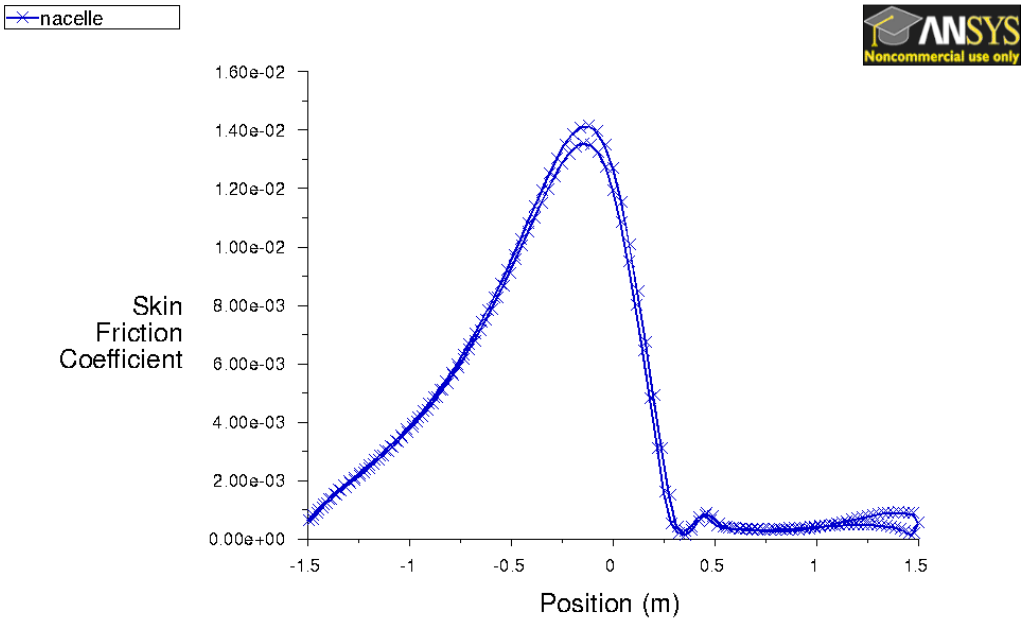

Skin Friction Coefficient (Time=3.0000e+01)

Jul 19, 2010
ANSYS FLUENT 12.1 (2d, dp, pbns, ske, transient)

A.4.5 Contour of static pressure

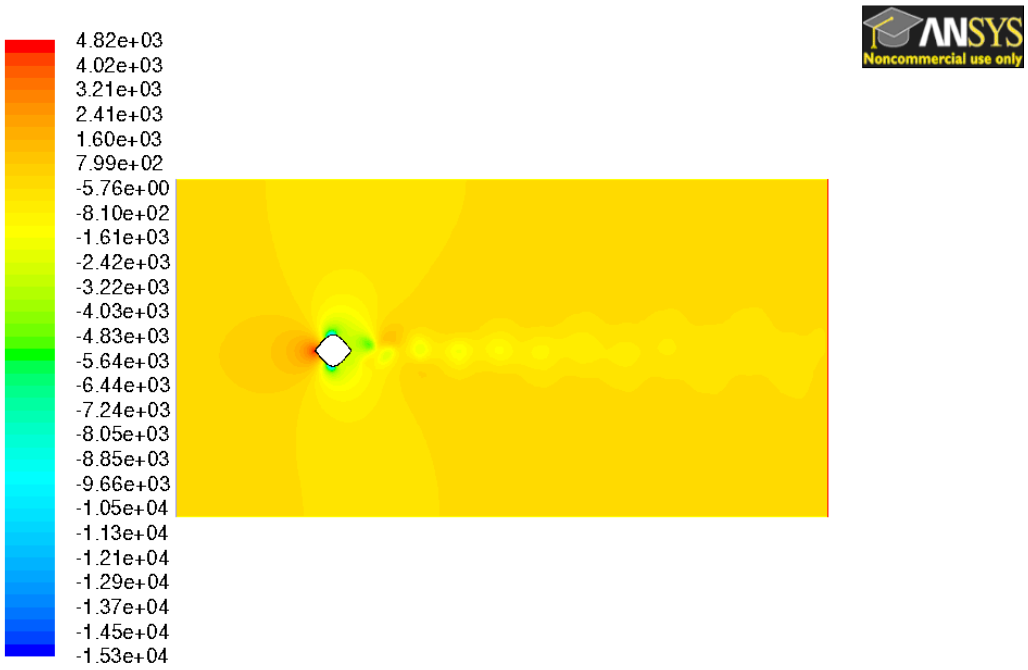

Contours of Static Pressure (pascal) (Time=3.0000e+01) Jul 19, 2010
ANSYS FLUENT 12.1 (2d, dp, pbns, ske, transient)

A.4.6 Turbulence intensity

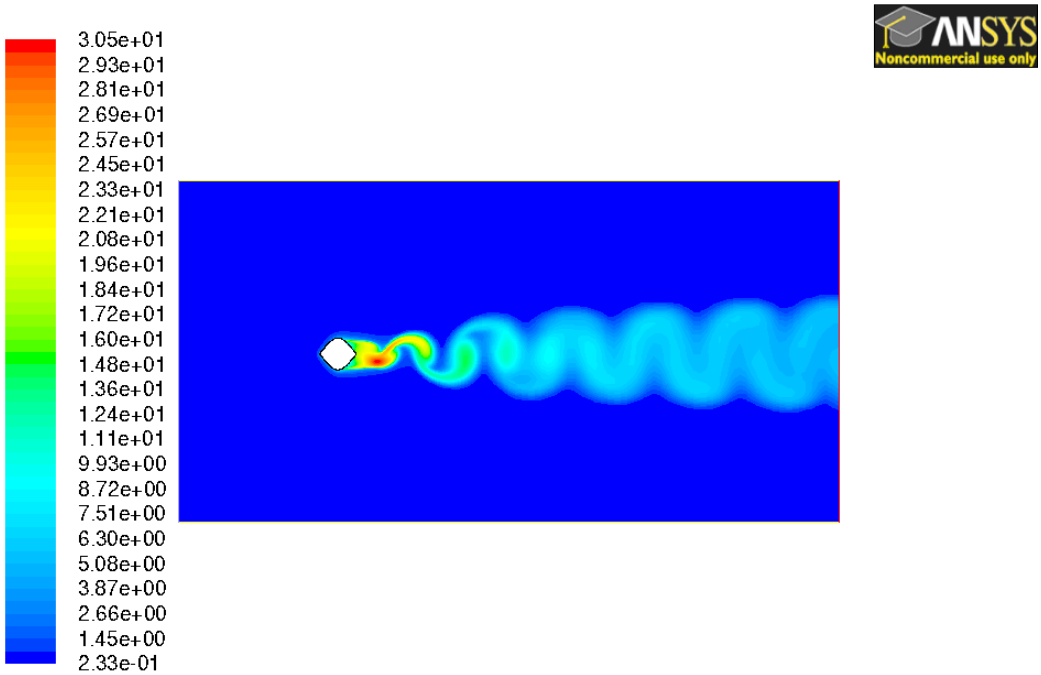

Contours of Turbulent Intensity (%) (Time=3.0000e+01) Jul 19, 2010
ANSYS FLUENT 12.1 (2d, dp, pbns, ske, transient)

A.4.7 Velocity vectors

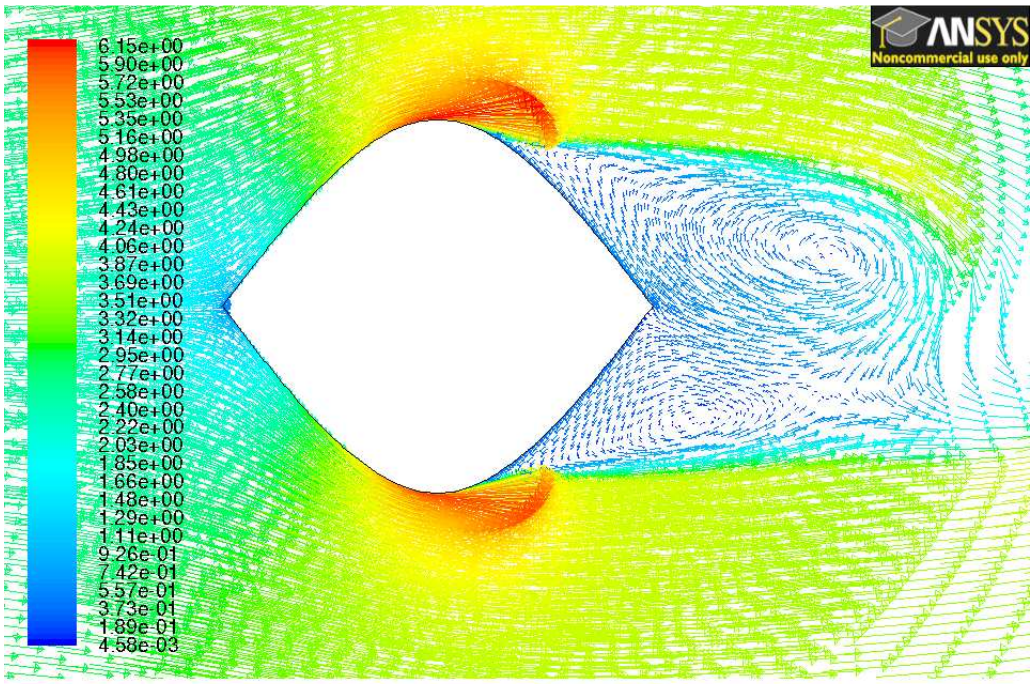

Velocity Vectors Colored By Velocity Magnitude (m/s) (Time=3.0000e+01) Jul 19, 2010
ANSYS FLUENT 12.1 (2d, dp, pbns, ske, transient)

A.4.8 Contours of velocity magnitude

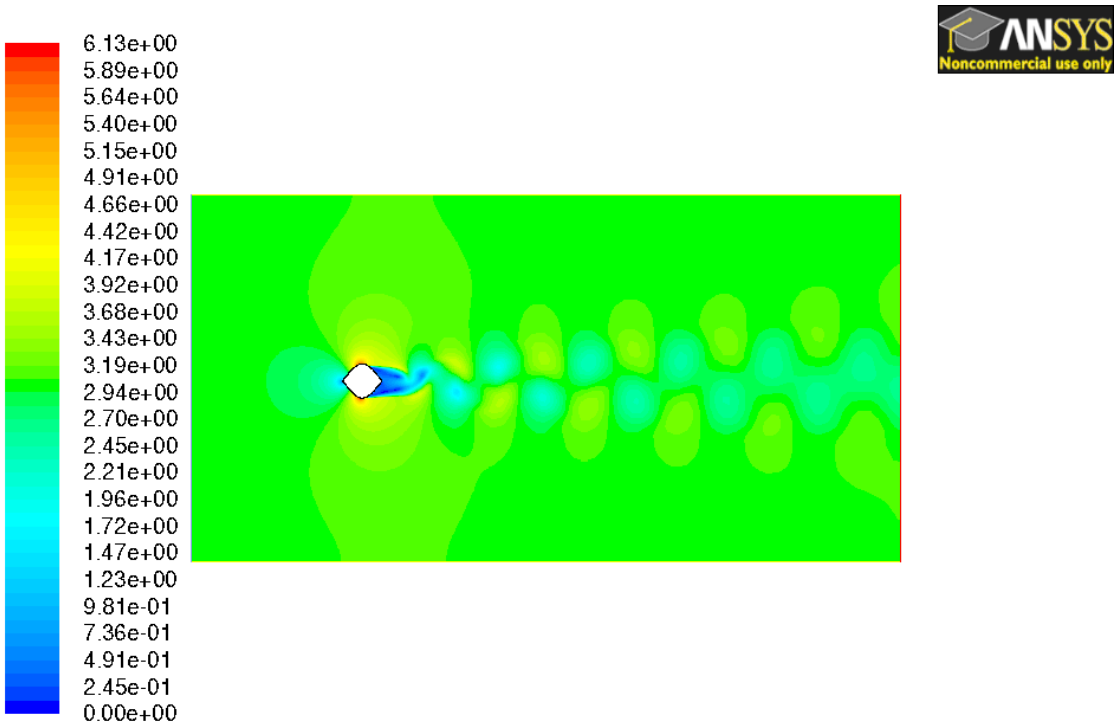

Contours of Velocity Magnitude (m/s) (Time=3.0000e+01) Jul 19, 2010
ANSYS FLUENT 12.1 (2d, dp, pbns, ske, transient)

A.5 Cross section shape F

A.5.1 Drag coefficient history

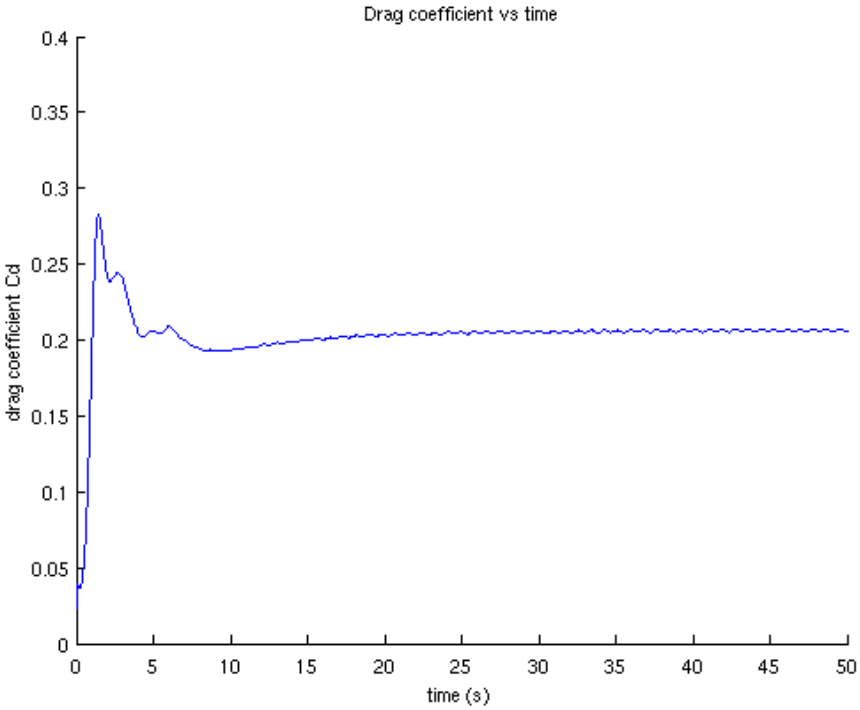

A.5.2 Lift coefficient history

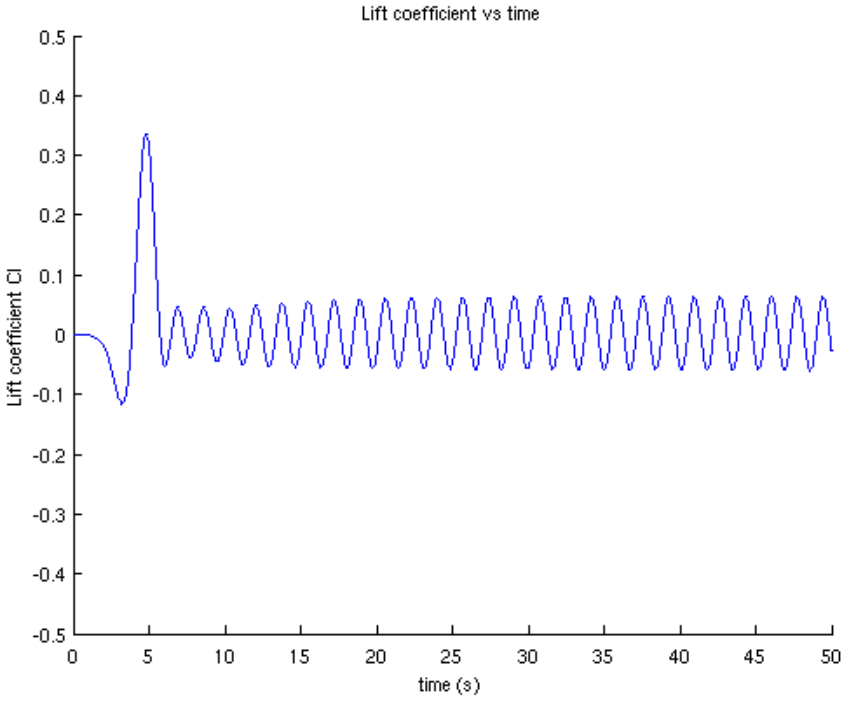

A.5.3 Pressure coefficient

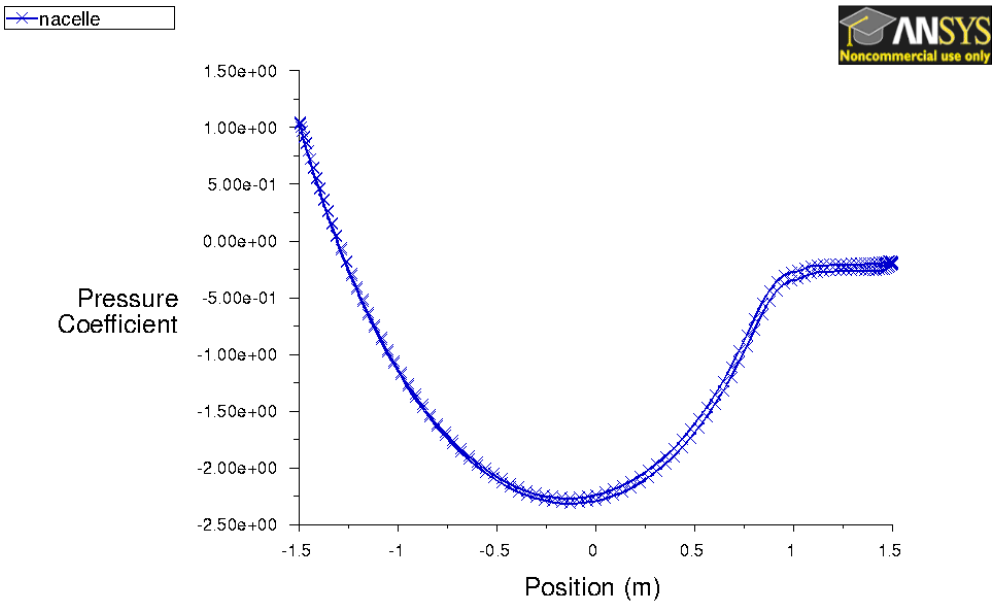

Pressure Coefficient (Time=3.0000e+01)

Jul 19, 2010
ANSYS FLUENT 12.1 (2d, dp, pbns, ske, transient)

A.5.4 Skin friction coefficient

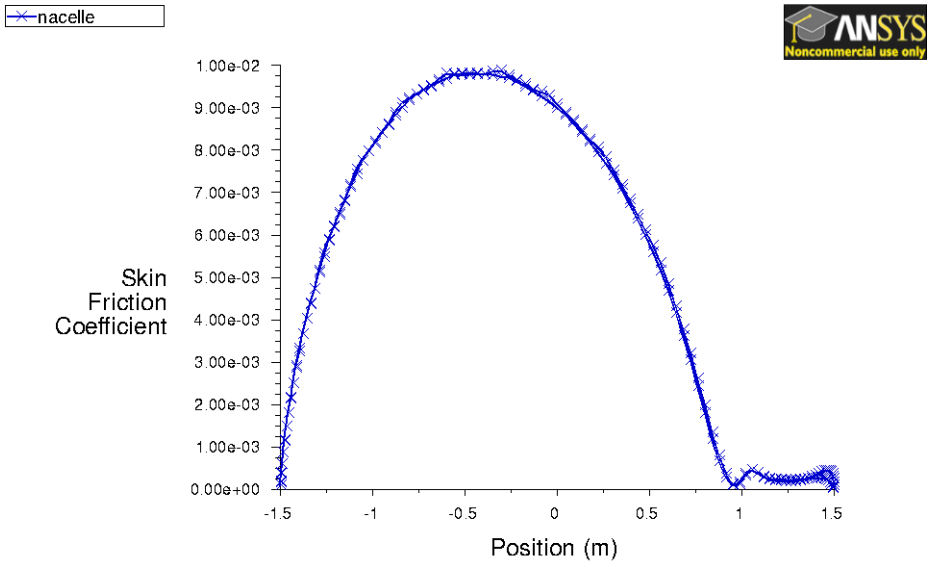

Skin Friction Coefficient (Time=3.0000e+01)

Jul 19, 2010
ANSYS FLUENT 12.1 (2d, dp, pbns, ske, transient)

A.5.5 Contour of static pressure

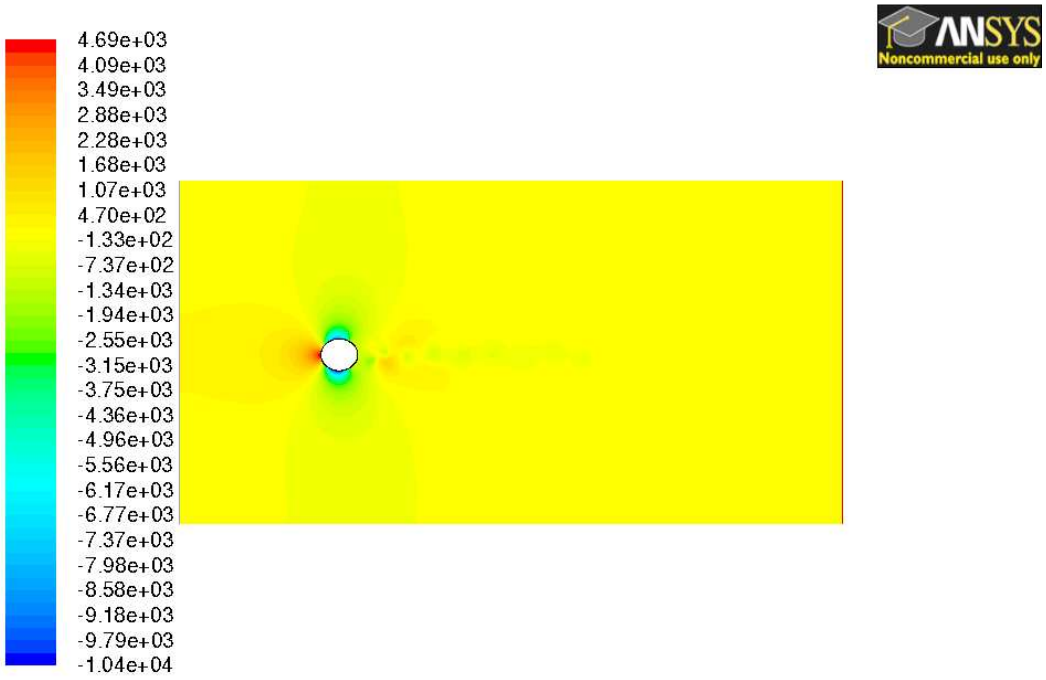

Contours of Static Pressure (pascal) (Time=3.0000e+01) Jul 19, 2010
ANSYS FLUENT 12.1 (2d, dp, pbns, ske, transient)

A.5.6 Turbulence intensity

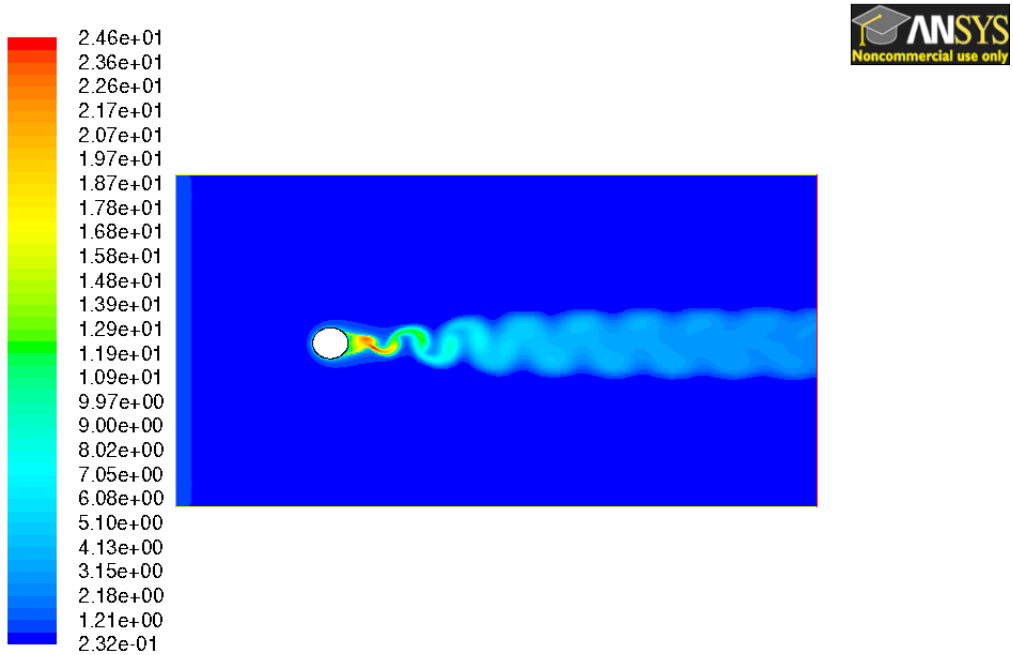

Contours of Turbulent Intensity (%) (Time=3.0000e+01) Jul 19, 2010
ANSYS FLUENT 12.1 (2d, dp, pbns, ske, transient)

A.5.7 Velocity vectors

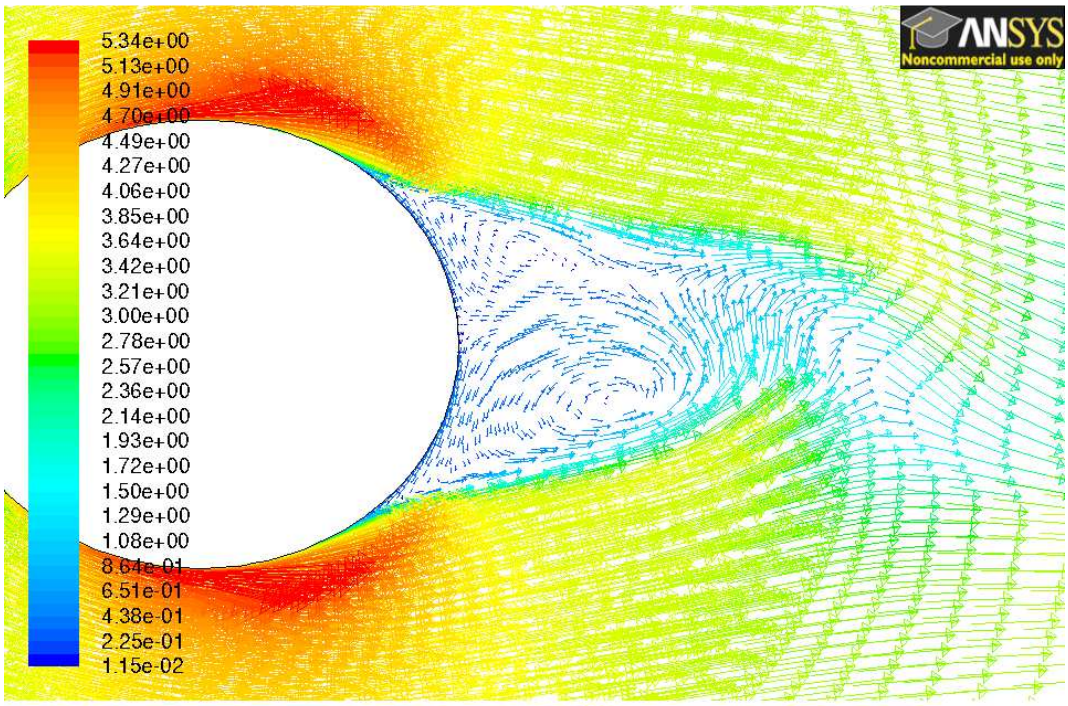

Velocity Vectors Colored By Velocity Magnitude (m/s) (Time=3.0000e+01) Jul 19, 2010
ANSYS FLUENT 12.1 (2d, dp, pbns, ske, transient)

A.5.8 Contours of velocity magnitude

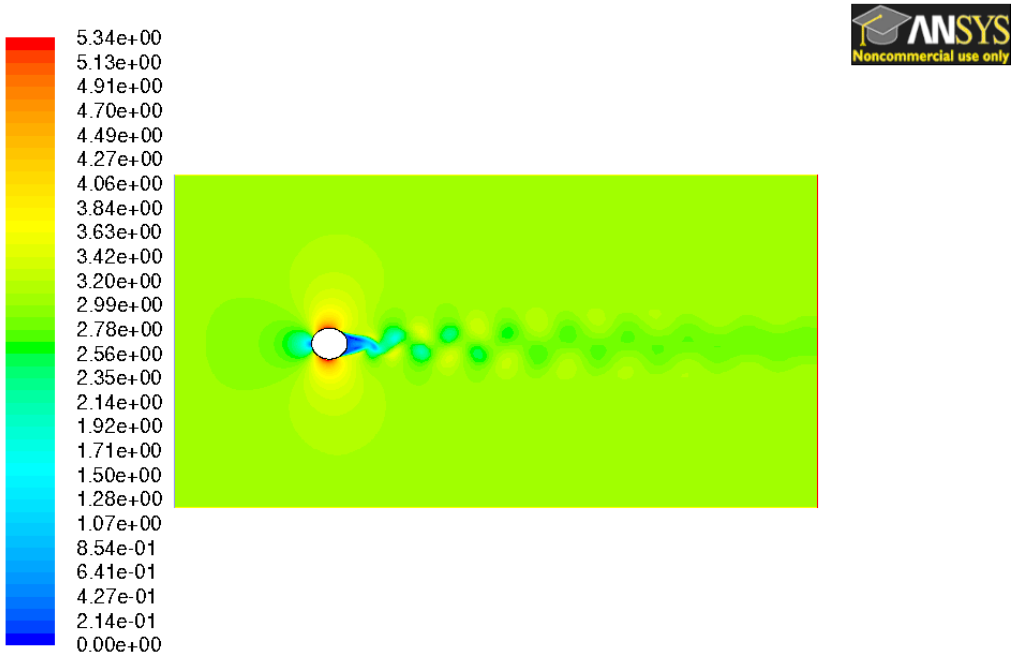

Contours of Velocity Magnitude (m/s) (Time=3.0000e+01) Jul 19, 2010
ANSYS FLUENT 12.1 (2d, dp, pbns, ske, transient)

Appendix B 2D Longitudinal section study

B.1 Original shape

B.1.1 Pressure coefficient

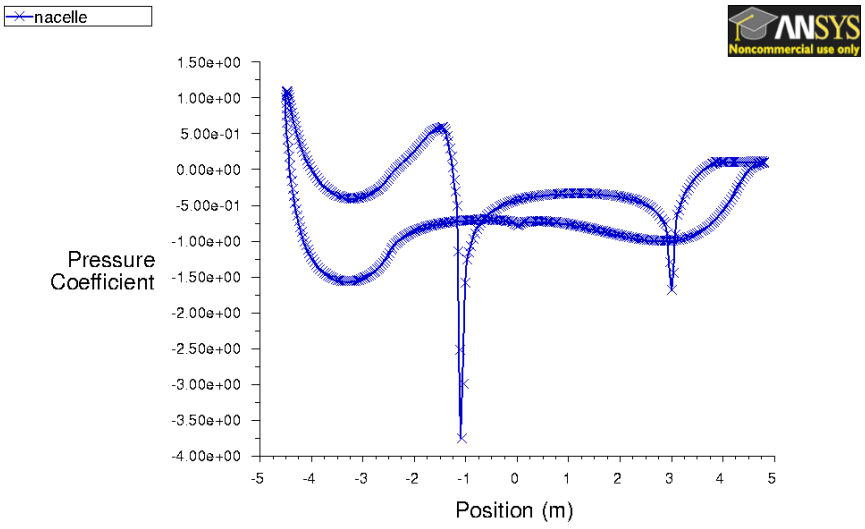

B.1.2 Contours of static pressure

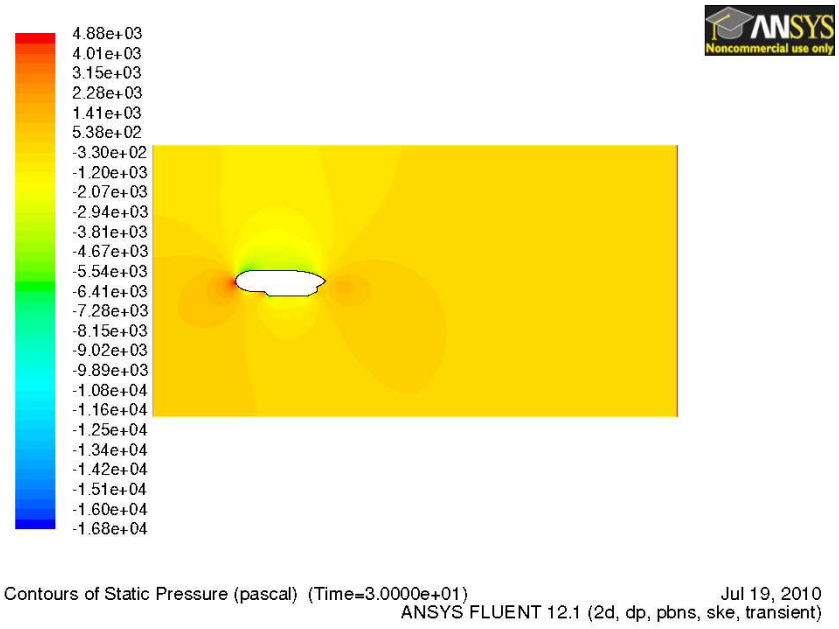

B.1.3 Contours of velocity magnitude

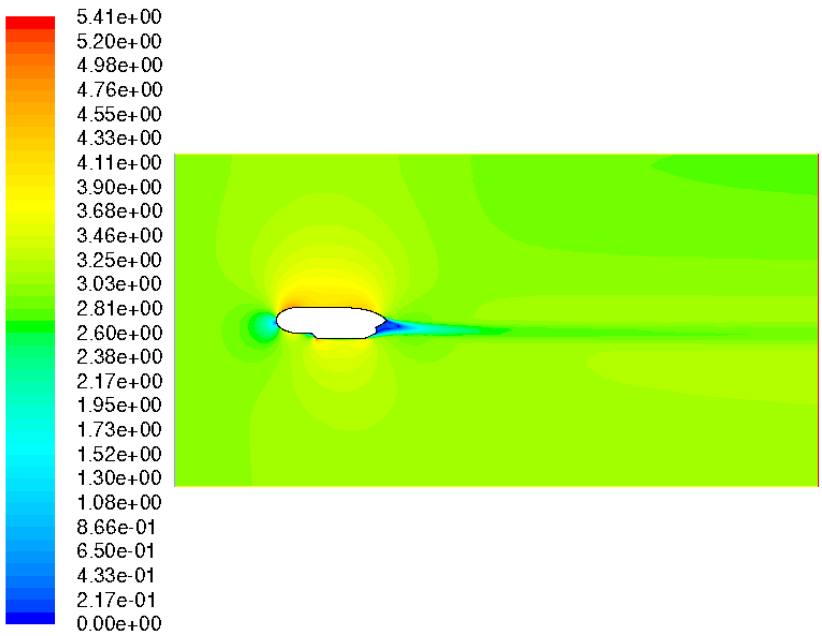

Contours of Velocity Magnitude (m/s) (Time=3.0000e+01) Jul 19, 2010
ANSYS FLUENT 12.1 (2d, dp, pbns, ske, transient)

B.2 Shape I

B.2.1 Pressure coefficient

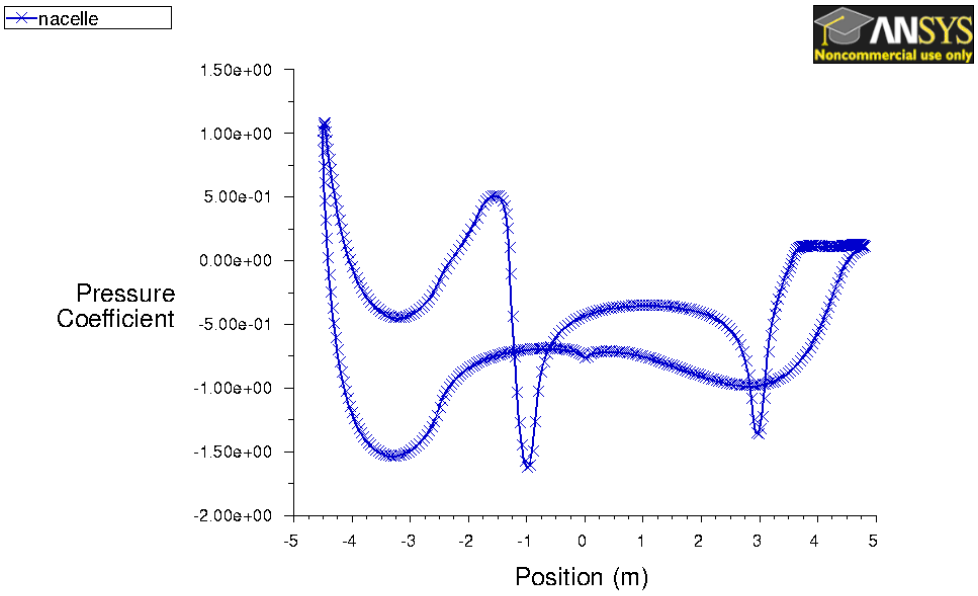

Pressure Coefficient (Time=2.8000e+01)

Jul 19, 2010
ANSYS FLUENT 12.1 (2d, dp, pbns, ske, transient)

B.2.2 Contours of static pressure

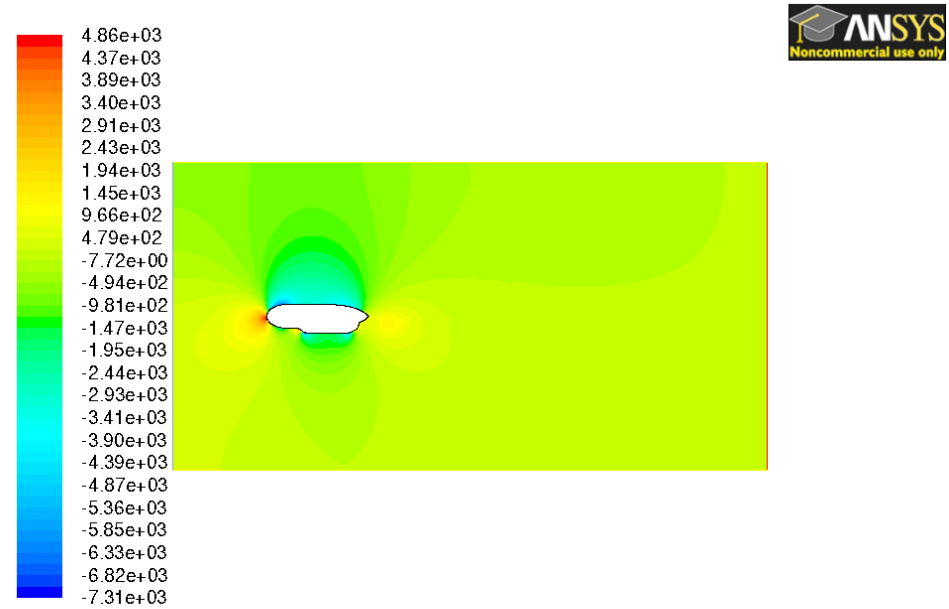

Contours of Static Pressure (pascal) (Time=2.8000e+01)

Jul 19, 2010
ANSYS FLUENT 12.1 (2d, dp, pbns, ske, transient)

B.2.3 Contours of velocity magnitude

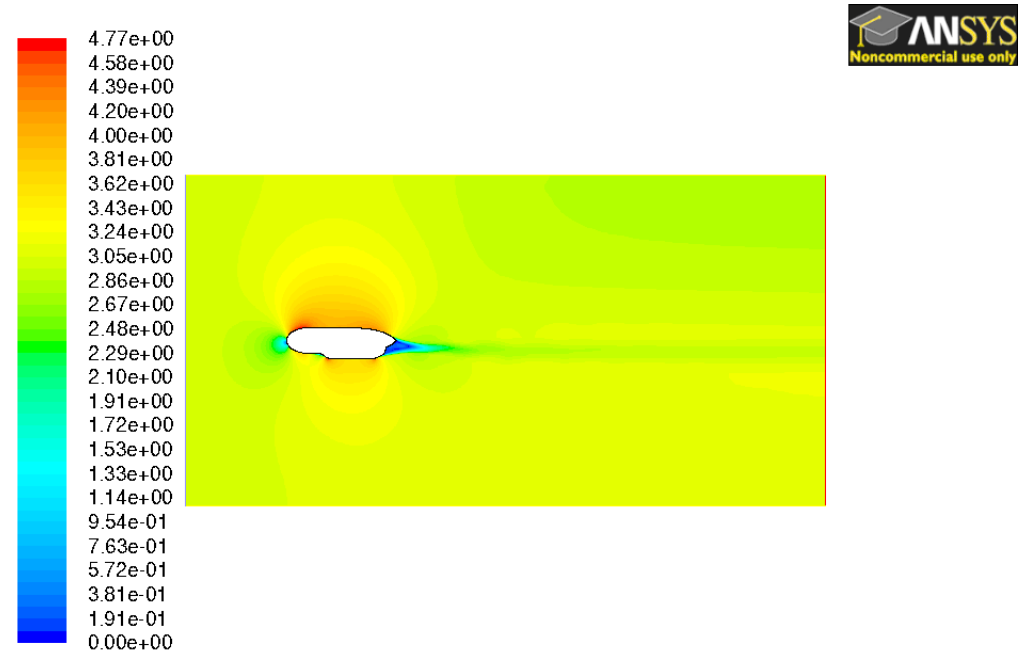

B.3 Shape II

B.3.1 Pressure coefficient

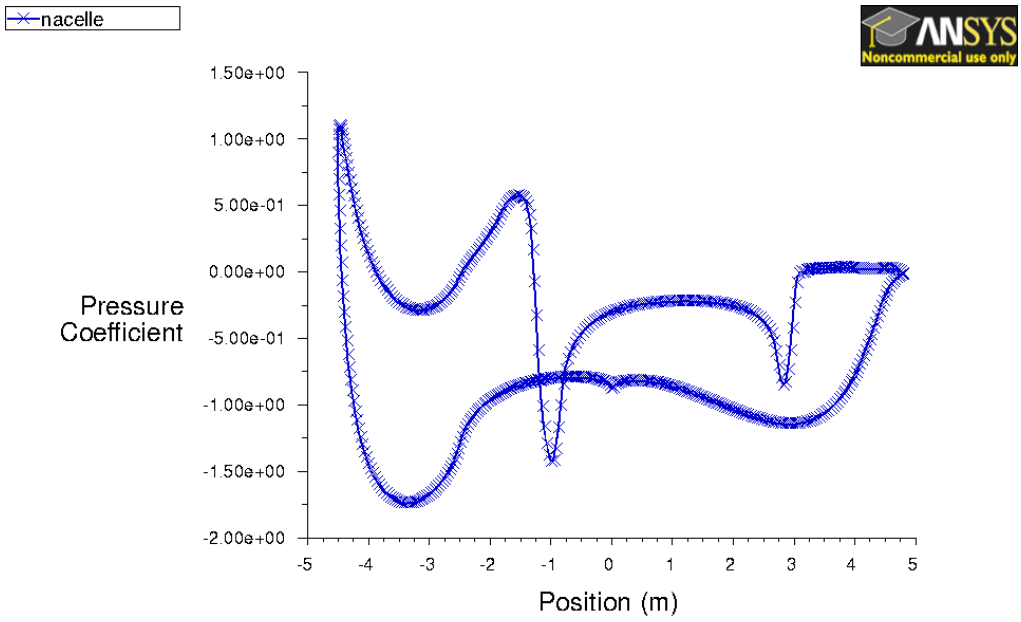

B.3.2 Contours of static pressure

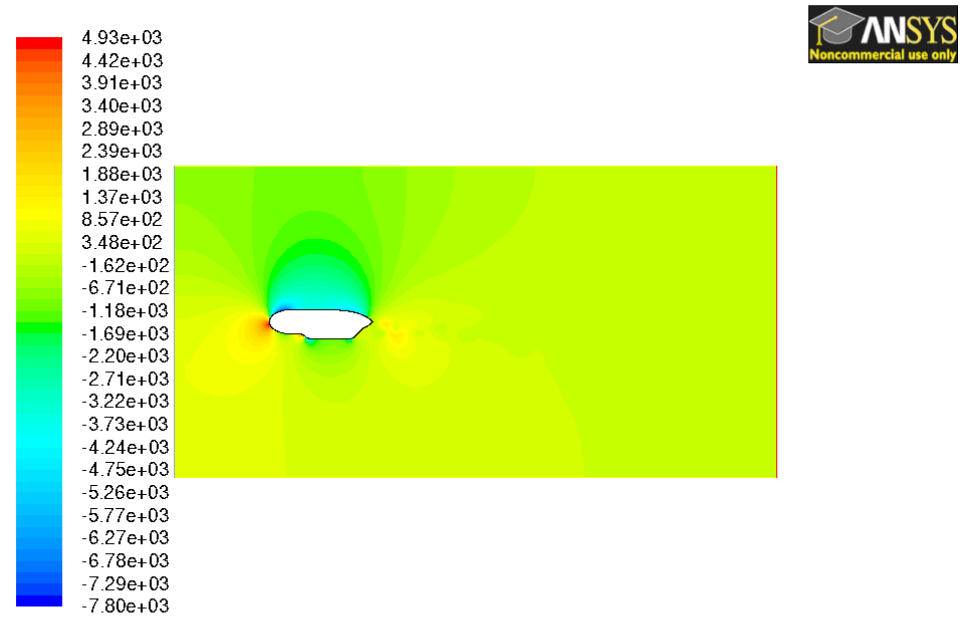

B.3.3 Contours of velocity magnitude

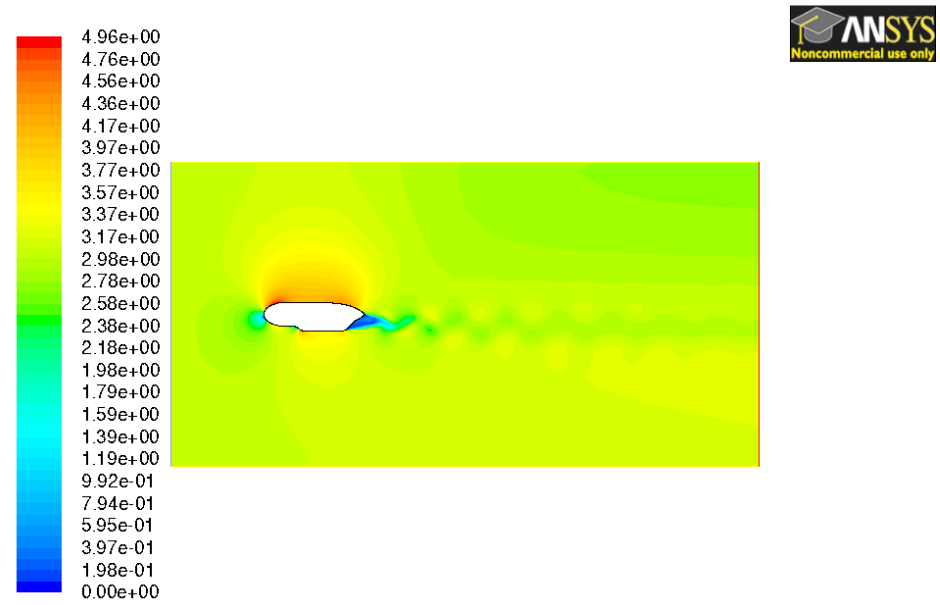

Contours of Velocity Magnitude (m/s) (Time=3.0000e+01) Jul 19, 2010
ANSYS FLUENT 12.1 (2d, dp, pbns, ske, transient)

B.4 Shape III

B.4.1 Pressure coefficient

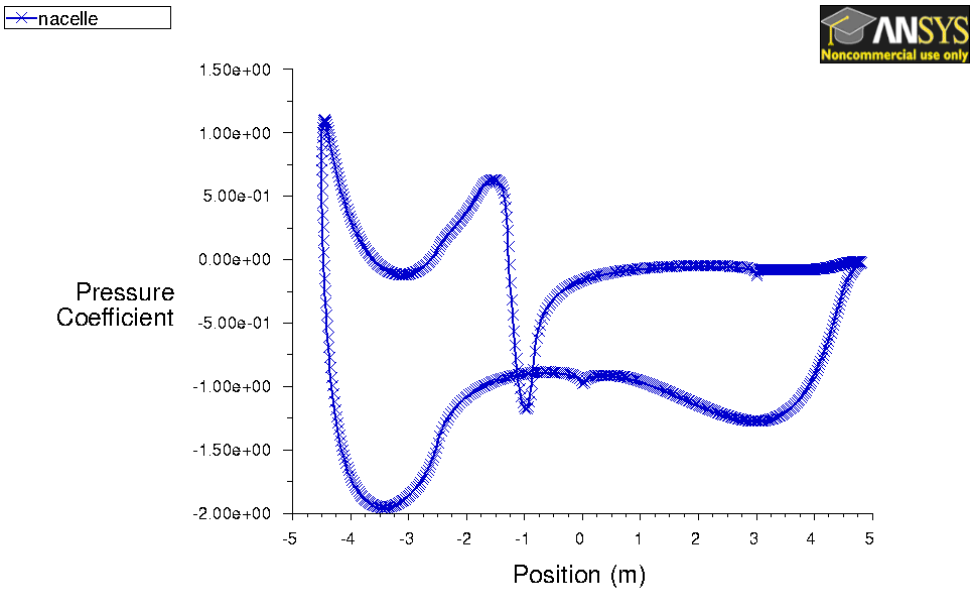

B.4.2 Contours of static pressure

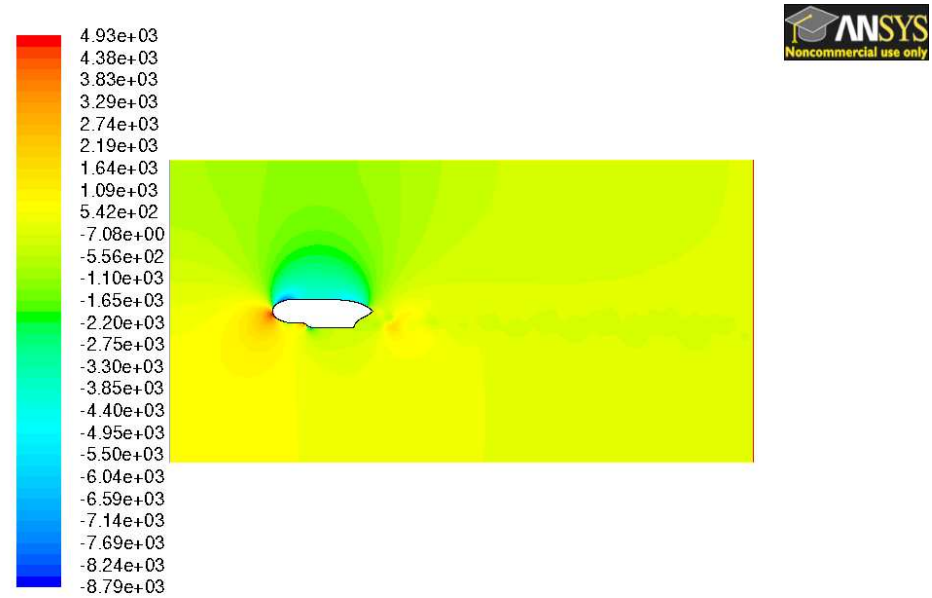

B.4.3 Contours of velocity magnitude

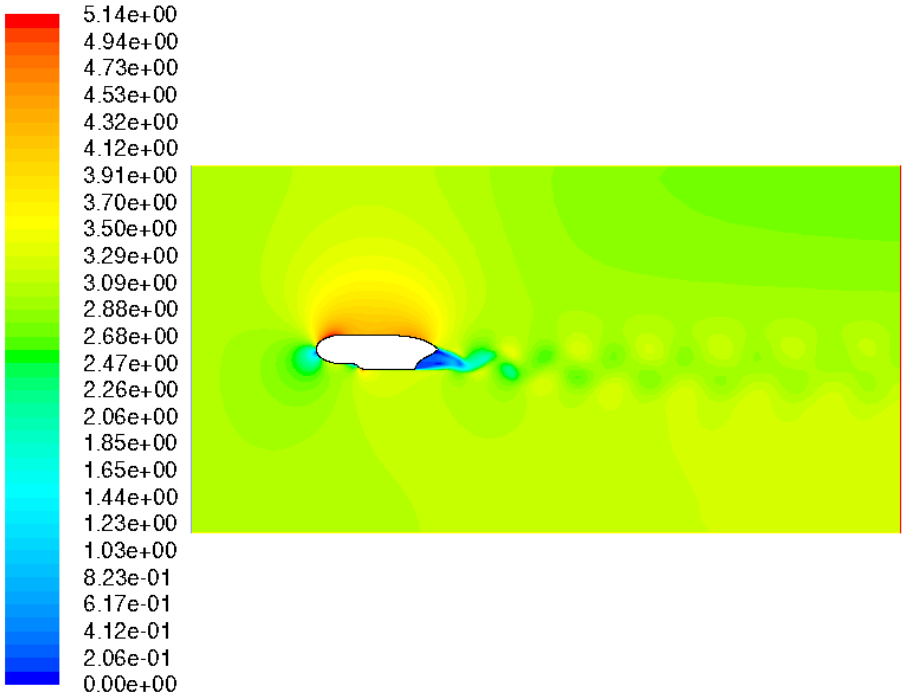

Contours of Velocity Magnitude (m/s) (Time=3.0000e+01) Jul 19, 2010
ANSYS FLUENT 12.1 (2d, dp, pbns, ske, transient)

B.5 Shape IV

B.5.1 Pressure coefficient

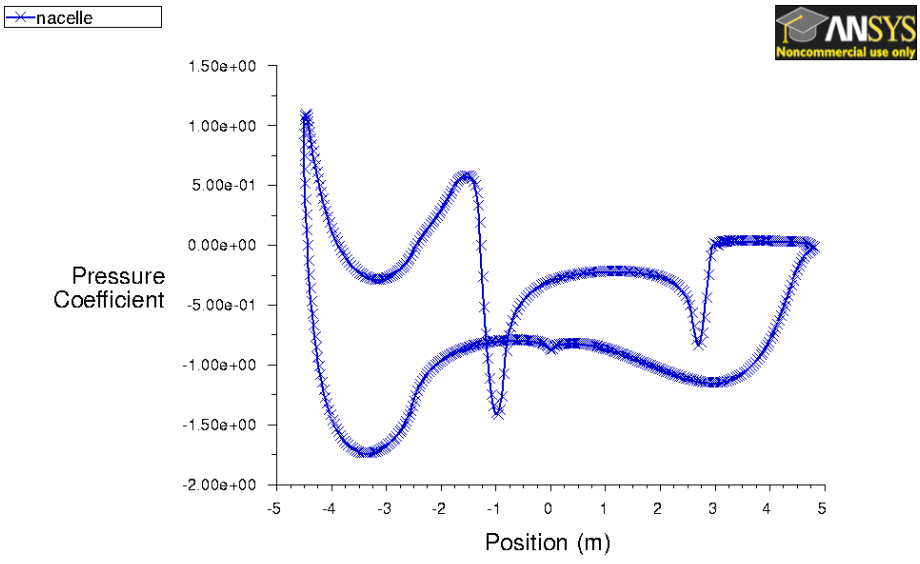

B.5.2 Contours of static pressure

B.5.3 Contours of velocity magnitude

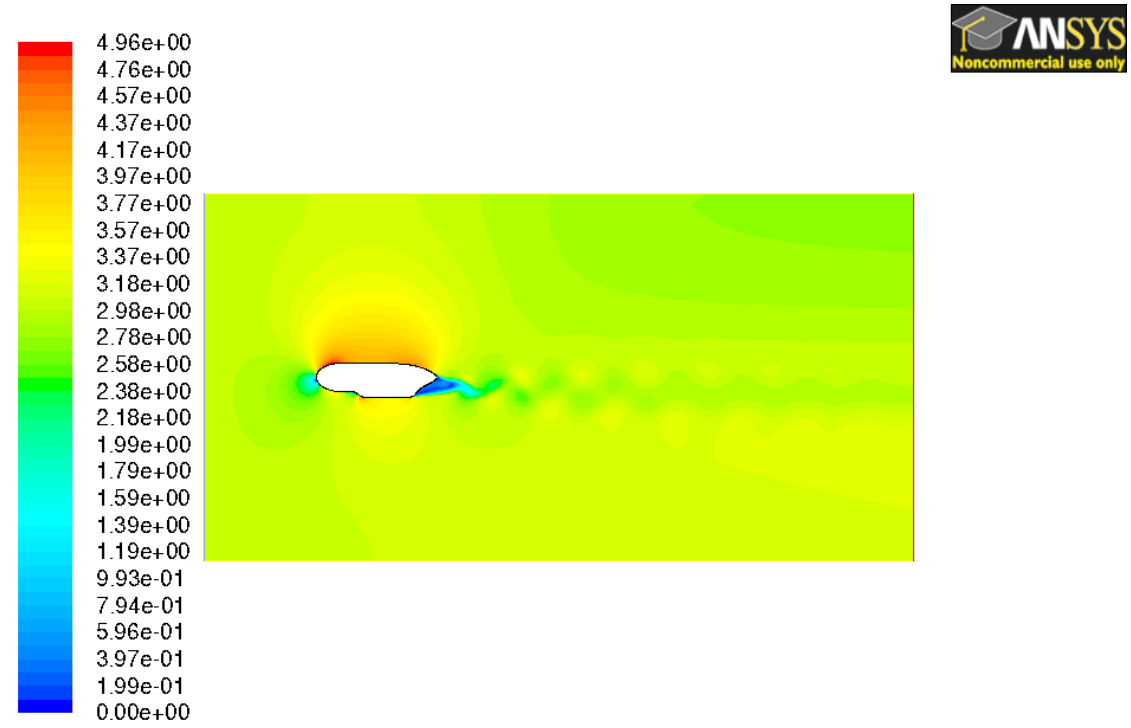

Contours of Velocity Magnitude (m/s) (Time=3.0000e+01) Jul 19, 2010
ANSYS FLUENT 12.1 (2d, dp, pbns, ske, transient)

B.6 Longitudinal elliptical shape

B.6.1 Pressure coefficient

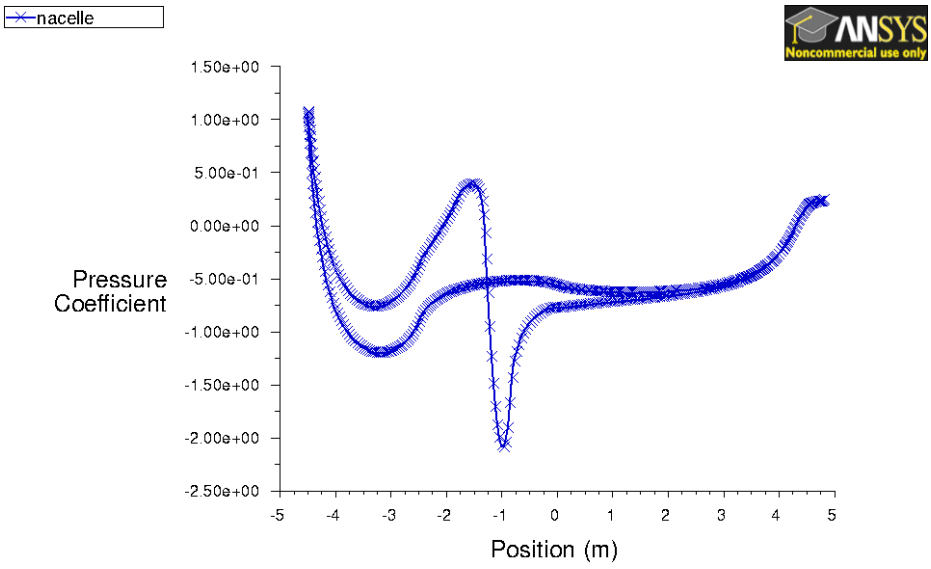

Pressure Coefficient (Time=3.0000e+01)

Jul 19, 2010
ANSYS FLUENT 12.1 (2d, dp, pbns, ske, transient)

B.6.2 Contours of static pressure

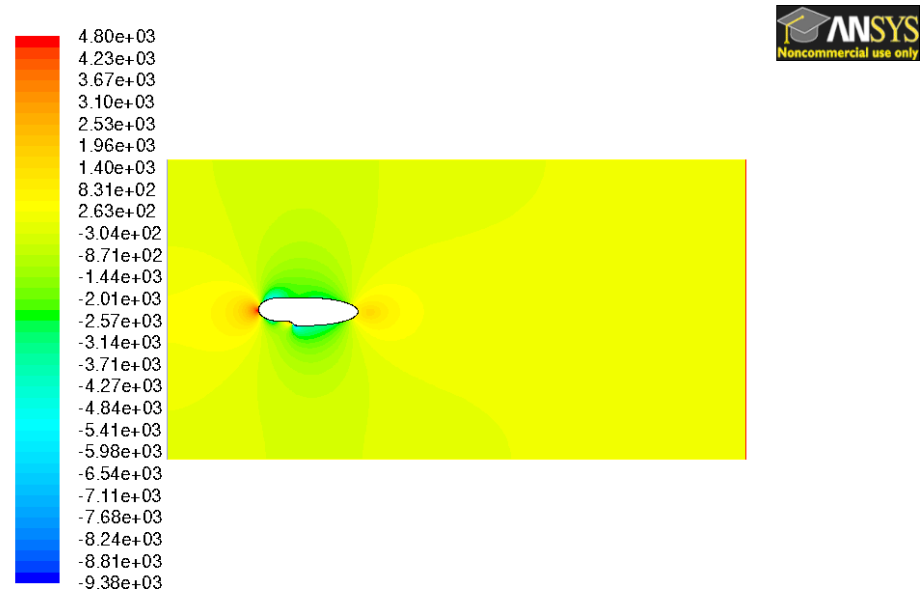

Contours of Static Pressure (pascal) (Time=3.0000e+01)

Jul 19, 2010
ANSYS FLUENT 12.1 (2d, dp, pbns, ske, transient)

B.6.3 Contours of velocity magnitude

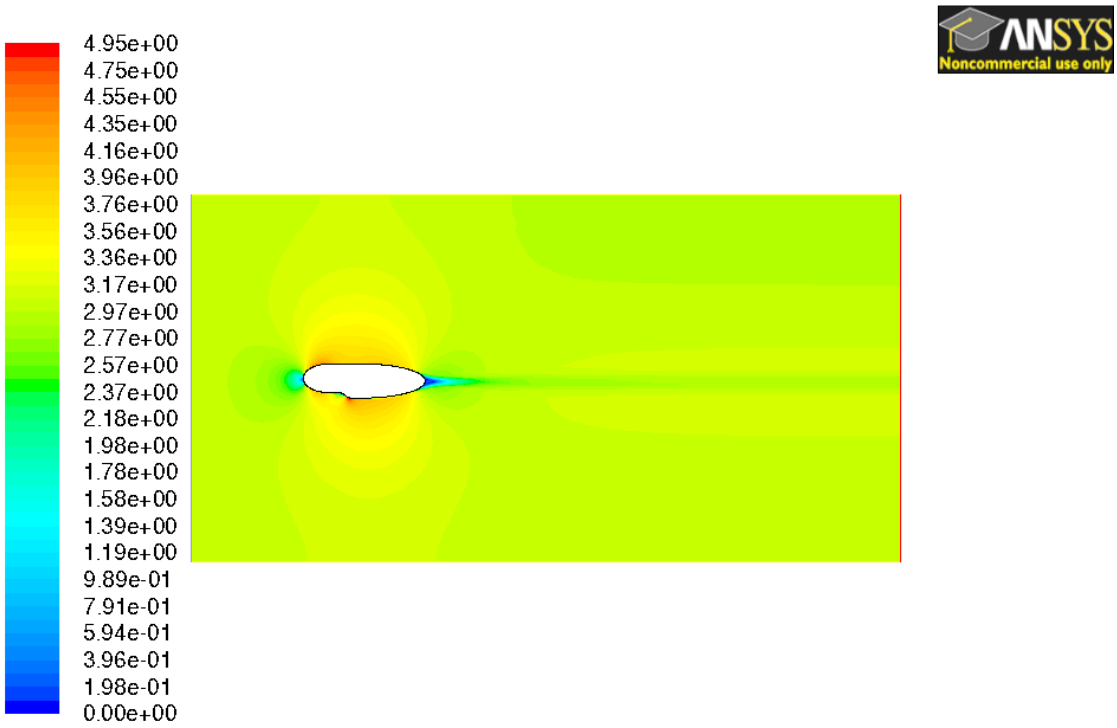

Contours of Velocity Magnitude (m/s) (Time=3.0000e+01) Jul 19, 2010
ANSYS FLUENT 12.1 (2d, dp, pbns, ske, transient)

Appendix C MatLab scripts

C.1 Drag

```
% Tuesday 20/07/2010 - 12:16

% Fabien - DRAG COEFFICIENT CALCULATOR - MatLab function


                % ** Function declaration **


                % Name of the function is 'drag'

                % Output is drag_coeff

                % Input is '.dat' file loaded in the command

                % window

                % Function returns drag_coeff


function [drag_coeff] = drag(file)


t=file(:,1);

                % Definition of vector t (time) 1st column of

                % the '.dat'.


cd=file(:,2)/2.6;

                % Definition of vector cd (drag coefficient).
```

```
                % This is the second column of the '.dat' file.
                % Each component is divided by the reference
                % value of 2.6 meters. This corresponds to the
                % height of studied profiles.


i=find(t==20);
                % i is an indice used to find the row number
                % corresponding to time t = 20 sec in the '.dat'

drag_coeff=mean(cd(i:length(cd)));
                % drag_coeff is the mean of the values of
                % vector cd from indice i to the end of the
                % vector. In other terms the mean of cd values
                % is calculated when convergence starts from
                % t = 20 sec until the end of the calculation.
```

C.2 Lift

```
% Tuesday 20/07/2010

% Fabien - LIFT COEFFICIENT CALCULATOR - MatLab function


                % ** Function declaration **


                % Name of the function is 'Lift'

                % Output is lift_coeff

                % Input is '.dat' file loaded in the command

                % window

                % Function returns lift_coeff


function [lift_coeff] = lift(file)


t=file(:,1);

                % Definition of vector t (time) 1st column of

                % the '.dat'.


cl=file(:,2)/2.6;

                %Definition of vector cl (lift coefficient).

                %This is the second column of the '.dat' file.
```

```
                %Each component is divided by the reference
                %value of 2.6 meters. This corresponds to the
                %height of the profiles.



i=find(t==20);
                %i is an indice used to find the row number
                %corresponding to time t = 20 sec in the '.dat'


lift_coeff=mean(cl(i:length(cl)));
                % lift_coeff is the mean of the values of
                % vector cl from indice i to the end of the
                % vector. In other terms the mean of cl values
                % is calculated when convergence starts from
                % t = 20 sec until the end of the calculation.
```

C.3 Plots

```
close all

clear all


%chargement fichier .dat

load('cd_origin_sv.dat')


%definition du temps (axe des abscisses)

t=cd_origin_sv(:,1);


%definition du coeff de drag (axe des ordonnees)

cd=(cd_origin_sv(:,2))/2.6;


%trace du graphique

hold on

figure(1)

plot(t,cd)

axis([0 50 0 0.6]);

title('Drag coefficient vs time');

xlabel('time (s)');

ylabel('drag coefficient Cd');
```

```
close all

clear all


%chargement fichier .dat

load('cl_origin_sv.dat')


%definition du temps (axe des abscisses)

t=cl_origin_sv(:,1);


%definition du coeff de drag (axe des ordonnees)

cl=(cl_origin_sv(:,2))/2.6;


%trace du graphique

hold on

figure(1)

plot(t,cl)

axis([0 50 0 2.5]);

title('Lift coefficient vs time');

xlabel('time (s)');

ylabel('Lift coefficient Cl');
```